TABLE OF CONTENTS

Editorial 5

The TANDEM AMS facility 7

Operation of the 6 MV TANDEM accelerator 8

A new control system for the TANDEM accelerator 9

^{10}Be and ^{26}Al measurements with the 6 MV TANDEM 10

Improved ^{10}Be sample preparation for the TANDEM 11

New primary ^{10}Be standard and $T_{1/2}$ for AMS at ETH 12

Re-calibration of the ETH chlorine-36 standards 13

The TANDY AMS facility 15

The upgraded 0.6 MV AMS system "TANDY" 16

Modified ion source for the TANDY 17

^{10}Be measurements on the 0.6 MV TANDY 18

^{129}I measurements at 0.5 MV 19

^{236}U at TANDY 20

The MICADAS AMS facility 21

The first years of MICADAS 22

DatingMICADAS 23

Ion source upgrade for MICADAS 24

Improving a gas ion source 25

^{14}C AMS measurements of small samples 26

Online ^{14}C analyses of carbonaceous aerosols 27

Detection and analysis 29

Compact gas ionization chambers 30

A new HIBS detector for RBI Zagreb 31

Energy-loss straggling measurements 32

Measurements at high counting rates 33

BATS: A new tool for AMS data reduction 34

^{14}C sample preparation 35

Extension of the ^{14}C laboratory 36

What's cooking in the ^{14}C lab? 37

AGE: A new graphitization system 38

Graphitization in 'closed tubes' 39

Compound-specific radiocarbon analysis 40

Alternative cellulose isolation from wood 41

Simplified radiocarbon dating of small samples 42

In situ cosmogenic ^{14}C 43

Radiocarbon applications 45

The ^{14}C samples 'pie' 46

Ultra-high precision radiocarbon dating 47

Is it time for a new calibration curve? 48

Carbon cycling in Damma Glacier forefield soils 49

45'000 year old Niederweningen mammoth 50

^{14}C based age-depth model of Soppensee 51

Radiocarbon analyses of aerosol components 52

Applications in geology 53

Alpine glacier and rock glacier activity 54

Alpine glaciers in the Jura Mountains 55

Glaciations in the Kackar Mountains (NE Turkey) 56

Glaciations in the Dedegöl Mountains (Turkey) 57

Pleistocene glaciations in the subtropical Andes 58

Comparing ^{14}C and ^{10}Be exposure dating results 59

Large mass movements in the Alps 60

A tool to reconstruct rock fall history? 61

Testing dual-cosmogenic isotope burial dating 62

A new view of Alpine erosion 63

Erosion rates in the Hörnli area 64

Erosion rates from the eastern Altiplano 65

^{10}Be based denudation rates in foreland basins 66

Denudation rates from fault footwalls 67

Building stones in Hattusha (Hittite Empire) 68
^{36}Cl production in limestones and dolomites 69

Ice and ocean sediments 71

Past and future solar activity 72
Solar irradiance since the Maunder Minimum 73
^{36}Cl in permafrost ice from Sibiria 74
Carrier free ^{10}Be/^{9}Be measurements at the TANDY 75
^{231}Pa/^{230}Th off West Africa 76

Environmental monitoring 77

^{14}C as tracer of fossil fuel CO_2 78
Iodine-129 in the environment 79
Oceanic transport of radioactive waste 80
Determination of plutonium using AMS 81
Plutonium isotopes from a nuclear test site 82

Biomedical applications 83

Bomb peak dating of French brandy 84
Tracing ethanol metabolism with a 1964 brandy 85
Isotopic labeling of a sheep skeleton 86

Materials sciences 87

Capillary microprobe 88
Simultaneous RBS and PIXE 89
A new set-up for Helium PIXE 90
New high temperature irradiation set-up 91
Analysis of PLD-grown ion-conductive films 92
Converting polycrystals into single crystals 93

Education 95

Learning by playing with your own samples 96
Development of new lab equipment 97

Publications 99

Talks

Invited talks 105

Talks and posters 108

Seminars

Spring semester 112

Fall semester 113

Theses

Internal 114

External 115

Collaborations 117

Visitors 122

EDITORIAL

In 2009, a new organizational structure for the **Laboratory of Ion Beam Physics** (LIP) has been implemented. After more than 24 years of successful operation under the auspices of ETH and the Paul Scherrer Institut, the LIP is now completely integrated into the ETH structure. A board of trustees has been formed to support and control the LIP activities. Members of the board of trustees are delegates from ETH (D-PHYS, D-ERDW), the Swiss Federal Institute of Aquatic Science and Technology (EAWAG), the Swiss Federal Institute of Material Sciences and Technology (EMPA) and the Paul Scherrer Institut (PSI). The laboratory is now part of the Department of Physics (D-PHYS) and is associated with the Institute of Particle Physics (IPP).

LIP serves as a national and international center for accelerator mass spectrometry (AMS) and for materials sciences based on ion beam technology. We have at our disposal sophisticated instrumentation with dedicated accelerator facilities covering the energy range from a few 100 keV to 50 MeV. The mission of the laboratory comprises fundamental research in ion beam technologies, instrumental developments and applications of ion beam technologies. In addition, we contribute to the educational program of ETH and provide service for external users.

Reorganization always offers a chance to present the activities of the laboratory from a somewhat different point of view. We decided to show the large breadth of our activities in this report with the focus on the day to day work, the little advances, and the significant progress made in 2009. Of course, a much deeper view of the scientific output can be obtained by studying the scientific publications compiled in the annex of this report.

This report was planned to give a comprehensive overview of the laboratory's activities of the past year and the outreach of our scientific capabilities into the network of external research groups we are collaborating with. The large number of contributions from our partners demonstrates the vast variety of applications of ion beam technologies for accelerator mass spectrometry as well as for the research activities in the materials sciences. It indicates the highly trans-disciplinary nature of our primary activities and shows the strong embedding of the laboratory into rapidly growing research fields.

All theses activities became only possible due to the dedicated work of the scientific and the technical staff of the laboratory. The equivalent of 24.6 full time positions was filled in 2009. Financing of personnel and operational costs relies on an innovative model for ETH, where about 50% of all expenses are covered directly from internally generated funds. Our primary research partners (D-ERDW, EAWAG, EMPA, and PSI) have a combined share of 25% and the Department of Physics covers the rest. Thus, a well balanced configuration has been found between maintaining the essential knowledge within the laboratory by a good number of long-term employed senior scientists and key people in technical positions as well as the necessary regeneration of the laboratory within the framework of flexible time-based contracts.

It was our pleasure to compile the information and merge it to this comprehensive report. We are grateful to all our own people who have contributed to successfully continue the activities of the Laboratory of Ion Beam Physics, and we thank all our external partners for their ongoing support. It is our desire to further develop the ion beam technologies and to make possible a more widespread use of these powerful techniques.

Hans-Arno Synal, Peter W. Kubik

THE TANDEM AMS FACILITY

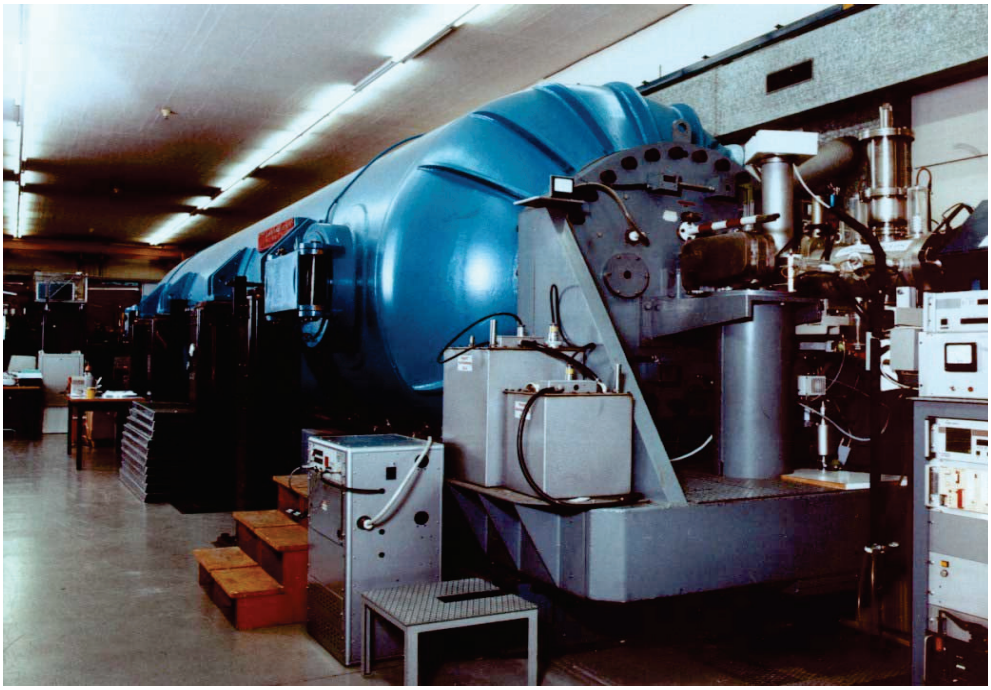

Operation of the 6 MV TANDEM accelerator

A new control system for the 6 MV TANDEM accelerator

^{10}Be and ^{26}Al measurements with the 6 MV TANDEM

Improved ^{10}Be sample preparation for the TANDEM

Re-calibration of the ETH ^{10}Be standards

Re-calibration of the ETH chlorine-36 standards

OPERATION OF THE 6 MV TANDEM ACCELERATOR

Beam time statistics and future upgrade plans

Scientific and technical staff, Laboratory of Ion Beam Physics

In 2009, the 6 MV EN TANDEM accelerator facility (Fig.1) was operated for more than 2000 hours (Fig. 2). About 1200 hours were spent on the routine AMS measurements of the three radionuclides ^{10}Be, ^{26}Al and ^{36}Cl, while the various experiments in the materials sciences took up about 500 hours. Due to the fact that all radiocarbon measurements have been moved to the MICADAS systems, the total number of operational hours has been significantly reduced. There is much more flexibility now to allocate beam time and to adjust the schedule to the needs of the different user programs. This is particularly true for the materials sciences program. All in all, the beam time of the accelerator could be provided with a minimum of effort.

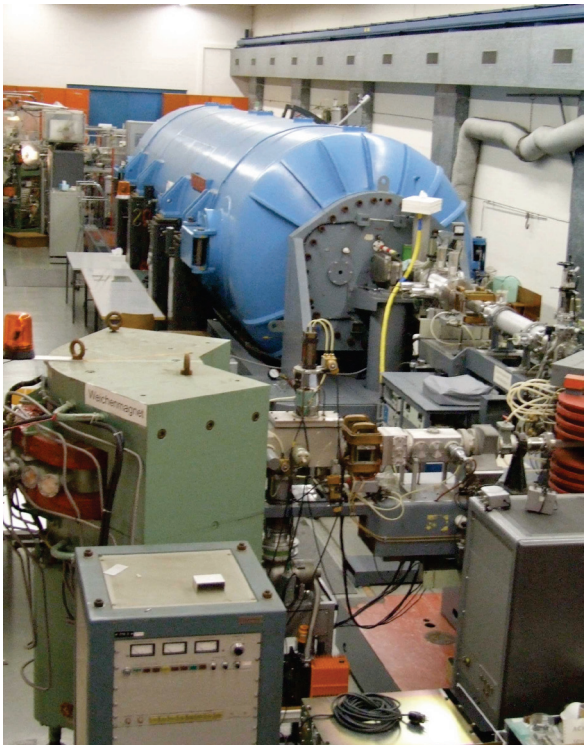

Fig. 1: *The EN TANDEM accelerator seen from the high-energy side of the accelerator hall.*

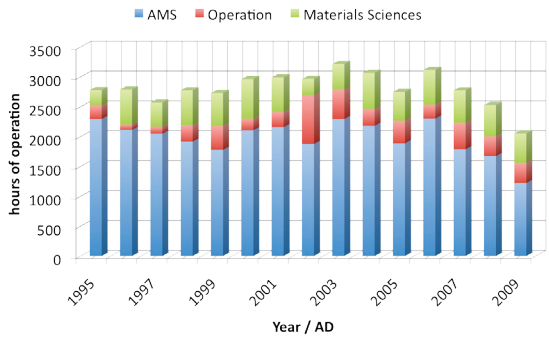

Fig. 2: *Statistics of accelerator operation subdivided into AMS, materials sciences, service and maintenance activities.*

The generation of the terminal voltage is still based on a belt charging system. Since new charging belts are not available any more, a new Pelletron type charging system will be needed to ensure the continuation of the very successful AMS and materials sciences programs. The proposed upgrade will bring the TANDEM accelerator in line with newly installed accelerators with only a modest investment. The infrastructure of various ion sources and beam lines, which have been optimized over the past decades, and the excellent expertise in ion beam physics will keep the TANDEM facility positioned among the top AMS laboratories.

Our R'Equip-SNF proposal has been approved in November and funding is now available for the upgrade. Detailed planning has begun and we plan to place the order for the new Pelletron charging system in early spring of 2010. We expect delivery within 9 month and should be ready for the replacement of the charging system in early 2011.

In parallel, a new ion source is planned to be set up at the 90° port of the TANDEM injection spectrometer. This source will be of the same type as the newly developed MICADAS ion sources.

A NEW CONTROL SYSTEM FOR THE TANDEM ACCLERATOR

Hardware and software update

R. Pfenninger, S. Bühlmann

The computer control system of our EN TANDEM accelerator, which was coming to the end of its life time cycle, has now been replaced with a new system based on an industrial PC. It uses our software *panda*, which for years has successfully controlled our other AMS systems (TANDY, MICADAS). The system supports three ion sources and two beamlines. The beamline setups are selected during startup of *panda*.

The industrial PC (Advantech) is composed of a dust-proof box with power supply and cooling system and a passive backplane with 14 PCI slots for the interface boards and for the CPU board. The setpoint values of the accelerator system power supplies are controlled by peripheral digital-to-analog converters (existing, homemade DACs) for optimum beam stability. The actual values are converted by two 16bit-ADCs (Measurement Computing) of 32 channels each.

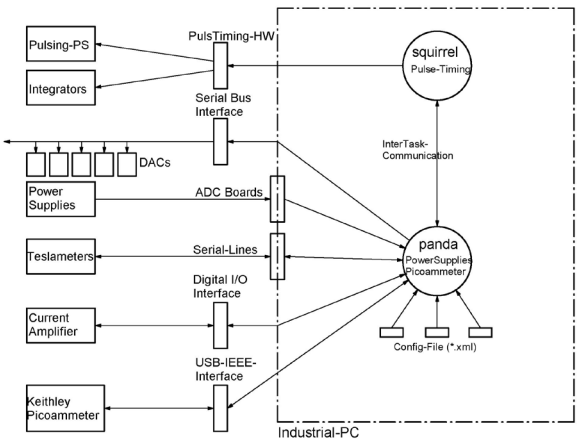

Fig. 1: *Block diagram of the control system.*

The timing signals for the fast pulsing system are produced by timer boards (National Instruments) and sent to the power supplies and current integrators with 50 Ohm drivers.

A relay/optocoupler board is available for the input and output of digital I/O signals.

Beam currents from Faraday cups are measured with pico-amperemeters (Keithley Instruments) which are controlled by an IEEE interface (Agilent Technologies). Range adjustments are made with the PC.

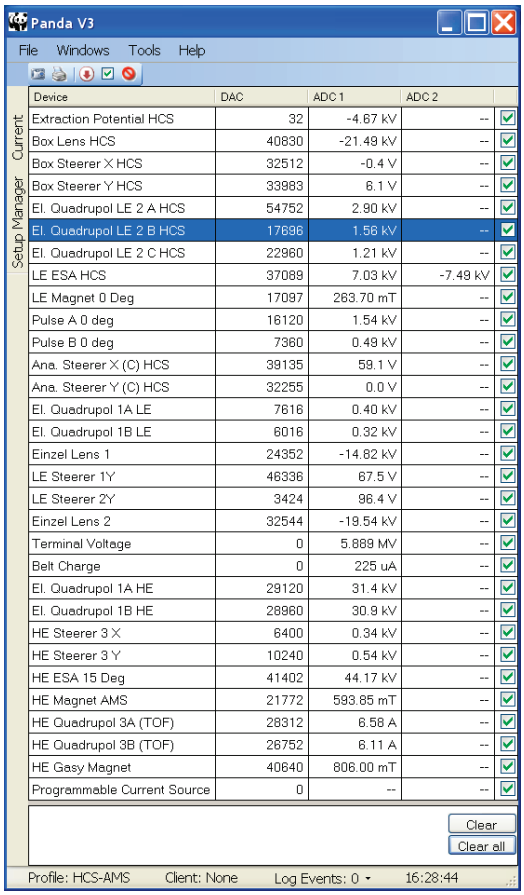

Device	DAC	ADC 1	ADC 2
Extraction Potential HCS	32	-4.67 kV	--
Box Lens HCS	40830	-21.49 kV	--
Box Steerer X HCS	32512	-0.4 V	--
Box Steerer Y HCS	33983	6.1 V	--
El. Quadrupol LE 2 A HCS	54752	2.90 kV	--
El. Quadrupol LE 2 B HCS	17696	1.56 kV	--
El. Quadrupol LE 2 C HCS	22960	1.21 kV	--
LE ESA HCS	37089	7.03 kV	-7.49 kV
LE Magnet 0 Deg	17097	263.70 mT	--
Pulse A 0 deg	16120	1.54 kV	--
Pulse B 0 deg	7360	0.49 kV	--
Ana. Steerer X (C) HCS	39135	59.1 V	--
Ana. Steerer Y (C) HCS	32255	0.0 V	--
El. Quadrupol 1A LE	7616	0.40 kV	--
El. Quadrupol 1B LE	6016	0.32 kV	--
Einzel Lens 1	24352	-14.82 kV	--
LE Steerer 1Y	46336	67.5 V	--
LE Steerer 2Y	3424	96.4 V	--
Einzel Lens 2	32544	-19.54 kV	--
Terminal Voltage	0	5.889 MV	--
Belt Charge	0	225 uA	--
El. Quadrupol 1A HE	29120	31.4 kV	--
El. Quadrupol 1B HE	28960	30.9 kV	--
HE Steerer 3 X	6400	0.34 kV	--
HE Steerer 3 Y	10240	0.54 kV	--
HE ESA 15 Deg	41402	44.17 kV	--
HE Magnet AMS	21772	593.85 mT	--
HE Quadrupol 3A (TOF)	28312	6.58 A	--
HE Quadrupol 3B (TOF)	26752	6.11 A	--
HE Gasy Magnet	40640	806.00 mT	--
Programmable Current Source	0	--	--

Fig. 2: *Screenshot of a panda program display.*

In the near future, the industrial PC is also envisioned to control the regular AMS measurements with our software *squirrel*. At present, these measurements are made with the data acquisition system *hamster*.

^{10}Be AND ^{26}Al MEASUREMENTS WITH THE 6 MV TANDEM

A status report

P.W. Kubik, M. Christl

The routine ^{10}Be and ^{26}Al measurements are still performed with the nominal 6 MV EN TANDEM accelerator (Fig. 1). About 2000 ^{10}Be and 150 ^{26}Al samples are measured per year (Tab.1).

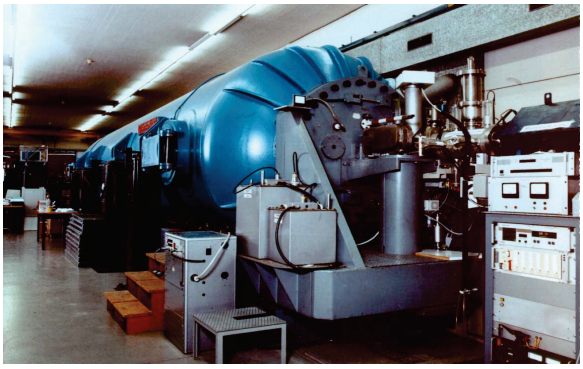

Fig. 1: *The nominal 6 MV EN TANDEM seen from the high-energy side.*

The typical negative ion beam output from the high-intensity ion source used in these measurements is shown in Table 1. The ions are injected sequentially into the TANDEM using a fast pulsing system. Argon gas is used to strip the ions at terminal voltages of 5.5 MV for Be and 4.5 MV for Al. The high-energy mass spectrometer consists of an electrostatic analyzer followed by the high-energy magnet.

nuclide	I^- [uA]	T [%]	BG	samples
^{10}Be	2-6	10	$<10^{-15}$	2000
^{26}Al	0.1-0.6	15	$<10^{-14}$	150

Tab. 1: *Performance parameters for ^{10}Be and ^{26}Al measurements. BG=background ratio, T= accepted to injected radionuclide counting rate.*

^{26}Al measurements are made in charge state 3+ with an overall transmission of ≈15%. ^{26}Al/Al ratios for commercial Al_2O_3 are $<10^{-14}$ (Tab. 1).

^{10}Be is first analyzed in charge state 3+ and then passed through a thin C foil at the entrance to a 180° magnet. Charge state 4+ is selected for ^{10}Be and the background inducing ^{10}B ions. This way, the ^{10}B counting rate is reduced about fivefold with only a 10% loss in the ^{10}Be rate. For this mode, beam-line restrictions require the use of ^{16}O instead of ^{9}Be of the injected ^{9}Be^{16}O molecule for the stable isotope measurement. The overall transmission for ^{10}Be is ≈10%. ^{10}B induced background ratios are $<10^{-15}$ for good quality samples (Tab. 1). An example of processed Be blanks is shown in Fig. 2.

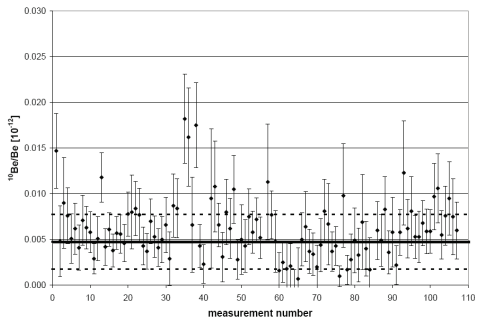

Fig. 2: *^{10}Be/Be ratios of chemistry blanks for an Antarctic ice core project.*

For an update on ^{10}Be standards at ETH see "New primary ^{10}Be standard and $T_{1/2}$ for AMS at ETH" in this report. For ^{26}Al we have made a similar decision to facilitate comparability of ^{26}Al data from different AMS laboratories. Effective April 1, 2010 we will use the ^{26}Al standard of K. Nishiizumi (01-4-1) [2] as our primary ^{26}Al standard together with a half-life of 0.705 Ma. Our in-house standard ZAL94 has thus been relabeled and recalibrated to ZAL94N=490·10^{-12} (±5%). Consequently, all pre-April 2010 ^{26}Al data from ETH will have to be reduced using the eqation: $^{26}Al_{new} = {}^{26}Al_{old}/1.072$ [1].

[1] P.W. Kubik and M. Christl, Nucl. Instr. & Meth. B 268 (2010) 880

[2] K. Nishiizumi, Nucl. Instr. & Meth. B 223-224 (2004) 388

IMPROVED ^{10}Be SAMPLE PREPARATION FOR THE TANDEM

A Fe-Ag matrix significantly enhances the BeO^- output

M. Christl, P.W. Kubik

Systematic tests have shown that both the output and the efficiency of the TANDEM high-intensity ion source are significantly enhanced for ^{10}Be samples, if a mixture of silver and iron oxide is used as sample matrix. The use of iron also facilitates the last steps of BeO cathode preparation, particularly for small (low carrier) samples. The complete cathode preparation scheme is available on request. Here, we summarize only the main steps of the method and the effects in the ion source.

After the chemical separation of Be about 0.5 - 1 mg of Fe (as $FeNO_3$) is added to the sample. The sample is homogenized and Be-hydroxide is co-precipitated with iron-hydroxide by adding NH_4OH. After several washing steps $AgNO_3$ is added to the precipitate. The suspension is mixed, dried and heated to 650°C so that the main constituents of the final sample matrix are Ag, Fe_2O_3, and BeO.

BeO cathodes prepared with the new Fe-Ag method produce high negative ion currents with good reproducibility (Fig. 1).

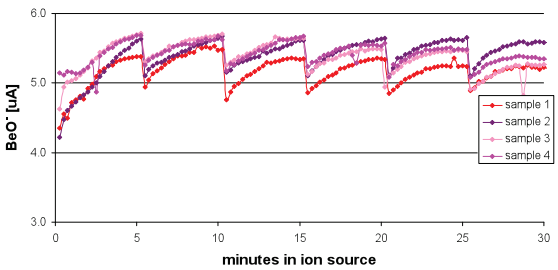

Fig. 1: *Low-energy current over time for four individual Fe-Ag-Be samples (200 µg-Be carrier).*

Compared to the standard preparation methods for the TANDEM (Ag-matrix, Cu-matrix) the Fe-Ag matrix significantly increases the apparent ionization efficiency for BeO^- (ratio of collected BeO^- ions to total BeO in the sample; 35 min collection time). This effect was tested with Be samples containing 100 µg and 200 µg of Be-carrier and is reproducible (Fig. 2).

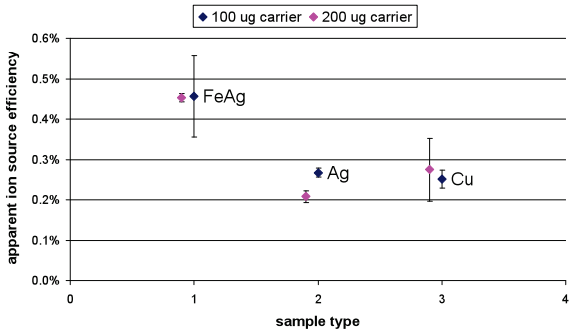

Fig. 2: *Apparent ion source efficiency for BeO^- after 35 min in the ion source for different sample matrices and 100 µg and 200 µg carrier.*

A dilution series of the in house standard S2007 was prepared to determine the apparent total efficiency in dependence of the amount of Be in the sample (Fig. 3). Our results show that after 20 min (representing a typical measurement time during routine ^{10}Be measurements) an apparent total efficiency (identified ^{10}Be counts vs. ^{10}Be in the sample) of $(1.9 - 2.5 \cdot 10)^{-4}$ is reached for samples containing between 50 µg and 250 µg of Be.

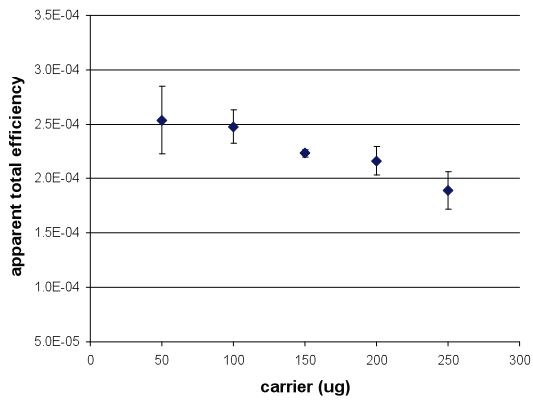

Fig. 3: *Apparent total efficiency as a function of carrier amount after 20 min of sputtering.*

NEW PRIMARY ^{10}Be STANDARD AND $T_{1/2}$ FOR AMS AT ETH

Recalibration of the in-house ^{10}Be standards

P.W. Kubik, M. Christl, V. Alfimov

Three in-house ^{10}Be AMS standards have been in use at ETH-Zurich (BEST433, S555 and S2007 with nominal ^{10}Be/Be ratios of $93.1\cdot10^{-12}$, $95.5\cdot10^{-12}$ and $30.8\cdot10^{-12}$, respectively). They are related to the material used to determine the ^{10}Be half-life of 1.51±0.06 Ma via an activity measurement and the reported ^{10}Be content of the ORNL-MASTER solution [1]. An extensive comparison shows very good agreement between S555 and the nominal values of the ICN ^{10}Be standards of K. Nishiizumi reported for a half-life of 1.5 Ma [2] (Fig. 1).

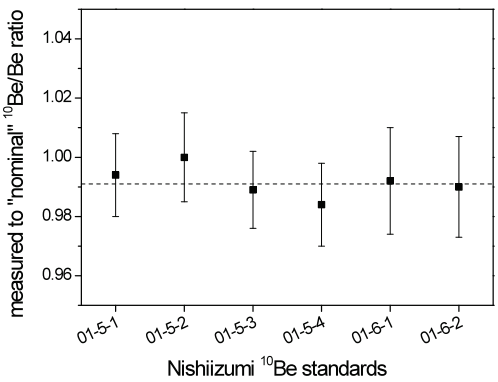

Fig. 1: *Measured to nominal ^{10}Be/Be ratios of the ICN standards (based on 1.5 Ma) normalized to S555. Error bars are 1σ.*

In the same paper [2], Nishiizumi et al., however, present new, half-life independent measurement data for the ICN standards. The results are lower by a factor of 1.106 relative to the nominal values for $T_{1/2}$=1.5 Ma implying that the ^{10}Be half-life is only 1.36±0.07 Ma [2].

Very recently, two very precise ^{10}Be half-life values measured with different methods have been published with a recommended weighted mean of 1.387±0.012 Ma [3, 4]. The evidence for a lower ^{10}Be half-life [2, 3, 4] and the agreement between our standard S555 and the ICN standards (for 1.5 Ma) necessitate a recalibration of the ETH ^{10}Be standards.

We have decided to use ICN standard 01-5-1 with the revised ^{10}Be/Be ratio of $2.709\cdot10^{-12}$ [2] as the new primary ETH ^{10}Be standard effective April 1, 2010. Accordingly, the ^{10}Be/Be ratios of the ETH in-house (secondary) standards need to be reduced by a factor of 1.096 [5]. To avoid confusion, we renamed our standards BEST433N, S555N and S2007N (with nominal values of $83.3\cdot10^{-12}$, $87.1\cdot10^{-12}$ and $28.1\cdot10^{-12}$, respectively). The 1σ error is 2.7% based on the 1σ errors of BEST433 and ICN 01-5-1 [1, 2].

All future ^{10}Be results from ETH will be referenced to standard ICN 01-5-1. The renormalization of the ETH standards to the ICN standards requires the use of a ^{10}Be half-life in agreement with 1.36±0.07 Ma [2]. We recommend and will use 1.387±0.012 Ma [3, 4].

As a consequence of this renormalization, all ^{10}Be results determined at ETH before April 1, 2010 will have to be reduced by a factor of 1.096. Examples are the ^{10}Be production rates by muons in quartz from Heisinger et al. [6] ($P_{sl\mu}$=0.097±0.007 and $P_{f\mu}$=0.085±0.012 ^{10}Be atoms/y/g quartz) and the sea level, high latitude ^{10}Be production rate from the Köfels landslide (4.96±0.17 ^{10}Be atoms/y/g quartz) [7].

[1] H. Hofmann et al., Nucl. Instr. & Meth. B 29 (1987) 32
[2] K. Nishiizumi et al., Nucl. Instr. & Meth. B 258 (2007) 403
[3] G. Korschinek et al., Nucl. Instr. & Meth. B 268 (2010) 187
[4] J. Chmeleff et al., Nucl. Instr. & Meth. B 268 (2010) 192
[5] P.W. Kubik and M. Christl, Nucl. Instr. & Meth. B 268 (2010) 880
[6] B. Heisinger et al., Earth and Planet. Sci. Lett. 200 (2002) 345 and 357
[7] P.W. Kubik and S. Ivy-Ochs, Nucl. Instr. & Meth. B 223-224 (2004) 618 (+ ref. therein)

RE-CALIBRATION OF ETH CHLORINE-36 STANDARDS

Improving the quality of ^{36}Cl/Cl ratio measurements

V. Alfimov, H.-A. Synal, R. Finkel[1,2], K. Wilcken[3]

In the past, ^{36}Cl measurements at ETH were normalized against the internal reference material K380 that had been produced by neutron activation of natural NaCl. Over the years, three solutions with ^{36}Cl/Cl isotopic ratios in the 10^{-11} range (K380/4, K381/4 and K382/4) were prepared. Careful internal calibrations of K381/4 to K380/4 and of K382/4 to K381/4 were made. Early on, the ^{36}Cl/Cl ratio of K380/4 was also calibrated against a reference material (^{36}Cl/Cl=$9.94\cdot10^{-12}$) kindly provided by Kuni Nishiizumi (UCSD).

	mean [10^{-12}]	σ [10^{-12}]	std used	samples
ETH	17.30	0.10	CLSTDN3	5
LLNL	17.37	0.05	KN5000	4
SUERC	17.42	0.13	Z93-0005	8

Tab. 1: *^{36}Cl/Cl ratios of ETH standard K382/4. The measured ratios were normalized to the standards indicated.*

A recent interlaboratory comparison indicated that the ^{36}Cl/Cl ratios of the ETH internal reference materials may be too low. This and the increasing demand for higher precision of ^{36}Cl measurements required a new approach to establish the absolute ^{36}Cl/Cl ratio of the Zurich reference materials. Three AMS laboratories, ETH, LLNL and SUERC, have measured the ETH ^{36}Cl standard K382/4 against other ^{36}Cl standards. At ETH, we measured against the standard CLSTDN3 with a nominal ^{36}Cl/Cl ratio of $1.003\cdot10^{-12}$ prepared by Kuni Nishiizumi in 1983. The LLNL measurements were made against the Nishiizumi standard KNSTD5000 (nominal ratio $5.00\cdot10^{-12}$) from 1989. The values of both standards were determined with a 301 kyr ^{36}Cl half-life. The SUERC measurements were made against standard Z93-0005 prepared at PRIME Lab of Purdue University. During the measurements at SUERC, another standard of Nishiizumi (^{36}Cl/Cl =$1.60\cdot10^{-12}$) was treated as an unknown. The result was within 1% of the nominal value.

All three K382/4 measurements agree within 0.5% (Tab. 1). The average of these results and its standard error are $(17.36\pm0.03)\cdot10^{-12}$. This material is now designated as K382/4N. The errors shown in Tab. 1 do not contain the uncertainties of the absolute values of the standards CLSTDN3, KNSTD5000, and Z93-0005. ETH materials with the new calibration values are now named K380/4N, K381/4N and K382/4N in order to separate them from the original standard materials.

The measured ratios between K381/4 and K382/4 and between K381/4 and K380/4 are 0.988±0.003 and 0.979±0.004, respectively. This yields a value of $(17.14\pm0.06)\cdot10^{-12}$ for K381/4N and $(16.78\pm0.09)\cdot10^{-12}$ for K380/4N.

We ask our ETH collaborators to use in the future the newly calibrated standard values and their labels (Tab. 2). To recalculate old (pre-2010) ^{36}Cl measurements we propose the scaling factors shown in Tab. 2.

	New	Old	Scaling
K380/4N	16.78±0.09	15.30	1.097
K381/4N	17.14±0.06	15.63	1.097
K382/4N	17.36±0.03	-	

Tab. 2: *The new ETH ^{36}Cl standard labels and values. Scaling factors are shown to convert pre-2010 AMS measurements to the new values.*

[1] *CEREGE, Aix en Provence, France*
[2] *Center for Accelerator Mass Spectrometry, LLNL, Livermore, USA*
[3] *SUERC, East Kilbride, United Kingdom*

THE TANDY AMS FACILITY

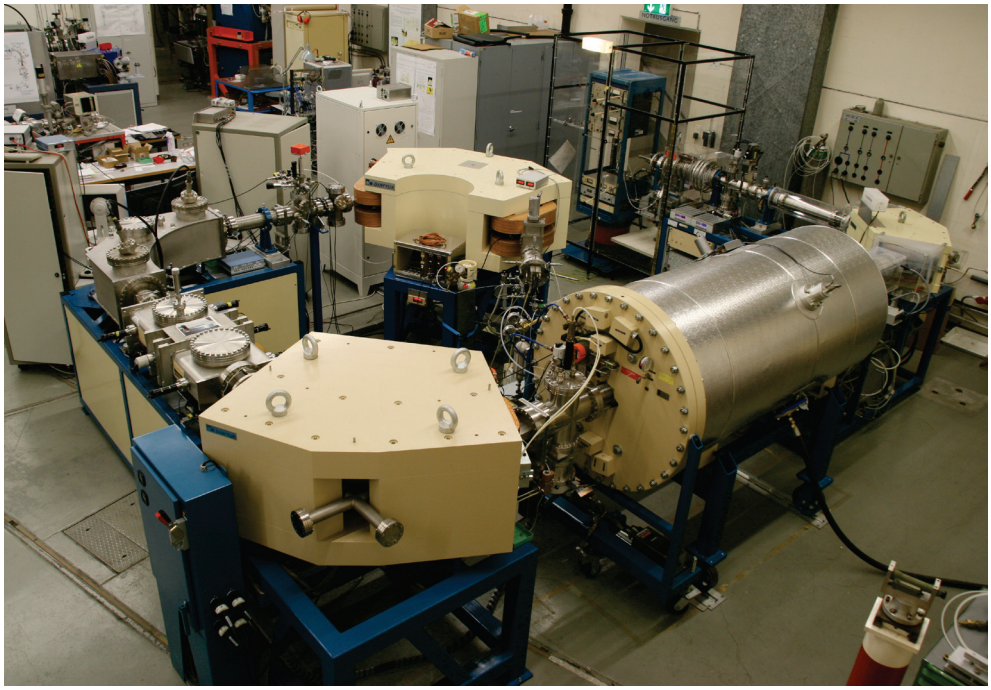

The upgraded 0.6 MV AMS system “TANDY”

Modified ion source for the TANDY

^{10}Be measurements on the 0.6 MV TANDY

^{129}I measurements at 0.5 MV

^{236}U at TANDY

THE UPGRADED 0.6 MV AMS SYSTEM "TANDY"

A new 130° magnet improves the high energy spectrometer

A.M. Müller, J. Bourquin, M. Christl, R. Gruber, J. Lachner, M. Suter, H.-A. Synal, C. Vockenhuber

AMS systems operating at low terminal voltages may suffer from an increased probability of ion scattering and charge exchange processes in the accelerator tubes. Due to these processes, neighboring masses can pass the TANDY high energy spectrometer consisting of a 90° bending magnet and an electrostatic analyzer (ESA). In the case of ^{10}Be measurements, the ^{9}Be induced background is intensified by scattering processes in the SiN degrader foil in front of the electrostatic deflector (Fig. 1) [1].

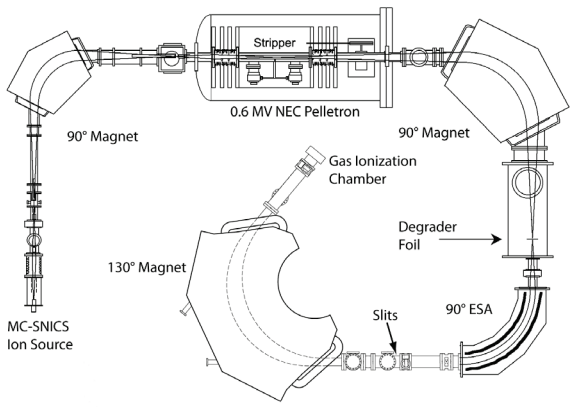

Fig. 1: *Schematic view of the upgraded TANDY spectrometer.*

To suppress this background, an additional 130° magnet spectrometer was designed and installed, which is usable over the full radionuclide mass range (^{10}Be - Pu) measured with the TANDY system (Tab. 1).

For ^{10}Be measurements the straggling losses in the degrader foil are minimized by designing the combination of ESA and 130° magnet as an achromatic and angular focusing system. Figure 2 shows how a beam of 0.5% energy dispersion is refocused after passing the ESA. With this setup, a ^{10}Be transmission (from the low energy side of the system to the detector) of up to 11% was achieved, which is comparable to our 6 MV tandem facility (see "^{10}Be and ^{26}Al measurements with the 6 MV TANDEM" in this annual report volume).

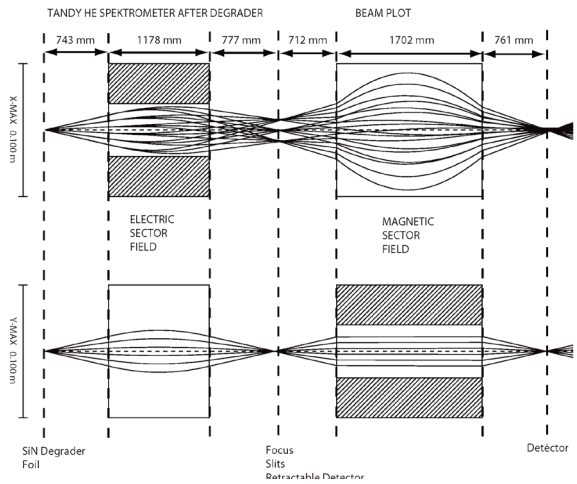

Fig. 2: *GICOSY [2] beam plot of the achromatic system consisting of the 90° ESA and the new 130° bending magnet for ΔE/E = 0.5%.*

The ^{10}Be/Be background ratio of $8{\cdot}10^{-14}$ without the 130° magnet was reduced to < $1{\cdot}10^{-15}$. This demonstrates that the TANDY AMS system is ready for routine ^{10}Be measurements.

Bending angle	130°
Entrance / exit angle	48.5°
Bending radius	750 mm
Pole gap	50 mm
Total weight	4410 kg
Manufacturer	Danfysik

Tab. 1: *Specifications of the new 130° magnet.*

[1] A.M. Müller et al., Nucl. Instr. & Meth. B 266 (2008) 2207
[2] http://www-linux.gsi.de/~weick/gicosy/

MODIFIED ION SOURCE FOR THE TANDY

Evolution of the MC-SNICS ion source

M. Christl, J. Lachner, C. Vockenhuber, R. Gruber, A. Herrmann, J. Bourquin

Several changes were made to the MC-SNICS ion source at the TANDY. The changes of the interior largely followed the suggestions by Southon and Santos [1].

The original NEC ionizer was replaced with a spherical Spectramat® ionizer - now used in all ETH AMS systems. A new ionizer housing was built with a fixed Cs delivery line that is heated by thermal conduction from the ionizer. Accordingly, the Cs oven was rebuilt with a vacuum insulated Cs feeding line. The Cs lens was removed from the system and an immersion lens at cathode potential was installed close to the ionizer, which significantly increases the field gradient between ionizer and immersion lens. The ion optics of the new geometry was modeled using SimIon® (Fig. 1).

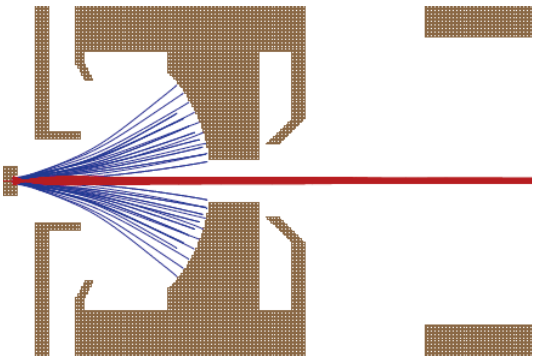

Fig. 1: *SimIon® simulation of the ion source. Blue: Cs^+ ions; red: extracted negative ions.*

Similar to modifications at the VERA AMS facility [2], an online target positioning system was implemented. During the measurement the target can be tilted or moved along the beam axis by individually turning three Lucite rods that are connected to the original positioning screws via chains (Fig. 2). The movement of the target can be observed with an IP-camera mounted on the viewport of the low energy magnet (Fig. 3).

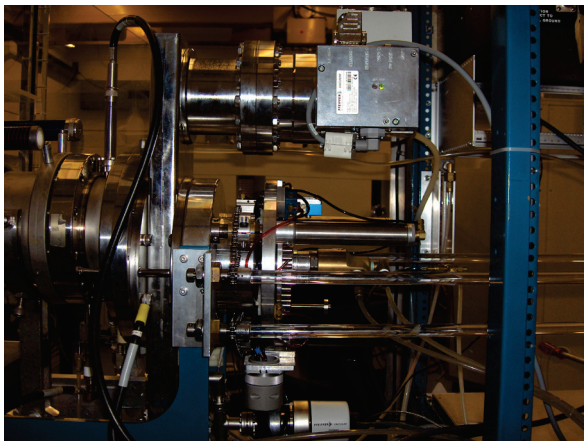

Fig. 2: *Picture of the rebuilt ion source showing the online positioning system and the new gate valve with the mounted turbopump.*

The installation of a MDC® gate valve with an additional port for a turbopump (Fig. 2) reduced the waiting time for a wheel change to about 2 to 3 hours. The ion source pressure during operation now is in the 10^{-8} mbar range.

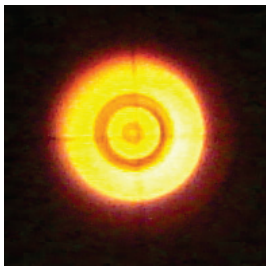

Fig. 3: *Picture of the IP-camera showing a target in measurement position.*

During first tests with BeO^- at a sample potential of 10 kV, currents of up to 8 µA were observed. However, the source has still to be thoroughly tested for reliability under routine operation.

[1] J. Southon and G.M. Santos, Nucl. Instr. & Meth. B 259 (2007) 88

[2] A. Priller et al., Nucl. Instr. & Meth. B 259 (2007) 94

^{10}Be MEASUREMENTS ON THE 0.6 MV TANDY

Starting routine operations

M. Christl, J. Lachner, A. Müller

After the installation of an additional magnet to the high-energy side of the spectrometer and after significant changes in the ion source, the compact (0.6 MV) AMS system TANDY is now ready for routine measurements of ^{10}Be (see other reports in this volume).

The efficiency of the system (ε) defined as the accepted to injected radionuclide counting rate is about 10 % (Tab. 1), which is competitive to the large (6 MV) TANDEM AMS system. Details of the measurement setup are described in [1].

	I^- [µA]	Tra [%]	ε [%]	BG
^{10}Be	2-4	>50	9-10	$<10^{-15}$

Tab. 1: *Performance parameters for the first ^{10}Be runs with TANDY. I^- = LE current, Tra = transmission, BG = background ratio.*

The first routine ^{10}Be measurements were very robust: The measured ^{10}Be/^{9}Be ratio of the standard S2007 varied by only 1.4 % (mean error for a single measurement) over one sample wheel (Fig. 1).

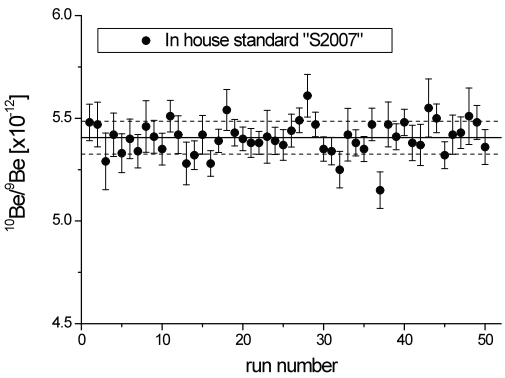

Fig. 1: *Standard S2007 over 17h (raw data).*

A low level Be carrier from the University Hannover (provided by F. v. Blanckenburg) was measured to estimate a background value for the new setup. ^{10}Be/^{9}Be ratios for this carrier material reported by other AMS laboratories (SUERC, VERA, ASTER) range between $4\cdot10^{-16}$ and $12\cdot10^{-16}$ (1σ conf.). The mean ^{10}Be/^{9}Be ratio of our measurements is $(1.0 \pm 0.4)\cdot10^{-15}$ (Fig. 2) clearly showing that no background on the 10^{-15} level is observed with the TANDY system.

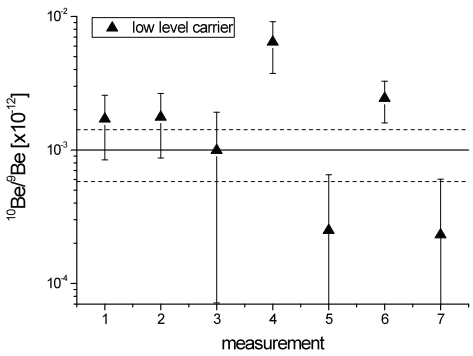

Fig. 2: *Low level Be-carrier measurements*

At ion energies of about 0.7 MeV complete separation of ^{10}Be and ^{10}B is achieved in the detection system (Fig. 3). The ^{10}B counting rate in the detector can be adjusted by changing the slit width at the exit of the electrostatic analyzer. This allows to adapt the measurement setup to the boron content of the samples.

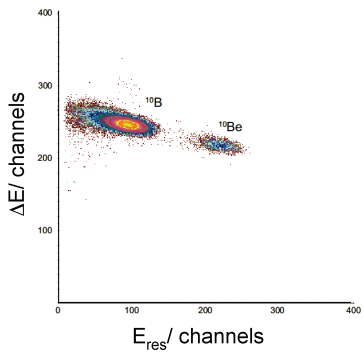

Fig. 3: *2d energy spectrum of a S2007 standard measurement*

[1] A. M. Müller et al., Nucl. Instr. & Meth. B 266 (2008) 2207

^{129}I MEASUREMENTS AT 0.5 MV

Benefits and pitfalls of going 3+

V. Alfimov, H.-A. Synal

To improve the conditions of our routine ^{129}I measurements at the 0.5 MV Pelletron accelerator TANDY we changed from measuring in charge state 4+ to 3+ at the high-energy side [1]. This resulted in a 3-4 times better machine background (^{129}I/I ≈ 9·10^{-14}, Fig. 1) and a 2 times better transmission (8%). Although a better performance was achieved, parasitic beams can cause severe problems and can interfere with the detection of ^{129}I. The observed interferences depend strongly on the stripper gas pressure.

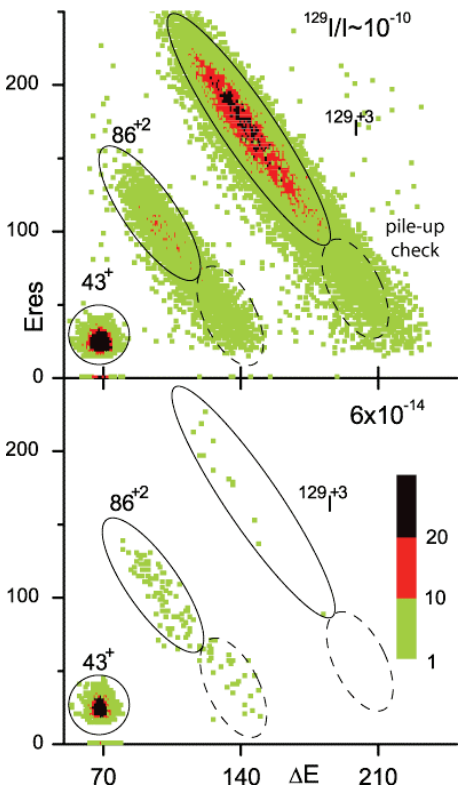

Fig. 1: *ΔE-E$_{res}$ spectra of a ^{129}I/I≈10^{-10} user sample and of a machine blank for a stripper pressure of 0.22 μg/cm^2. The right dashed ellipse in the tail of the ^{129}I peak is the likely receptor of 3x pile-ups from 43^{+1} molecules (see also Fig. 2).*

At low gas pressure, too many (mass 43)$^{+1}$ molecules enter the detector and cause pile-ups in the 2$^+$ or even 3$^+$ ΔE-E$_{res}$ windows (Fig. 2). Higher stripper pressure destroys the 43^{+1} molecules reducing the 2x pile-ups. Lowering the stripper density brings the molecules back. Note, that the up–down pressure scans were made quickly without giving the stripper pressure distribution time to homogenize itself.

We think that the 43^{+1} molecule is ^{27}Al^{16}O$^+$ and that its precursor at the terminal is (Al$_2$O$_3$+Al)$^-$. Other expected isobaric interferences such as ^{43}Ca^{+1} and ^{86}Sr^{+2} turned out to be negligible. We can control the 43^{+1} interference by comparing the tail-to-peak ratio of ^{129}I^{3+} (Fig. 1).

The new measurement conditions are sufficient for the measurement of nearly all ^{129}I samples submitted to ETH Zürich over the last few years.

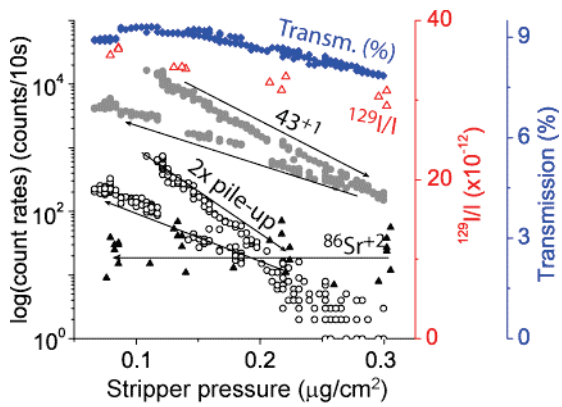

Fig. 2: *Dependence of 43^{+1}, ^{86}Sr^{+2}, 2x pile-ups (in +2), and ^{129}I^{+3} counting rates (left axis, log scale) on gas stripper pressure. Transmission and ^{129}I/I are plotted with the right axes (normal scale).*

[1] V. Alfimov et al., Nucl. Instr. & Meth. B 268 (2010) 769

^{236}U AT TANDY

Demonstration of excellent background suppression at high masses

C. Vockenhuber, M. Christl, J. Lachner

AMS measurements of ^{236}U at natural levels are particularly challenging because of the required high suppression of neighboring masses. Whereas measurements of other actinides (e.g. Pu isotopes, ^{231}Pa), which do not have abundant isotopes, have been successfully with the original setup of the TANDY AMS system, ^{236}U measurements were hampered by background from ^{235}U.

With the newly installed 130° magnet (HE magnet 2), this type of interference should be considerably reduced. We performed first measurements with uranium from the Joachimsthal mine in the Czech Republic as well as with material enriched in ^{236}U. UO$^-$ ions were selected with the low-energy magnet (LE magnet), accelerated as 3+ ions to about 1.2 MeV and detected in an ionization chamber with a 30 nm silicon nitride entrance window.

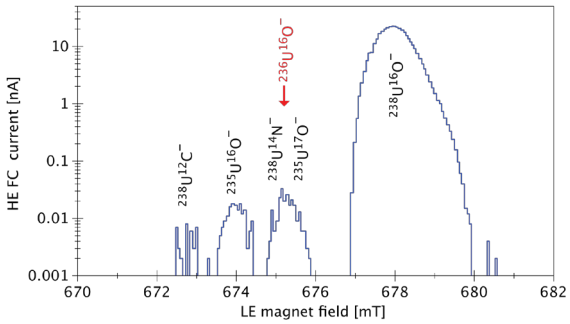

Fig. 1: *LE magnet scan of a U_3O_8 sample.*

Figures 1 to 3 demonstrate the important steps of background suppression with the main elements. The LE magnet scan (Fig. 1) shows a mass spectrum of the Joachimsthal sample. At the field for ^{236}U^{16}O$^-$ (mass 252) a substantial amount of ^{238}U is injected as ^{238}U^{14}N$^-$ as well as ^{235}U from ^{235}U^{17}O$^-$.

The scans of the high-energy side were made with uranium enriched in ^{236}U. While most of the ^{238}U is well separated by the first high-energy magnet and the electrostatic analyzer (ESA), ^{235}U is still at the level of ^{236}U/^{238}U≈10^{-9} (Fig. 2). This ^{235}U is finally well separated from ^{236}U at the HE magnet 2 (Fig. 3). First measurements of the Joachimsthal material fully agreed with the reference value of ^{236}U/^{238}U=7.0·10^{-11} (sample Vienna-KkU) from the VERA AMS facility in Vienna.

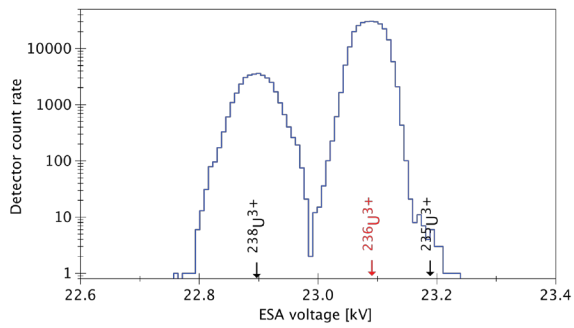

Fig. 2: *ESA scan: the positions of the U isotopes with the same p/q as ^{236}U are indicated.*

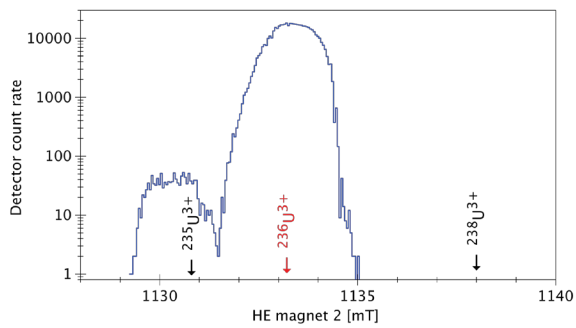

Fig. 3: *HE magnet 2 scan: positions of the U isotopes with the same E/q as ^{236}U are indicated.*

An overall efficiency of up to 10^{-4} was determined with a sample spiked with a known amount of a ^{233}U. This includes a measured transmission of around 9% in charge state 3+.

With this high overall efficiency and the excellent background suppression we are now ready to embark on ^{236}U measurements at natural levels.

THE MICADAS AMS FACILITY

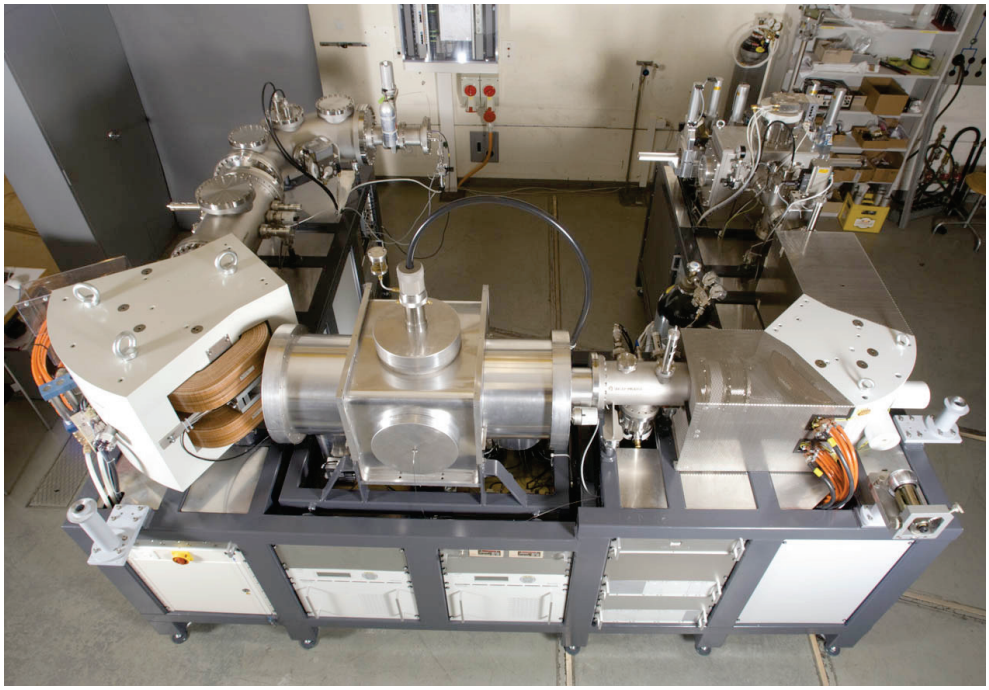

The first years of MICADAS

DatingMICADAS

Ion source upgrade for MICADAS

Improving a gas ion source

^{14}C AMS measurements of small samples

Online ^{14}C analyses of carbonaceous aerosols

THE FIRST YEARS OF MICADAS

Routine and ultra-high precision radiocarbon dating

L. Wacker, G. Bonani, I. Hajdas, T. Schulze-König, H.-A. Synal, C. Vockenhuber

The prototype MICADAS (Mini-Carbon-Dating-System) AMS facility at ETH Zurich has now been routinely operating for almost two years. More than 4000 solid samples and 1000 gaseous samples have been measured so far.

The system is usually set up on Monday and is then left running unattended and without or only minor retuning for the rest of the week or even longer (Fig. 1).

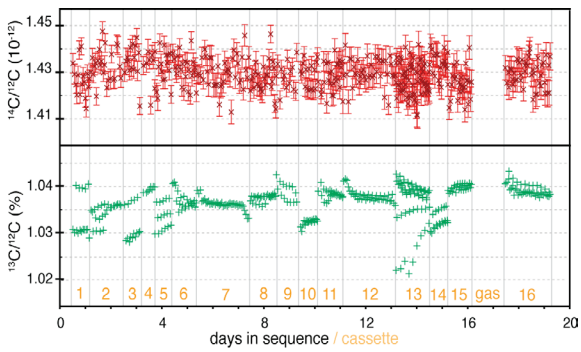

Fig. 1: *Fractionation corrected $^{14}C/^{12}C$ (top, red) and $^{13}C/^{12}C$ (bottom, green) ratios of single measurements of the OXII standard during a measurement campaign of 19 days without retuning.*

Measurements were carried out with $^{12}C^-$ currents of around 30 µA and a mean transmission ($^{12}C^-/^{12}C^+$) of (43.1±0.4) % (based on all OXII standards measured during the first half of 2009). Higher currents of up to 50 µA are possible with the new ion source (see "Ion source upgrade for MICADAS" in this annual report volume).

In the gas ionization detector we observe a background of molecular break-up components ($^{12}C^+$ and $^{13}C^+$) corresponding to typically 0.005 Fraction Modern Carbon ($F^{14}C$), which is about twice that of a typical processing blank. This background scales with the measured $^{13}C^+$ current from the break-up of $^{13}CH^-$ molecules (Fig. 2). Applying a correction we obtain blank values of 0.002–0.003 $F^{14}C$ with a standard deviation of 0.0005 $F^{14}C$.

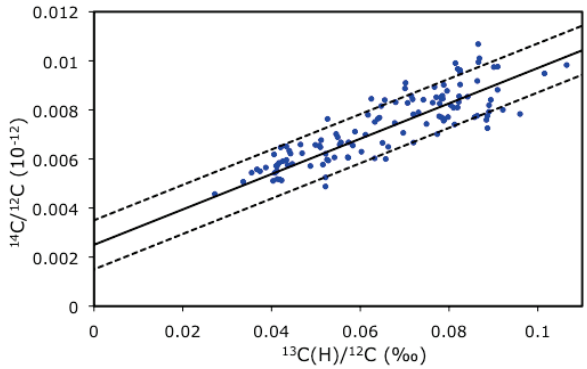

Fig. 2: *Correlation between $^{14}C/^{12}C$ ratios and normalized currents from molecular break-up ($^{13}C_H/^{12}C$) for processed blank samples.*

The excellent stability of the instrument is responsible for the good performance in ultra-high precision measurements where results for a sample can be reproduced to within less than 2 ‰. In this case, the blank variability is 0.0003 $F^{14}C$.

The performance of routine analyses is checked with IAEA reference samples. Good agreement with those reference values is achieved. The standard deviation of these measurements is only slightly higher than the combined uncertainty from counting statistics and blank correction for a single measurement. We have an additional unknown uncertainty of 3 ‰ in sample reproducibility (external uncertainty). This value is added to all our routine measurement results.

The stability of the measurements over time allows us to make even ultra-high precision measurements that until recently were a niche for gas counters and advanced liquid scintillation facilities.

DatingMICADAS

The next generation AMS system for ultra-high precision dating

H.-A. Synal, L. Wacker, T. Schulze-König, B. Kromer[1]

Following up on the developments of compact and user friendly AMS instrumentation for biomedical applications and the latest improvements on the performance of our MICADAS radiocarbon dating system we began a collaboration with the "Curt-Engelhorn-Zentrum für Archäometrie gGmbH" to develop a dedicated system for ultra-high precision radiocarbon dating.

The new instrument, DatingMICADAS (Fig. 1) was completed in February 2009. Due to delays during the construction of the building in Mannheim, Germany, where the new facility will be located, we have agreed to host the instrument at our laboratory for one more year. After a short commissioning phase, the final acceptance criteria have been met and the system was fully integrated into the research and measurement program of our laboratory where it is routinely used by its future users for routine dating measurements.

Fig. 1: *Picture of the new DatingMICADAS system, at present probably the most precise instrument for radiocarbon dating.*

As an example of the superb performance capabilities of the new system, the measurement results for standard reference materials obtained during an ultra-high precision radiocarbon dating run in October 2009 are shown in Fig. 2 and Tab. 1. In more than 50 hours of data taking, counting statistics of approx. 1‰ (10^6 ^{14}C counts) for individual standards was reached.

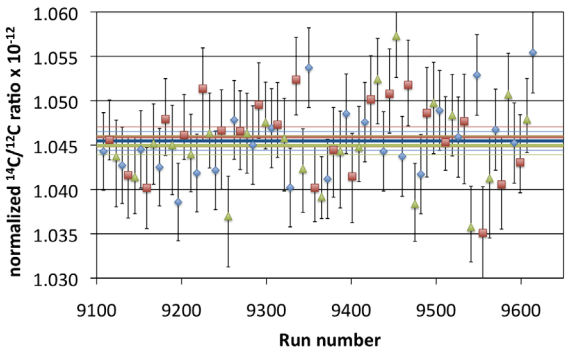

Fig. 2: *Measurements for 3 standard reference materials. Each data point represents 300 seconds of measurement time.*

standard	normalized $^{14}C/^{12}C$ (10^{-12})	σ-stat (‰)	σ-stdev (‰)
OxaII-1	1.04547	0.91	0.86
OxaII-2	1.04594	1.00	0.93
OxaII-3	1.04497	0.94	1.00
mean of runs	1.04543	0.55	0.54
mean of means	1.04544	0.55	0.27

Tab. 1: *Summary table of mean values derived from the 58 measurements shown in Fig. 2.*

The dataset demonstrates the impressive potential of the new instrument. It is certainly capable to perform measurements of isotopic ratios below the 1‰ level. Thus, it is closer to a conventional mass spectrometer than to a traditional AMS system.

---

[1] *Heidelberg Academy of Sciences, Germany*

ION SOURCE UPGRADE FOR MICADAS

Routine ^{14}C analyses with the new ETH universal sputter ion source

H.-A. Synal, T. Schulze-König, C. Vockenhuber, L. Wacker

The improvements made on the sputter ion sources of the BioMICADAS and DatingMICADAS systems were significant enough to decide on a replacement for the existing ion source at our MICADAS accelerator mass spectrometer. The new model of the ETH type universal sputter ion source (Fig. 1) was installed in July/August 2009. The improved sample changer (Fig. 2) is equipped with a dual vacuum lock system, which allows the loading of one sample magazine while a second magazine is being analyzed. This permits a flexible and continuous ion source operation. Neither breaking of the source vacuum nor a shutdown of any of the high voltage potentials is required. Each of the 23 samples in the magazine can be accessed in any order and loaded into the sputtering position of the ion source.

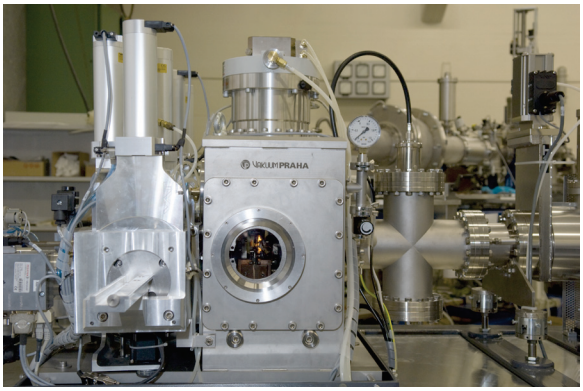

Fig. 1: *The new type ion source of the MICADAS AMS series.*

During the design of the source we carefully considered user safety issues and avoided any open high-voltage (HV) potentials. All HV potentials in the ion source are fed through the vacuum housing from a well shielded voltage deck integrated into the support stand of the ion source. The vacuum box itself is kept on ground potential.

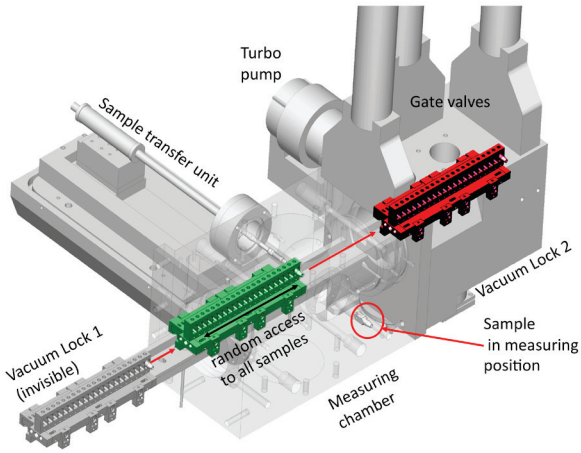

Fig. 2: *The sample changer of the new ETH universal ion source.*

In addition, the ion optics for the Cs focusing has been redesigned. Following the original idea of Middleton [1] and the experience made by the Livermore group [2], we replaced the Cs focusing lens system by a simple immersion lens geometry.

The ion source operates routinely at 10 to 15 kV Cs potential. The negative ions are extracted with an energy of up to 45 keV. The best measurement performance is reached with ^{12}C currents of up to 50 µA, although more than 100 µA can be obtained at higher Cs temperatures.

The source is also equipped with a gas inlet system allowing the extraction of more than 10 µA $^{12}C^-$ from a mixture of CO_2 and He gas that is flushed over a titanium catalyst.

[1] R. Middleton, Nucl. Instr. & Meth. B 214 (1983) 139

[2] T.A. Brown, M.L. Roberts and J.R. Southon, Nucl. Instr. & Meth. B 172 (2000) 344

IMPROVING A GAS ION SOURCE

Towards high-precision radiocarbon dating of gaseous samples

S. Fahrni[1], S. Szidat[1], L. Wacker, H.-A. Synal

The gas ion source of the MICADAS AMS facility has now been in use for three years and about 1000 small samples (1-35 µg C) have been measured so far [1, 2]. For small samples it is advantageous to measure them as CO_2 samples because graphitization is difficult and prone to contamination.

However, the MICADAS gas ion source had a major drawback. Gaseous samples produced only about 2.5 µA of $^{12}C^-$ in contrast to graphitized samples (40-60 µA). This has limited the measurement precision (counting statistics) - obtained in a reasonable measurement time - to a moderate value of about 1 %. However, for many dating applications higher precision is needed. It could be achieved with higher negative ion currents, preferably due to an increase in ionization efficiency.

After the installation of the new MICADAS ion source (see report "Ion source upgrade for MICADAS"), we tested a number of gas target geometries and varied the cesium reservoir and ionizer temperatures, cathode cooling, CO_2 concentration and the gas inlet pressure.

The following changes were the most effective in these early tests:

1. Defocusing the cesium beam by increasing the distance between the ionizer and sample to sputter a larger area of the cathode,
2. Increasing the Cs reservoir temperature (from 154 to 175 °C) for a more intense Cs beam,
3. Changing the sample gas inlet pressure (from 1200 to 1500 mbar) to increase the mass flow rate from 0.7 to 1.1 µg C/min.

Higher mass flow rates are also useful because for some reason the current reaches steady conditions faster at the beginning of a measurement. However, increasing the gas flow too much can lead to a loss in efficiency (Fig. 1). This problem can be somewhat reduced by increasing the primary Cs beam intensity.

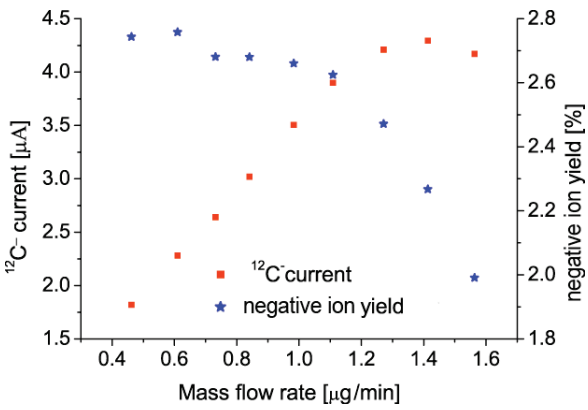

Fig. 1: *$^{12}C^-$ currents and usable negative ion yield as a function of carbon mass flow rate (standard conditions: 4.5% CO_2 in helium; 154 °C Cs temperature).*

Optimizing a combination of parameter changes led to negative ^{12}C currents of on average 9 µA with an increase in the integrated yield from 1.7% to 4% for real samples. A standard gas sample even produced a maximum of 16 µA $^{12}C^-$ corresponding to a usable yield of 7%. The measurements were generally very stable and no significant fractionation was observed. A Cs reservoir temperature of more than 175°C would likely lead to a further increase in yield and ion current.

Precise radiocarbon dating in the range of 5‰ seems now possible for samples with <50 µg carbon opening a range of new applications.

[1] H.-A. Synal et al., Nucl. Instr. & Meth. B 223-224 (2004) 339
[2] M. Ruff et al., Radiocarbon 49 (2007) 307

[1] *Chemistry and Biochemistry, University of Bern*

^{14}C AMS MEASUREMENTS OF SMALL SAMPLES

Graphite target material versus CO_2 gas measurements

J. Liebl[1], P. Steier[1], L. Wacker, S. Fahrni[2]

At ETH Zürich, an AMS method was developed to measure ^{14}C samples in the µg carbon range with a gas ion source [1], while at the Vienna Environmental Research Accelerator (VERA) laboratory, the focus of the development was on the graphitization and the measurement of small graphitized samples [2]. Comparative measurements of small samples were made at both laboratories. Possible variations in the results coming from sample isolation and combustion are ignored in this comparison.

A large amount of CO_2 (from an organic material) was split into one aliquot of about 100 µg C and two smaller aliquots of about 10 µg C each. The larger aliquot was graphitized and measured at VERA. The two smaller aliquots were welded in DURAN® glass vials and randomly assigned to be measured at ETH (as CO_2) or at VERA (as a graphitized sample).

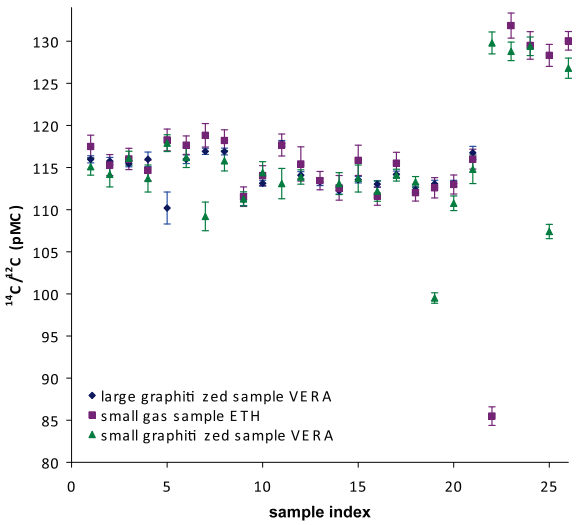

Fig. 1: *AMS results for all measured samples.*

Figure 1 shows the AMS results of all measurements. The ^{14}C content of samples 1-21 was unknown. Samples 22–26 were IAEA C-3 standards.

The measurement of three graphitized 'dead carbon' materials at VERA resulted in a $^{14}C/^{12}C$ background of 0.02±0.01 pMC for 100 µg C and 0.23±0.05 pMC for 10 µg C samples. Gas ion source measurements of 10 µg C samples yielded a $^{14}C/^{12}C$ background of typically 1 pMC. Though 1 pMC for small samples is a very acceptable value, the results suggest that there is room for improvement with the gas ion source technique.

The measured $^{14}C/^{12}C$ ratios of sample and standard materials at both laboratories agree very well, except for five outliers (see Fig. 1), which were excluded from further analysis. Samples of the size of 10 µg C were typically measured with a precision of about 1 %. A reduced X^2 test shows that the stated measurement precisions are correct both at VERA and at ETH.

(1) X_r^2 = 0.63 (VERA large graphite to ETH gas)

(2) X_r^2 = 1.29 (VERA large to small graphite)

(3) X_r^2 = 1.08 (VERA small graphite to ETH gas)

The results of this intercomparison are very encouraging for the development of small samples with either method.

[1] M. Ruff et al., Nucl. Instr. & Meth. B 268 (2010) 790

[2] J. Liebl et al., Radiocarbon (2010) accepted

[1] *VERA, Faculty of Physics, University of Vienna, Austria*

[2] *Chemistry and Biochemistry, University of Bern*

ONLINE ^{14}C ANALYSES OF CARBONACEOUS AEROSOLS

Coupling a commercial OC/EC analyzer to the MICADAS gas ion source

N. Perron[1], A.S.H. Prévôt[1], U. Baltensperger[1], S. Szidat[2], S. Fahrni[2], M. Ruff[2], L. Wacker

By convention, atmospheric carbonaceous aerosols are divided into organic and elemental carbon, respectively OC and EC. Their carbon amounts can be analyzed with an OC/EC analyzer whereas their fossil and non-fossil origins are determined with ^{14}C AMS [1]. To merge these two operations we developed an on-line system connecting a commercial OC/EC analyzer (RT 3080 thermo-optical OC/EC analyzer from Sunset Laboratories Inc.) to the gas ion source of the MICADAS AMS system using its CO_2 feeding system [2], which consisted of (Fig. 1):

- a zeolite sieve to trap the CO_2 emitted by the analyzer,
- a gas-tight syringe to mix the CO_2 with helium and inject it into the gas ion source,
- a 6-port valve for switching between those two elements.

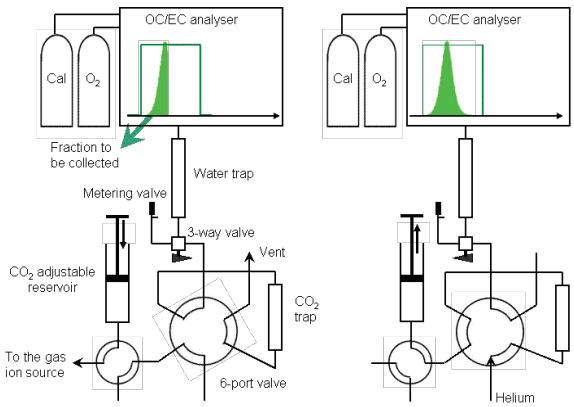

Fig. 1: *Coupling system between the OC/EC thermo-optical analyzer and the gas interface during CO_2 trapping (left) and during injection into the gas ion source (right).*

In addition, we installed upstream of the interface:

- a $Mg(ClO_4)_2$ water trap and
- a 3-way valve to direct the instrument exhaust either to the interface or to the outside.

Either the first fraction (OC) or the second fraction (EC) combusted under pure oxygen in the analyzer can be trapped with the gas interface for the subsequent radiocarbon analyses.

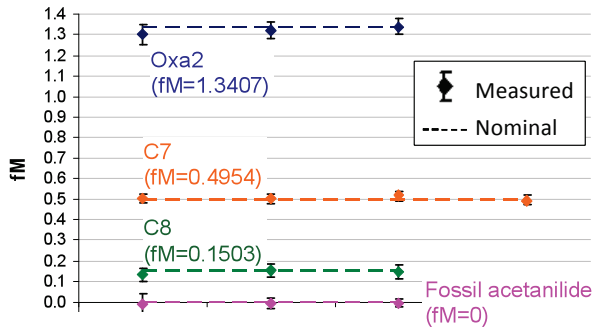

Fig. 2: *fM (fraction modern carbon) values of ^{14}C standards for the filter measurements. A filter blank correction of 2.0±0.4 µg C and fM=0.54 was applied.*

To validate the method, bunches of pre-baked quartz filters were spiked with IAEA standards (10-20 µgC) (Fig. 2). The use of those filters led to the adsorption of volatile organic compounds during sample preparation. After correcting for this artifact, amounting to 2.0 µgC with a fM=0.54, the ^{14}C values agreed well with the nominal values.

[1] S. Szidat et al., Geophys. Res. Lett. 34 (2007) L05820
[2] M. Ruff et al., Radiocarbon 49 (2007) 307

[1] *Paul Scherrer Institute, Villigen*
[2] *Chemistry and Biochemistry, University of Bern*

DETECTION AND ANALYSIS

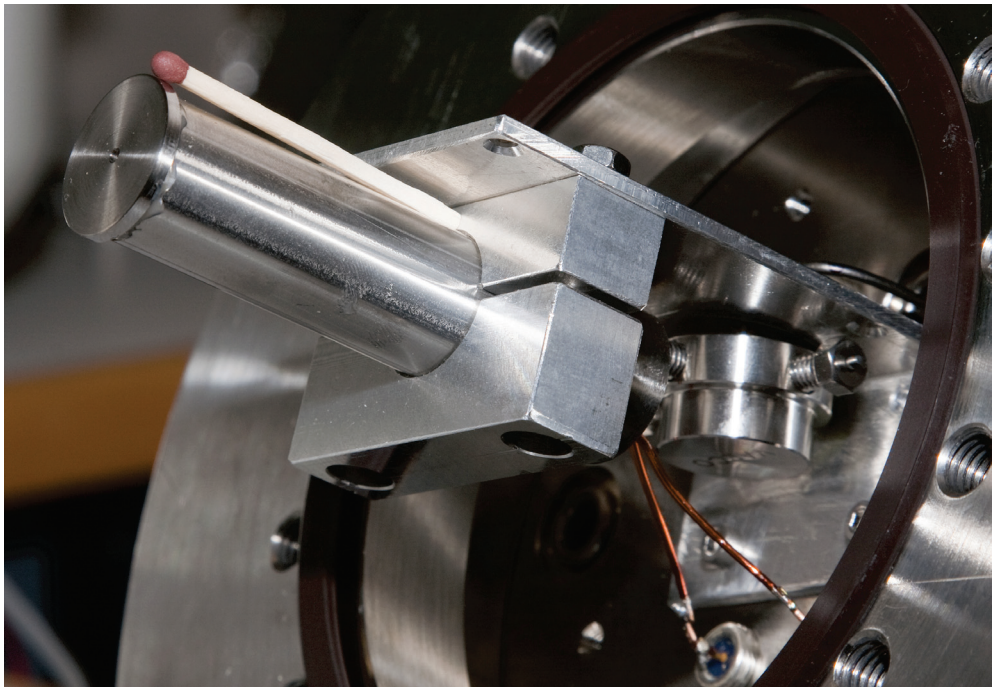

Compact gas ionization chambers

A new HIBS detector for RBI Zagreb

Energy-loss straggling measurements

Measurements at high counting rates

BATS: A new tool for AMS data reduction

COMPACT GAS IONIZATION CHAMBERS

Development of new small gas detectors for IBA and AMS

A.M. Müller, M. Döbeli, R. Gruber, M. Mallepell, M. Suter, H.-A. Synal, W. Wiederkehr

Gas ionization chambers are well established devices for particle identification in AMS and ion beam analysis (IBA). Recent developments have significantly improved the energy resolution [1]. The design however was optimized for applications with counting rates below 10 kHz. We decided to develop a gas ionization detector also for higher counting rates.

For this purpose, two prototypes were built this year and tested on the 0.6 MV TANDY AMS system. The detector anodes are mounted on an insulator inset inside a stainless steel tube of 20 mm diameter and 60 mm length (Fig. 1 & 2). One prototype did not use a Frisch grid.

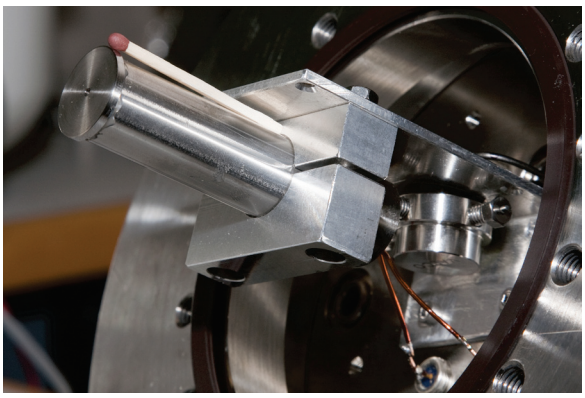

Fig. 1: *The new small gas ionization chamber prototype mounted on a flange, which can be adjusted in x- and y- direction.*

Since very small SiN membranes (1x1 mm^2) were used as entrance windows, the detector could be operated under gas pressure (C_4H_{10}) of more than 1 bar. For 600 keV protons an energy resolution of about 25 keV was achieved (Fig. 3). The resolving power of this detector was stable at counting rates of up to 30 kHz.

New prototypes are already planned and will be built and tested during the next year.

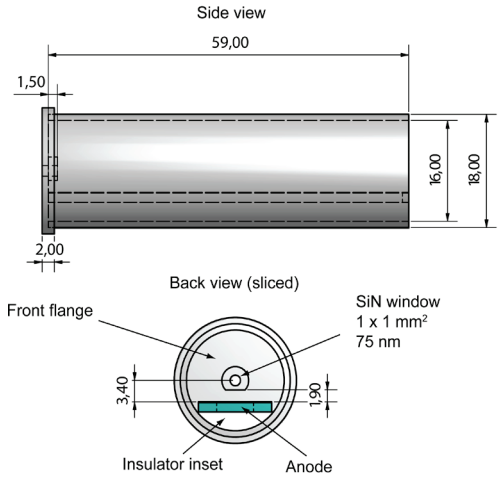

Fig. 2: *Perspective view of the small gas ionization chamber. Dimensions are in mm.*

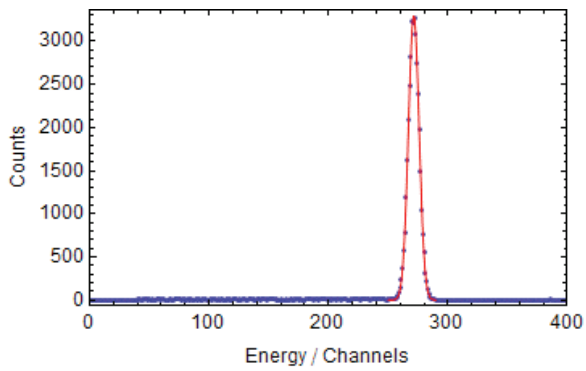

Fig. 3: *Energy spectrum of 600 keV protons taken by the small gas ionization chamber without a Frisch grid. FWHM is about 25 keV.*

[1] M. Suter et al., Nucl. Instr. & Meth. B 259 (1) (2007) 165

A NEW HIBS DETECTOR FOR RBI ZAGREB

Knowledge exchange between ETHZ, RBI Zagreb and KUL Leuven

A.M. Müller, M. Döbeli, R. Gruber, M. Mallepell, H.-A. Synal, W. Wiederkehr

The Laboratory of Ion Beam Physics (LIP) is member of the SPIRIT (Support of Public and Industrial Research using Ion Beam Technology) consortium [1]. This framework supports among other projects networking activities concerning the development of detection systems for ion beam analysis (IBA).

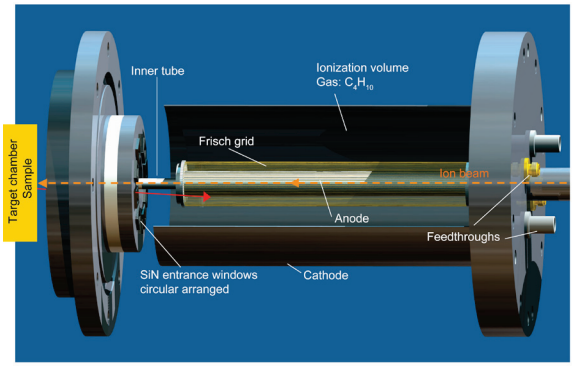

Fig. 1: *Perspective view of the annular gas ionization detector*

In this context LIP built a heavy ion back-scattering (HIBS) detector (Fig. 1) for the Ruder Boskovic Institute (RIB) in Zagreb. This annular gas ionization improves the mass resolution for heavier masses compared with "classical" RBS measurements with He ions [2]. Tests with a prototype at the ETH 6 MV TANDEM accelerator have shown a resolution of 13-16 keV for 1 MeV He particles. The energy resolution of this detector is therefore comparable to that of silicon detectors even for light ions.

The new detector for RBI is adapted to the mechanical dimensions of the local analysis beam line. It was assembled and tested during a 2 week visit of Zdravko Siketic (RBI) and Qiang Zhao (KUL) to Zurich, in November 2009. The visit was organized like a small workshop on gas ionization chambers with as much know-how transfer as possible. For training purposes, the visitors were involved in the detector assembling (wrapping the Frisch grid, etc.) to obtain a realistic view of how to build a gas ionization chamber of the newest generation.

The performance of the HIBS detector was tested under realistic conditions at the 0.6 MV TANDY AMS system (Fig. 2). The device was shipped to Zagreb in December, where it will be commissioned this year.

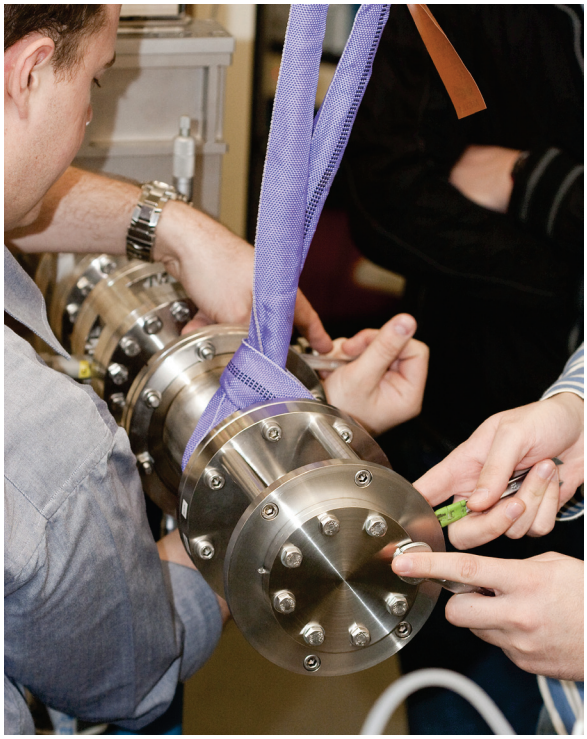

Fig. 2: *LIP members together with the visitors are mounting the new HIBS detector on the 0.6 MV TANDY spectrometer beamline for tests under a direct beam.*

[1] http://www.spirit-ion.eu/Start.html
[2] M. Mallepell et al., Nucl. Instr. & Meth. B 267 (7) (2009) 1193

ENERGY-LOSS STRAGGLING MEASUREMENTS

Determination of a critical parameter for the ^{36}Cl – ^{36}S isobar separation

C. Vockenhuber, V. Alfimov, M. Döbeli, M. Suter, H.-A. Synal, M. Martschini[1], P. Steier[1]

Energy-loss straggling is a crucial parameter for isobar separation based on the specific energy loss of ions e.g. in ionization chambers and with the passive absorption method. Several physical processes contribute to energy-loss straggling, with collisions and charge-changing effects being the most important ones. Thickness variations in the stopping medium due to foil inhomogeneities have an additional effect on the energy distribution and often mask the effects of the physical processes. Theoretical predictions for energy-loss straggling are difficult and still unreliable, thus semi-empirical formulae have been developed [1]. Following early measurements with various ions at the TANDY facility [2], we extended the measurements to the TANDEM accelerator to energies at and below the stopping power maximum.

Stable ^{35}Cl and ^{32}S beams were used to investigate the separation of ^{36}Cl and ^{36}S. Highly homogeneous silicon nitride (SiN) foils of various thicknesses were placed at the object point of the high-energy magnet. The energy distribution was measured by scanning the beam over a narrow slit in front of the ionization chamber at the image point. Energy-loss straggling was determined by quadratically subtracting the contribution of the initial beam energy spread and measurement resolution, measured without a foil in place. The stoichiometry of the foils was measured with RBS. The thickness was determined by the energy loss of the ions and using the stopping power from SRIM-2008 [3].

Figure 1 shows the results of the straggling measurements for Cl and S, plotted as a function of the velocity parameter ξ and relative to the velocity independent Bohr straggling (Ω_bohr). Also shown are predictions from SRIM-2008 and from the empirical Yang formula [1]. The blue points were measured at TANDY and are already published in [2]; green points are measured at the Tandem; yellow and orange points are from a similar measurement at VERA, which connects the two other data sets and also allows checking for systematic errors.

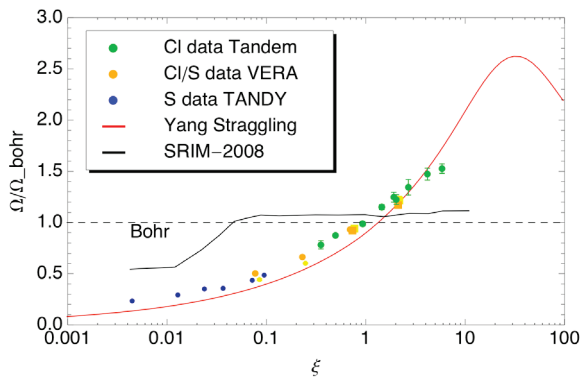

Fig. 1: *Straggling data for Cl and S in SiN*

While the SRIM-2008 straggling curve obviously fails to represent the measurements, the Yang formula reproduces the velocity dependence quite well. Clearly, more data at higher velocities are necessary to check the extent of the straggling peak of the Yang formula.

Due to the large energy range available at the ETH accelerators and systematic checks at VERA (0.4 to 50 MeV) we were able to produce a reliable dataset over a large velocity range which should help us to improve the detection method for ^{36}Cl and ultimately also to refine theoretical models of energy-loss straggling.

[1] Q. Yang et al., Nucl. Instr. & Meth. B 61 (1991) 149
[2] G. Sun et al., Nucl. Instr. & Meth. B 256 (2007) 586
[3] www.srim.org

[1] *VERA, Faculty of Physics, University of Vienna, Austria*

MEASUREMENTS AT HIGH COUNTING RATES

Pile-up correction to extend the range of radiocarbon AMS

T. Schulze-König, J. Giacomo[1], J. Vogel[1], H.-A. Synal

Biomedical tracer studies utilizing AMS typically generate radiocarbon concentrations in a range of 0.1 fMC to 1'000 fMC. Hence, a detection system is desirable with a negligible dark-counting rate and capabilities to accept event rates of 100 kHz and more. The MICADAS AMS systems [1] use a gas ionization chamber in connection with a level discriminator for event detection. To extend the range of this detection system from ≈ 15 kHz up to 150 kHz, a detailed analysis of event loss was made. Event loss occurs, when an ion enters the detector while the detection system is still converting a previous event. This period is called dead time. Detection systems can be classified based on their dead time behavior (Fig. 1). Once classified, event losses can be calculated and thus corrected for. Detection systems can typically be described as an arrangement of those classifiable systems.

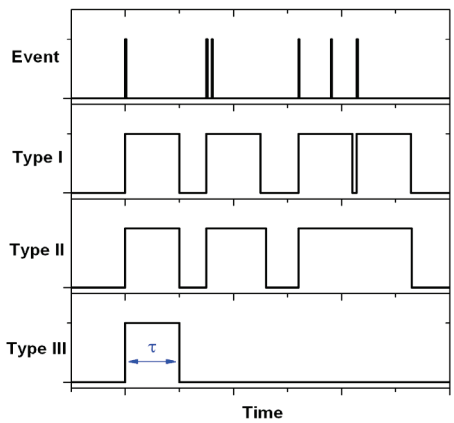

Fig. 1: *Classification of detection systems. Type I: non-extendable dead time; type II: extendable dead time; type III: pile-up rejection.*

The MICADAS detection system can be described by a serial arrangement of a type I and a type II detector. For such a circuit, an analytical equation to quantify counting losses exists [2].

The suppression of molecular isobars in the terminal stripping process is independent of ion intensity and depends only on the molecule dissociation cross-section and the density of the stripper medium. Anticipating constant isobar suppression, it is possible to observe the actual counting losses by measuring the rate of surviving molecules at different ion source currents and thus at different true event rates. Hence, the effectiveness of the correction procedure can be analyzed without requiring ^{14}C enriched standard samples.

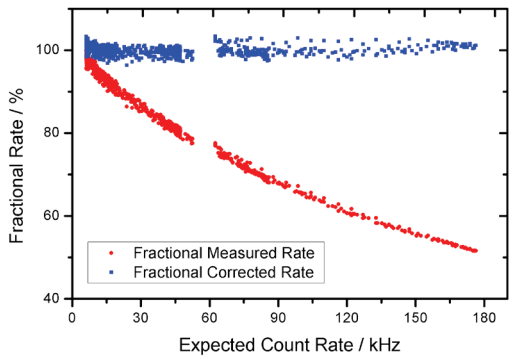

Fig. 2: *Measured and corrected event rates of ^{14}C isobars relative to expected count rates assuming a constant isobar suppression factor.*

The range of acceptable counting rates could be improved by a factor of 10 (Fig 2). The system is now tested for rates of up to 180 kHz corresponding to $^{14}C/C \approx 1'500$ fMC. It is therefore usable for the full range applied in biomedical tracer studies.

[1] H.-A. Synal, M. Stocker and M. Suter, Nucl. Instr. & Meth. B 259 (2007) 7
[2] S. Pommé, Appl. Radiat. Isot. 66 (2008) 941

[1] *Vitaleascience, Davis, USA*

BATS: A NEW TOOL FOR AMS DATA REDUCTION

Development of a data evaluation program for radiocarbon

L. Wacker, M. Christl, H.-A. Synal

The AMS data reduction software used at ETH Zurich was developed 20 years ago. Although the software was powerful for its time, it lacks some nice-to-have features, is rather cumbersome and time-consuming in operation. Additionally, our compact AMS systems MICADAS and TANDY need modified data reduction procedures for the high-precision measurements. This led to the development of a new, platform-independent data reduction software named BATS [1].

BATS calculates the final results for a set of samples with uncertainties based on multiple measurements of the set. Typically, a set consists of one sample cassette or one sample wheel stacked with "unknown" samples, standards and blanks. BATS has also the option to combine several independently measured sample sets, if measurement conditions had been stable enough to evaluate such a large sample set.

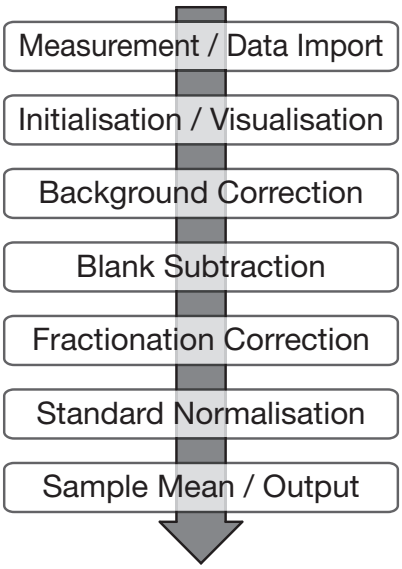

Fig. 1: *Order of the steps performed in data reduction for radiocarbon samples measured on MICADAS.*

Besides the straightforward normalization and background reduction procedure, a number of corrections can by applied to the raw data (Fig. 1). These corrections are applied to the result of each single measurement of an individual sample before sample means are calculated. The idea behind this approach is to separate systematic effects from the uncertainty based on counting statistics (internal error). Such systematic effects, if present, can introduce a significantly higher standard deviation for repeated measurements of a single sample than would be expected from counting statistics alone. Under favorable conditions, the applied corrections reduce the standard deviations towards the internal uncertainty. BATS shows this reduction of the standard deviation based on X^2 tests.

Over the last year the BATS program has proven to be an easy-to-use data reduction program. Little user input is required for reliable end results. Data tables with X^2 tests and 2D-plots help to visualize and monitor the quality of the data. Because the program is designed to automatically calculate and update the results, the quality and status of the acquired data can be monitored quasi-online. This helps to decide, when the desired precision including the error propagation of the data reduction is reached.

Next, the program will be intensively tested for use with the other measured AMS nuclides besides radiocarbon.

[1] L. Wacker, M. Christl and H.-A. Synal, Nucl. Instr. & Meth. B 268 (2010) 976

^{14}C SAMPLE PREPARATION

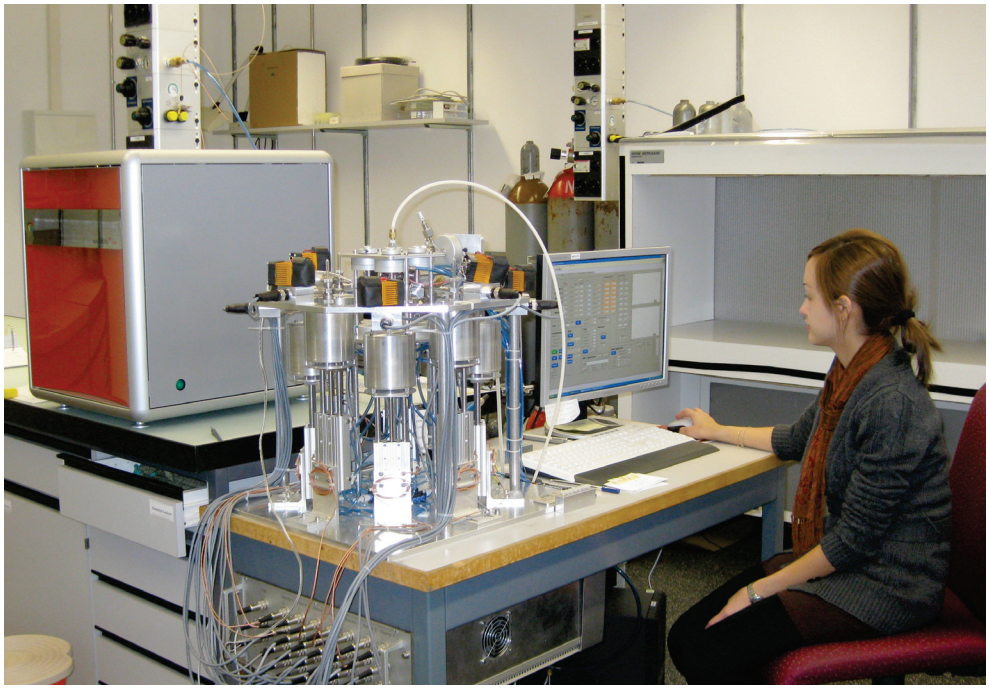

Extension of the ^{14}C laboratory

What's cooking in the ^{14}C lab?

AGE: A new graphitization system

Graphitization in 'closed tubes'

Compound-specific radiocarbon analysis

Alternative cellulose isolation from wood

Simplified radiocarbon dating of small samples

In situ cosmogenic ^{14}C

EXTENSION OF THE ^{14}C LABORATORY

More space for the preparation of smaller samples

I. Hajdas, G. Bonani, S. Iglesias, M. Maurer, H. A. Synal, L. Wacker

Our ^{14}C preparation laboratory 'expanded' this summer to the room next door and gained so additional space for its activities. A connection between both rooms was made and some of preparation steps were moved to the new room. The new graphitization system based on an elemental analyzer (EA) for sample combustion (see AGE report) is now placed in this new laboratory (Fig. 1).

In the new room clean samples, standards and blanks, which are ready for graphitization with AGE, are weighed on a micro-balance and loaded into the EA, which is connected to the fully automated AGE graphitization system. The graphite samples taken out of AGE are then pressed into cathodes and organized into cassettes ready for the AMS measurement.

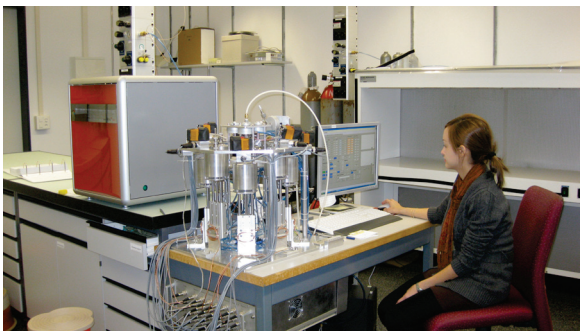

Fig. 1: *View of the new laboratory. Most of the organic samples are graphitized using the new AGE system.*

All cleaning steps remain in the original laboratory. Also, the graphitization line built in 1999 is still in this room and is now used exclusively to graphitize foraminifera and other carbonates (for example mortar) as well as CO_2 samples in tubes (for example extracted from groundwater or air).

Some samples contain very low amounts of carbon (often unknown). These samples are combusted in Vycor tubes and graphitized with the old system. The amount of carbon can only be estimated after the tubes are broken in the graphitization line. If the amount of C is less than 200 µg, the samples are re-frozen with LN_2, sealed into a Pyrex tube (ϕ = 4 mm) for use with the gas ion source [1].

Fig. 2: *View of the original laboratory. A new vacuum system is used to re-freeze CO_2 of microgram size samples that are later measured with the gas ion source.*

A new vacuum line dedicated to re-freezing very small samples for the gas ion source (Fig. 2) is extensively used by Ph.D. students working on the radiocarbon dating of biomarkers (see report CSRA). The very small amount of CO_2 obtained from combustion of specific compounds in Vycor tubes (ϕ = 9 mm) can be estimated by measuring the pressure in a calibrated volume of the vacuum line. The sample is then re-frozen into the small tube (ϕ = 4 mm) for use with the gas ion source.

[1] M. Ruff et al., Radiocarbon 49 (2007) 307

WHAT'S COOKING IN THE ^{14}C LAB?

Recent advances in preparation methods

I. Hajdas, G. Bonani, S. Iglesias, M. Maurer, C. Vockenhuber, L. Wacker

Development in the preparation of samples for radiocarbon dating has always focused on the reduction of contamination and the selection of the appropriate carbon fraction (suitable for dating or as an environmental tracer). Most of the samples submitted to our laboratory aim to date various archaeological or art objects or archives of past environmental changes. The reliability of the ages is related to the treatment methods and their ability to select the right fraction of carbon (for example cellulose from wood or gelatine from bone). Another issue is the contamination with 'young' or 'old' carbon, which might occur during the preparation process.

A set of measurements was performed on samples containing 0.1 to 1.5 mg of C prepared from coal (^{14}C free) to investigate contamination by young carbon (Fig. 1).

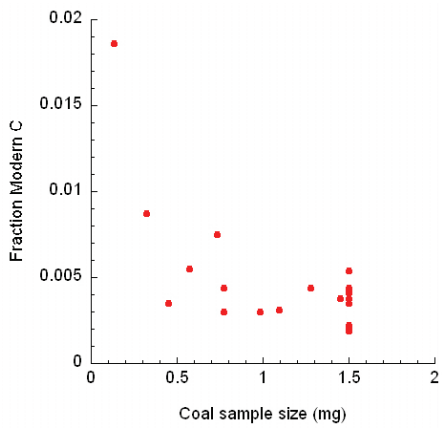

Fig. 1: *"Fraction of Modern Carbon" measured for coal samples of different size. The correction for contamination seems to remain size-independent for samples containing >1.0 mg of C. Smaller samples require an additional correction. Presently small blanks are always measured together with small samples.*

Bones are typical archaeological finds, which are not always well preserved. Our laboratory uses a procedure of separation and purification (Ultra Filtration) of gelatine. Recently, we tested the separation of C from the mineral fraction of bones. This method is typically applied to dating of cremated bones. First results show that for bones younger than 5000 years, ages are comparable to those obtained for gelatine. However, very old bones show contamination with young carbonates.

Mortar belongs to materials, which are difficult to date. Charcoal fragments will be prepared for dating, if they are present, but that is not often the case. We apply a method (Fig. 2) to select carbonate, which was formed when CaO (quicklime) hardened and re-absorbed CO_2 from the atmosphere [1]. First results from Roman objects show clear differences in ages of various fractions.

Fig. 2: *Mortar samples are disintegrated in water and sieved to separate the smallest fraction (<32µm), which is then dissolved in acid.*

These examples illustrate the importance of development and modifications of existing methods for specific dating projects.

[1] J. Heinemeier et al., Nucl. Instr. & Meth. B 123 (1997) 487

AGE: A NEW GRAPHITIZATION SYSTEM

Development and optimization of the equipment

L. Wacker, M. Němec[1]

Graphitization of carbon is the standard sample preparation method for ^{14}C AMS. The Automated Graphitization Equipment (AGE) was designed as a compact system for routine sample preparation. In contrast to other systems, AGE dispenses with the cryogenic transport of CO_2. Samples are combusted in a standard elemental analyzer (EA). The resulting CO_2 is absorbed in a zeolite trap. The CO_2 is released by heating the trap and expands to the individual reactors, where it is reduced by H_2 to graphite on the surface of an iron catalyst. The preparation procedure is described in Figure 1 and the detailed instrumental setup in [1].

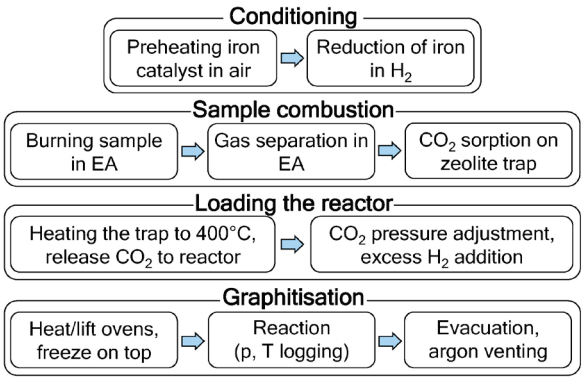

Fig. 1: *Final sample preparation procedure.*

Each of the seven 4.4 mL reactors consists of two vertically mounted vials. The upper part of a reactor is cooled during the reaction by a Peltier cooler to less than -10 °C. The bottom vial can be heated in an electric oven to up to 700 °C. During the reaction, pressure and temperature values are logged as function of time.

To find the optimal conditions, CO_2 was graphitized at temperatures between 545 and 620°C and H_2/CO_2 ratios of 1.9 to 2.5. The graphite samples were measured on the 200 kV MICADAS AMS system to determine which procedure would minimize isotopic fractionation ($\delta^{13}C$) and the formation of molecular $^{13}CH^-$ currents. The influence of various parameters on the reaction time was also investigated (Fig. 2).

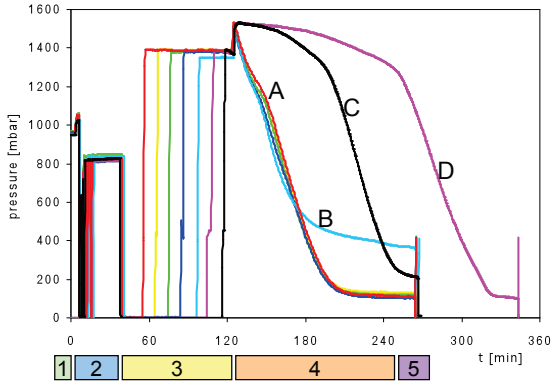

Fig. 2: *Pressure readings during graphitization: (A): optimized scenario (catalyst oxidation with air (1), cleaning of catalyst with H_2 (2), reactor filling (3), combustion with cooling below -10 °C (4), reactor venting (5)). (B): reactor top cooled to outside temperature. (C): no reactor cooling. (D): without iron oxidative preheating.*

Catalyst oxidation with air at the beginning of the conditioning steps reduces the reaction time significantly. The oxidation time was tuned with respect to the final reaction time and the pressure profile over time. In the end we selected 580°C and 2.3 H_2/CO_2 together with the 150 s for catalyst preheating and a reaction time of less than 2 hours. The procedure to graphitize 7 samples including combustion and pre-treatment of the iron takes now ≈4.5 hours.

[1] L. Wacker, M. Němec and J. Bourquin, Nucl. Instr. & Meth. B 268 (2010) 931

[1] *also Chemistry and Biochemistry, University of Bern*

GRAPHITIZATION IN 'CLOSED TUBES'

Testing a quick and inexpensive method for dating purposes

I. Hajdas, D.J. Michczyńska[1], G. Bonani, S. Iglesias, M. Maurer, C. Vockenhuber, L. Wacker

The growing demand for AMS analyses as well as the expansion of applications into new fields requires effective sample preparation. For many applications the need for high precision is less important than for high sample throughput. The standard procedure of graphitization used by AMS laboratories needs quite expensive equipment (pumps, pressure transducers, ovens). This limits the number of reactors, in which CO_2 and H_2 react to graphite, and can hamper a speedy target production. A method of quick and inexpensive graphitization was proposed for biomedical studies and recently modified for environmental samples [1].

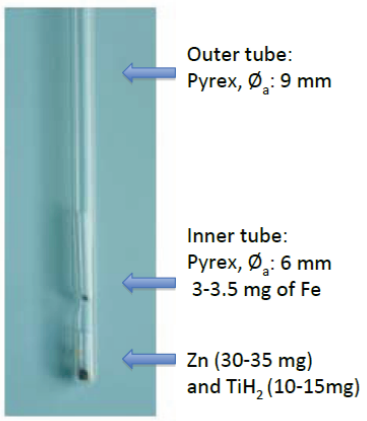

Fig. 1: *Pre-heated tubes are attached to a vacuum line, sample CO_2 is frozen in the inner tube and torch sealed. The shown amounts of reagents are for ca. 1 mg of C.*

In this method graphite is produced in 'closed tubes' (Fig. 1) and the only requirement is a vacuum line with the possibility to attach the tubes to transfer the sample CO_2 and torch seal it. The tubes can be prepared in advance and in batches. Batches of tubes can be placed in an oven (500 °C for 1 hr, then 550°C) for the CO_2 reduction reaction that is completed in ca. 7 hrs. Graphite is formed on the surface of the iron powder in the inner tube (Fig. 1). The biggest drawback of this method is the lack of control over the completeness of the reaction and thus the fractionation that occurs during the reaction.

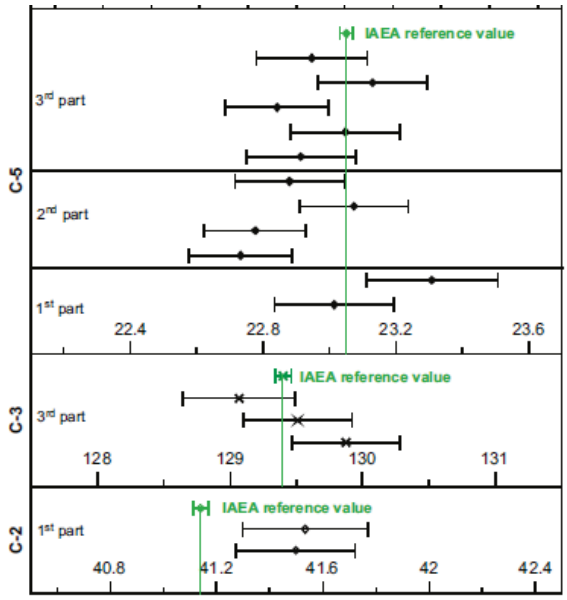

Fig. 2: *^{14}C content (± 1σ) measured in samples of IAEA C-2 (carbonate), C-3 (cellulose) and C-5 (wood) was corrected for fractionation ($\delta^{13}C$). The agreement with nominal values (green) is within 1σ for 9 samples out of 16 and within 2σ for the other 7 samples.*

Our results (Fig. 2) show that when a correction for fractionation is made, graphite produced in 'closed tubes' can be used for dating purposes. The observed fractionation can potentially be reduced with more precise reagent to carbon additions.

[1] X. Xu et al., Nucl. Instr. & Meth. B 259 (2007) 320

[1] *GADAM Centre of Excellence, Silesian University of Technology, Gliwice , Poland*

COMPOUND-SPECIFIC RADIOCARBON ANALYSIS

Analytical developments and application for lake sediments

A. Birkholz[1], R. H. Smittenberg[1], M. Gierga[1], S.M. Bernasconi[1] I. Hajdas, L. Wacker

Over the past decades, substantial progress has been made in understanding past climate and environments. Much of the information gained has been derived from lake and ocean sediments. However, there are still many gaps in our knowledge of global climate change, because practical issues hampered research in this direction. We are tackling two of these issues using compound-specific radiocarbon analysis.

First, we aim at improving our understanding of the build-up and the dynamics of the terrestrial soil organic carbon (SOC) pool throughout the last 20,000 years. SOC constitutes an important reservoir in the global carbon cycle and a better knowledge of its dynamics is of paramount importance for the prediction of its behavior in response to climate change. By comparing radiocarbon ages of soil-derived molecular compounds in lake sediments with the actual age of deposition of the sediment it is possible to estimate rates of organic carbon build-up in the catchment area of a lake.

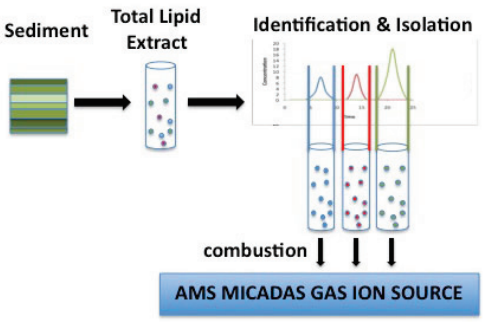

Fig. 1: *Schematic of the sediment processing and organic compound separation methods.*

Our second aim is to further develop the technique of compound-specific radiocarbon dating of sediments that do not contain recognizable macrofossil remains. For this purpose, we are further developing organic geochemical methods to isolate individual organic compounds from lake sediments in sufficient quantities for radiocarbon analysis. Purification and isolation methods include preparative high pressure liquid chromatography (HPLC) and gas chromatography (GC) depending on the type of target compounds (Fig. 1).

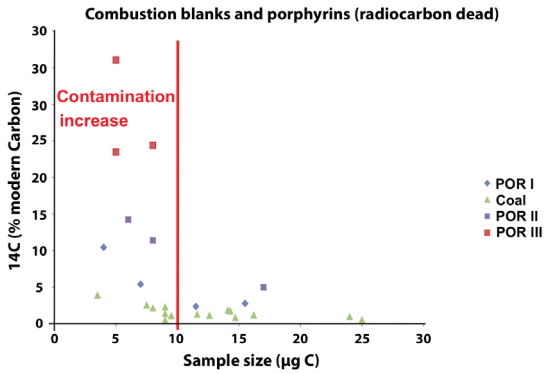

Fig. 2: *^{14}C content of procedural blanks and porphyrins vs. sample size.*

In a first step we extensively tested multiple substances to be used as system- and procedure-blanks, respectively standards. For example, we used chlorophyll-derived compounds purified from a millions of years old (radiocarbon dead) rock, and subjected different sample sizes to our purification procedure with HPLC. The same procedure was performed using a modern cholesterol standard. Different sample sizes of radiocarbon-dead coal were also analyzed. We concluded from these measurements that samples smaller than 10 µg were increasingly being influenced by contamination and thus require a large correction resulting in large uncertainties.

---

[1] *Geology, ETHZ*

ALTERNATIVE CELLULOSE ISOLATION FROM WOOD

Two new cellulose extraction techniques for radiocarbon dating

M. Němec[1], L. Wacker, I. Hajdas, H. Gäggeler[2]

Radiocarbon dating is very often applied to various types of wooden artifacts and tree-ring sequences. The main methods used to clean plant material for radiocarbon dating are not compound specific and generally remove only the easily exchangeable components. These are normally clean enough for standard radiocarbon measurements, but in some cases it is desirable to have pure cellulose, which is supposed to stay unchanged and immobile over long times, thus representing the original plant material.

In this work, two compound specific but still simple methods were tested to separate cellulose from wood. The first one, the viscose method, is based on the xanthification process. Cellulose converted to alkali cellulose forms with CS_2 a soluble cellulose xanthate, which is then extracted and decomposed to cellulose. The second procedure is based on the wood/cellulose dissolution in ionic liquid 1-butyl-3-methylimidazolium chloride [BMIM]Cl [1], where the dissolved cellulose could be precipitated again by simply adding a water-acetone mixture. These processes were never used for radiocarbon dating. The standard acid-base-acid method (ABA) and its variation called BABAB (base-acid-base-acid-bleaching) were used to look for potential contamination.

None of wood samples was fully dissolved, but reasonable amounts of cellulose could be prepared in all cases. The α-cellulose yield from the IAEA-C3 cellulose standard was almost 50% for the viscose method and the holocellulose yield for the ionic liquid method was even 75%. For wood samples the absolute yields were approx. 30% for BABAB, 10% - 20% for viscose and 14% for ionic liquid.

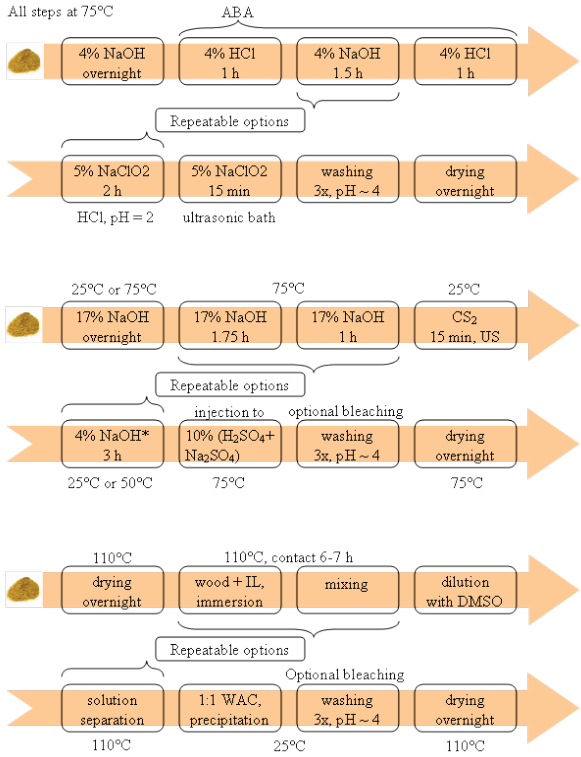

Fig. 1: *Sample preparation procedures. From the top: BABAB, viscose, ionic liquid [1].*

In general, the radiocarbon ages of cellulose from dendrochronologically dated wood obtained using the ionic liquid and viscose procedures agree very well with the values obtained with our reference BABAB method. However, the values are slightly older when compared with the IntCal04 calibration curve in the investigated time interval, while the ABA ^{14}C ages lie on the curve or are slightly younger.

[1] M. Nemec et al., Radiocarbon (2009) submitted

[1] *also Chemistry and Biochemistry, University of Bern*
[2] *Chemistry and Biochemistry, University of Bern*

SIMPLIFIED RADIOCARBON DATING OF SMALL SAMPLES

Direct gas measurements of ^{14}C samples after oxidation in quartz tubes

S. Fahrni[1], L. Wacker, M. Ruff[1], I. Hajdas, S. Szidat[1]

Sample combustion in quartz tubes with copper oxide and subsequent graphitization is a common procedure used in many ^{14}C AMS laboratories. However, since there is strong demand for measurements of small samples (<100 µg C), e.g. in the environmental sciences and dating of ice cores, it is important to adapt sample preparation and AMS measurements to such samples. Because the conversion of CO_2 to graphite contributes to contamination and is time consuming, we suggest to oxidize small ^{14}C samples in quartz ampoules using copper oxide followed by the direct measurement of the CO_2 with a gas ion source.

Quartz tubes closed at one end (4.0 mm O.D., 3.5 mm I.D., length: 15 cm) were used. About 0.1 g of copper oxide was filled into the tubes and heated to 950 °C for 2 h in a muffle furnace. Sample material weighed on a microgram balance was then filled into the quartz tubes. The tubes were evacuated to about 1 mbar with an oil-free turbo scroll pump for 5 minutes each. After evacuation, the tubes were sealed and heated for 2 h at 950 °C.

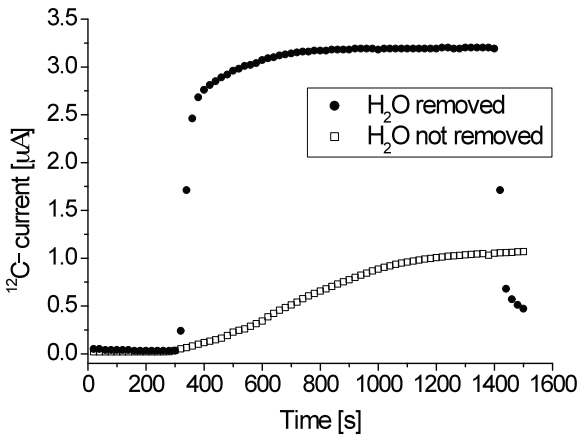

Fig. 1: *The effect of water removal on $^{12}C^-$ currents of small samples measured with the gas ion source.*

The ampoules were put directly into the cracker system [1] together with $CaSO_4$ as a drying agent. The measurements were made with the gas ion source at the MICADAS facility. Tests with artificial gas mixtures showed a strong effect of H_2O on the ionization efficiency for CO_2. A water content of 15% in the sample reduced the C^- current to about one third (Fig. 1). The removal of water is therefore crucial for high C^- currents and has to be made prior to every measurement. Other combustion by-products do not need to be removed.

C5	average	22.35 ± 0.35 pmC
(n=6)	nominal	23.05 ± 0.02 pmC
C7	average	49.03 ± 0.47 pmC
(n=8)	nominal	49.53 ± 0.12 pmC
OX-2	average	134.14 ± 1.00 pmC
(n=8)	nominal	134.07 pmC

Tab. 1: *Weighted averages with 1σ uncertainties for measurements of IAEA C5, C7 and NIST OX-2 reference materials normalized with OX-1.*

The AMS results for reference materials with 14 to 38 µg C are summarized in Table 1. 68% of the ^{14}C values lie within the 1σ interval and 95% within the 2σ interval, which demonstrates good agreement with a normal distribution. Blank values of coal samples had 0.95 pmC (38'000 years). The method in now widely used and has also been shown to be suitable for ^{14}C measurements of aqueous samples when water is gently evaporated prior to sample combustion.

[1] M. Ruff et al., Radiocarbon 49 (2007) 307

[1] *Chemistry and Biochemistry, University of Bern*

IN SITU COSMOGENIC ^{14}C

A new extraction line for terrestrially produced ^{14}C in quartz

K. Hippe[1], F. Kober[1], H. Baur[1], L. Wacker, M. Ruff, R. Wieler[1]

In situ produced cosmogenic ^{14}C is a not yet fully explored tool in Quaternary geochronology. Compared to other commonly used cosmogenic radionuclides (^{10}Be, ^{26}Al, ^{36}Cl), *in situ* ^{14}C has a short half-life (5730 a) giving it great sensitivity for studies in fast changing environments. Its rapid approach to secular equilibrium allows the evaluation of processes of rapid landscape formation. Extracting the tiny amounts of ^{14}C from terrestrial samples is the most challenging task in the application of the *in situ* ^{14}C method. The new ^{14}C extraction line at the Dept. of Earth Sciences, ETH Zürich (Fig. 1) is designed to extract ^{14}C from quartz samples in the form of pure CO_2 gas for analysis with AMS [1].

Fig. 1: *Close-up view of the ETH in situ ^{14}C extraction line.*

Up to 5 g of quartz are degassed at 1550 to 1600 °C in a flow of ultra-pure O_2 without the use of a fluxing agent. Samples are heated in a 6 kV electron bombardment furnace consisting of a sapphire tube that encloses a Pt-crucible holding the quartz. Gas purification is achieved in a series of cryogenic traps and passage through hot Ag and Cu wool/mesh (Fig. 2). The cleaned CO_2 gas is not graphitized but fed directly into the gas ion source of the MICADAS 200 kV AMS system to measure the $^{14}C/^{12}C$ ratio. Addition of C carrier is thus not required.

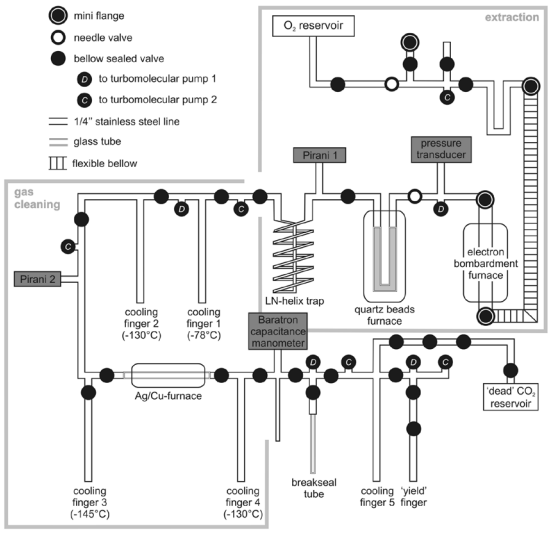

Fig. 2: *Schematic diagram of the extraction and gas cleaning system.*

Tests to determine the efficiency of CO_2 recovery after gas extraction and cleaning yielded consistently good recovery rates of >99.8 % (n=7). The ^{14}C blank contribution from the all-metal tubing system is negligible. Our preliminary procedural blank estimate derived mostly from the hot extraction furnace is $<9\cdot 10^4$ ^{14}C atoms. Extraction tests on two quartz samples by stepped heating show a quantitative separation of atmospheric ^{14}C at ≤500°C from the *in situ* component above 1200°C. First runs of quartz degassing by two-step heating indicate constant recovery rates. The extraction efficiency needs however to be improved.

[1] K. Hippe et al., Quat. Geochr. 4 (2009) 493

[1] *Geology, ETHZ*

RADIOCARBON APPLICATIONS

The ^{14}C samples 'pie'

Ultra-high precision radiocarbon dating

Is it time for a new calibration curve?

Carbon cycling in Damma Glacier forefield soils

45'000 year old Niederweningen mammoth

^{14}C based age-depth model of Soppensee

Radiocarbon analyses of aerosol components

THE ^{14}C SAMPLES 'PIE'

An overview of sample types, applications and collaborations for 2009

I. Hajdas, G. Bonani, S. Iglesias, M. Maurer, H-A. Synal, C. Vockenhuber, L. Wacker

In 2009, more than 2200 samples have been prepared as solid graphite samples or as CO_2 gas samples for analyses with our MICADAS AMS systems. A large part of prepared targets are standards (oxalic acid II) and blanks as well as IAEA reference materials (wood, cellulose, oxalic acids). These samples are measured along with unknown samples to ensure the quality of the preparation and measurements procedures. A significant number of samples are related to our internal projects (237). There, the focus is on improvements of preparation methods and, in particular, on technical innovations to enhance the reproducibility of the applied techniques. An increasing demand is also observed for analyses of very small samples (<50 µg carbon). This class of samples is analyzed as CO_2 using the gas feed option of our ion sources. About 400 gas samples were analyzed last year. They have been prepared predominantly by our collaborators.

Sample type	**Number of samples**
Standards (OXA II)	324
Blank samples	230
Reference materials (IAEA)	85
Subtotal	639
Category	
Internal	237
Gas samples	450
Archaeology	518
Past climate	118
Environmental	118
Art	144
Subtotal	1535
Grand total	**2224**

Tab. 1: *Numbers of samples from various projects as prepared and measured in 2009.*

Nearly 50 % of all the submitted samples have an archaeological context. This explains the big share of bones and charcoal in the samples 'Pie' (Fig. 1). However, the material analyzed most often is wood. It occurs in all categories of Table 1. Other materials, which occur less frequent, are also much more diverse. For example, carbonate samples include foraminifera, corals, pearls and mortar.

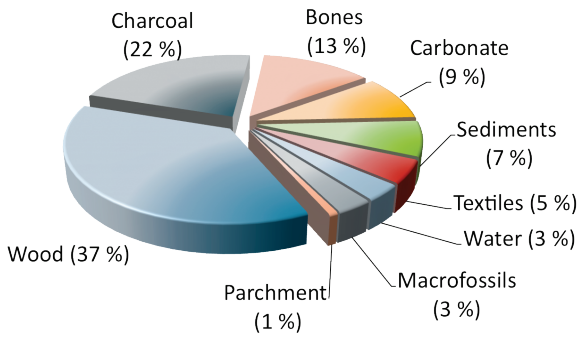

Fig. 1: *Samples 'Pie' showing the percentage of various types of graphitized material analyzed in 2009.*

Most samples originate from Switzerland due to close collaborations with archaeologists and climate researchers (Fig. 2) followed by samples from Germany and France where we have established long-standing collaborations.

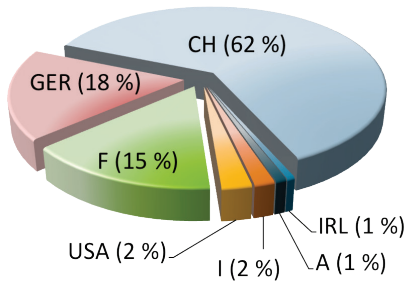

Fig. 2: *Fractions for samples submitted by users from Switzerland (CH) and other countries.*

ULTRA-HIGH PRECISION RADIOCARBON DATING

Case study of the Middle Ages: The "Goldene Handefeste" of Berne

L. Wacker, G. Bonani, I. Hajdas, H.-A. Synal, P. Martig[1], B. Studer[1]

The "Goldene Handfeste" of Berne is a medieval charter dated to April 15, 1218 purporting to have been issued by Holy Roman Emperor Frederick II (Fig. 1). It establishes the town privileges of Berne making it an Imperial Free City and, effectively, an independent state. For the last about 150 years, there is an ongoing controversy among scholars that the document might be a Bernese forgery from the middle of the 13th century. However, the charter was formally confirmed by King Rudolf I in 1274 and thus, without doubt, one of the most important documents in the history of Berne. In order to establish the true age of the charter it was agreed to conduct a radiocarbon test. New experimental opportunities to perform dating with ultra-high precision raise hope to resolve this controversial issue.

Fig. 1: *The "Goldene Handfeste" of Berne*

Samples were taken from the parchment and the seal cord. Each sample was cleaned twice, graphitized four, respectively five times and measured independently. The results show two distinct ages with perfect repeatability. The averages of the subsamples result in final uncertainties of ≈1‰ or 8-10 years (Tab. 1).

sample	type	age (BP)
ETH-36716.1	parchment	888 ± 20
ETH-36716.2	parchment	878 ± 19
ETH-36716.3	parchment	882 ± 19
ETH-36716.4	parchment	875 ± 19
ETH-36716	**parchment**	**881 ± 10**
ETH-36717.1	seal cord	800 ± 20
ETH-36717.2	seal cord	808 ± 19
ETH-36717.3	seal cord	833 ± 18
ETH-36717.4	seal cord	808 ± 18
ETH-36717.5	seal cord	800 ± 17
ETH-36717	**seal cord**	**809 ± 8**

Tab. 1: *Measured ages for the parchment and the seal cord with their corresponding means (in radiocarbon years BP with ±1σ uncertainties).*

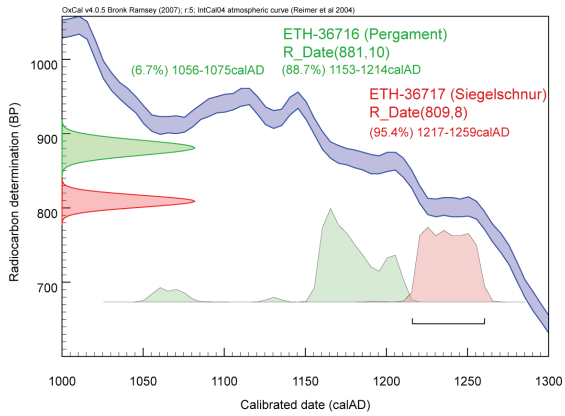

Fig. 2: *Calibrated ages of the two samples.*

Based on these results the parchment originates clearly from a time before 1218, but the seal cord appears to be younger. There remains a minor probability that the document might have existed in 1218. At present, the quality of the calibration does not allow a distinct conclusion. Only by improving the calibration data we will potentially be able to give a final answer.

[1] *Staatsarchiv Bern*

IS IT TIME FOR A NEW CALIBRATION CURVE?

Partial re-evaluation of the Intcal09 radiocarbon calibration curve

L. Wacker, M. Němec[1], M. Friedrich[2], B. Kromer[3], I. Hajdas, H.-A. Synal

The uncertainties of our latest highest-precision measurements are often lower than those of the IntCal09 calibration curve, which has an uncertainty of 12 – 13 years in radiocarbon ages for the past 2000 years (with only a decadal resolution in the samples entering IntCal09).

We decided to re-measure dendrochronologically dated tree-ring samples of the Southern German oak chronology in the time range of 1000 to 1200 calendar years BP. The samples covering 5 years each were measured to a precision of about 15 years (2 ‰), including an uncertainty of 0.8 ‰ for sample preparation (see Fig. 1).

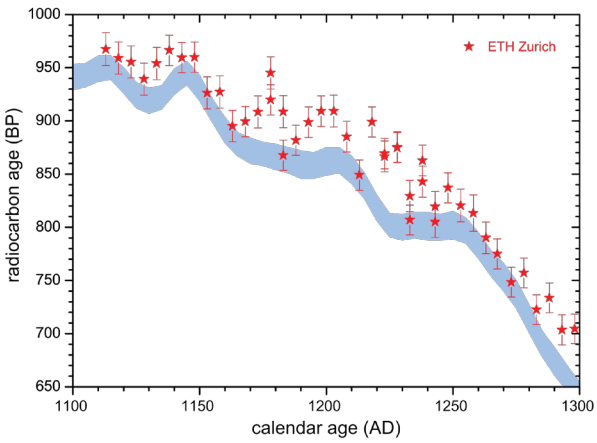

Fig. 1: *The 5-year oak tree-ring samples from Southern Germany are plotted with 1 σ uncertainties together with the IntCal09 calibration band (also 1 σ).*

The sample-to-sample ^{14}C age variability (26 years) is very low and compares very well with the decadal IntCal09 raw data, which show a variability between 30 and 35 years from sample to sample with 10-year resolution. In principle, with our 5-year resolution we should include in our results some of the production signal variations caused by the 11 yr solar cycle. Hence, the lower sample-to-sample variability in our data is unexpected.

Though the dataset looks very consistent, we see on average a significant offset of 26 year (about 3 ‰) to IntCal09. At present this offset cannot be explained as all our measurements of secondary standards agree fully with the consensus values. We do not yet know whether the offset originates from systematic effects in our measurement procedures. Some of the wood samples were also treated with a simple acid-base-acid procedure for comparison and do not show such an offset. The rigorous pre-treatment with base-acid-base-acid bleaching applied to the samples could therefore be responsible for the observed offset.

The stability of the MICADAS AMS system over time allows us to make highest-precision measurements that until recently were exclusively a niche for gas-counters and advanced liquid-scintillation facilities. This capability goes well beyond high-precision measurements on larger accelerators suggesting that modern samples can be measured to a precision of 2 ‰ or better.

As a word of caution, we have seen a significant offset in our data when re-measuring tree-ring samples between 1100 and 1300 AD compared to the IntCal09 calibration curve. This discrepancy will be further investigated in order to clarify whether this offset is a yet unknown systematic effect of our measurement procedures or whether it is caused by the applied pre-treatment procedure.

---

[1] *also Chemistry and Biochemistry, University of Bern*
[2] *Botany, University of Hohenheim, Germany*
[3] *Heidelberg Academy of Sciences, Germany*

CARBON CYCLING IN DAMMA GLACIER FOREFIELD SOILS

Tracing the build-up of soil carbon using the 'bomb peak'

R.H. Smittenberg[1], I. Hajdas, L. Wacker, S.M. Bernasconi[1]

Soil Organic Carbon (SOC) is a vastly complex mixture of biomolecules that can theoretically be divided into various chemical and physical 'pools'. These form in reality a continuum of size, functionality, degree of association with the mineral fraction, aggregation, or protection against water-soluble microbial enzymes. Knowledge of SOC turnover rates is very important for the quantification of soils as sources and sinks of atmospheric CO_2 - the recalcitrant or stabilized fraction being ultimately responsible for long-term terrestrial carbon storage.

As part of a larger project, called 'Biglink' the early development of high Alpine soils that were gradually exposed after glacier retreat in Central Switzerland was investigated. An exponential increase in Total Organic Carbon (TOC) content along the 150 year long chronosequence clearly shows initial SOC accumulation. Chemical and physical separation techniques combined with chemical fingerprinting techniques of size and density fractions along the chronosequence gave a first insight in the build-up and relative importance of such-defined SOC pools through time.

The permeation and attenuation of the radio-carbon bomb peak in the natural carbon cycle (plants, soils, dissolved C) is a useful tool to gain insight in the Carbon cycle. In the investigated forefield, the atmospheric bomb peak was used as natural tracer for the age of various organic carbon pools and compounds (Fig. 1).

Comparison of the radiocarbon content of physically and chemically separated fractions, including some isolated organic compounds (Fig. 2), gave insight in the mean residence time of these fractions. Some of these fractions were quite small, and here the use of the MICADAS AMS facility with the gas source inlet proved to be critical to obtain results.

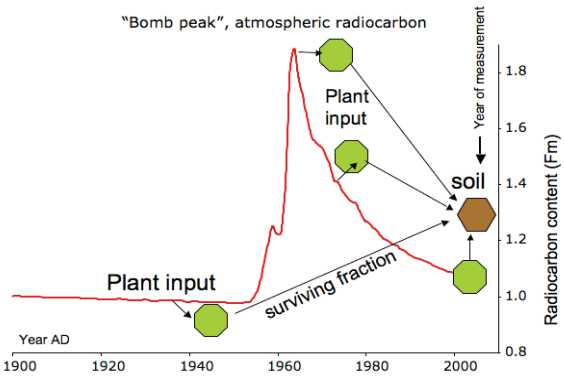

Fig. 1: *Schematic of the use of the radiocarbon 'bomb peak' in organic matter cycling studies. The soil carbon has an average age that is the mix of old, resilient carbon with high bomb-spike ^{14}C and newer plant input reflecting the present-day atmospheric ^{14}C content.*

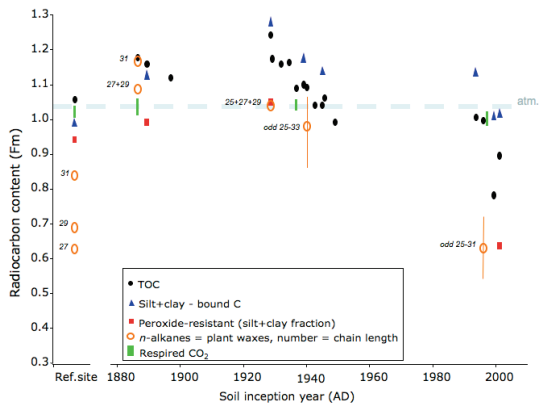

Fig. 2: *Radiocarbon contents of various SOC fractions over the soil chronosequence. Relatively high ^{14}C values of total SOC compared to the present-day atmosphere indicates that a considerable fraction withstands degradation. This is especially true for the mineral-bound fraction.*

---

[1] *Geology, ETHZ*

45'000 YEAR OLD NIEDERWENINGEN MAMMOTH

Bone preparation techniques at the limit of ^{14}C dating

I. Hajdas, A. Michczyński[1], G. Bonani, S. Iglesias, M. Maurer, C. Vockenhuber, L. Wacker, H. Furrer[2]

Mammoth finds are fascinating not only for the scientific community but are also for the public. The mammoth site in Niederweningen (ZH) is a good example of interplay between public curiosity and scientific interest (Fig.1). More than 100 years ago, numerous bones of mammoths were found and remained undated until recently. With the help of AMS ^{14}C dating the age of a mammoth bone was now determined to be 45'000 years. This is nearly 8'000 years older than that obtained with a previous AMS analysis of collagen (COL) (Tab. 1).

Fig. 1: *Mammoth tusk found in Niederweningen during construction work in 2004.*

The improved preparation method used now included additional treatment of collagen with base that removed contamination by younger carbon (mainly humic acid). The base cleaned gelatine fraction (GB) was then prepared for AMS ^{14}C analysis. The reliability of the age obtained is supported by ^{14}C ages of peat in which the mammoth bones were found [1].

Because the age of this mammoth is close to the detection limit of the ^{14}C method, dating its bones provided a great opportunity to test different preparation methods. As for the last 3 years our standard procedure in the preparation of bones was the purification of gelatine by ultra filtration (UF) [2], we also prepared and dated a sample using this method. Additionally, a base step was added to the UF method (BUF).

Fraction	Radiocarbon age (BP)
Collagen COL	40910 ± 830
Collagen COL	37910 ± 520
Base cleaned gelatine GB	45870 ± 1080
Gelatine Ultra Filtration UF	46760 ± 1470
Gelatine Ultra Filtration UF	44605 ± 1365
Gelatine Base+UF BUF	46765 ± 1370
Gelatine Base+UF BUF	44720 ± 1500

Tab. 1: *^{14}C ages on COL and GB [1] are compared with ages of UF and BUF fractions [2].*

Our results show that the radiocarbon ages of the GB, UF and BUF fractions are in very good agreement (Tab. 1). It is therefore possible to apply either of the cleaning methods to this specific bone. Similar studies are needed for bones in different preservation stages.

[1] I. Hajdas et al., Quat. Intern. 164 (2007) 98
[2] I. Hajdas et al., Radiocarbon 51 (2009) 675

[1] *GADAM Centre of Excellence, Silesian University of Technology, Gliwice, Poland*
[2] *Paleontology and Museum, University of Zurich*

^{14}C BASED AGE-DEPTH MODEL OF SOPPENSEE

OxCal Bayesian model of ^{14}C ages competes with varve chronologies

I. Hajdas and A. Michczyński[1]

High-resolution records of past environmental changes, such as tree rings, ice cores and laminated sediments, are valued for the possibility of detailed studies of temporal changes. Sedimentary records around the world belong to the most studied archives despite a common lack of annual resolution. Nowadays, a reliable ^{14}C chronology combined with Bayesian modeling, for example using OxCal4.0 [1], allows the construction of age-depth models of sedimentary deposits. This in turn provides new opportunities for new sites to be studied in more detail.

We have tested a depth-age model based on ^{14}C ages of terrestrial macrofossils selected from sediments of the laminated lake Soppensee (LU, Switzerland) (Fig. 1). A sequence of ^{14}C ages was introduced into the depositional model (P_Sequence) of the OxCal4.0 program, which is available on the web [2].

Fig. 1: *Examples of terrestrial macrofossils selected from laminated sediments of Soppensee (LU): seeds (birch on the left, alder on the right), fragments of flowers (top left corner) and a leaf. Because fragments of terrestrial plants have a ^{14}C content contemporary to the atmosphere they provide excellent material for radiocarbon dating.*

The resulting age depth-model was compared with the varve chronology i.e. the timescale based on counting annual layers preserved in sediments of Soppensee.

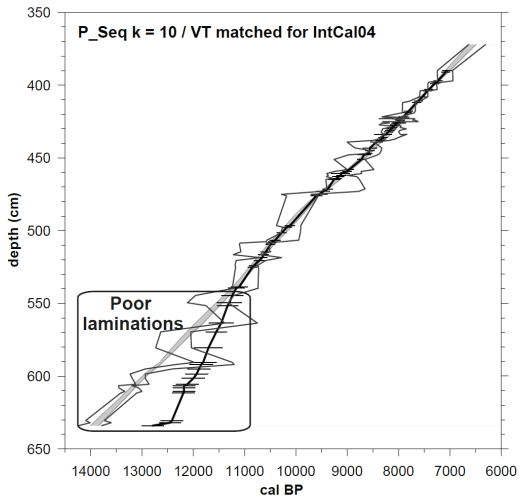

Fig. 2: *Results of the model (grey strip – 95% confidence intervals) are plotted together with the varve chronology (black line).*

Comparison between both chronologies (Fig. 2) shows a good agreement between the two chronologies and illustrates the importance of the quality of the laminations for the construction of varve chronologies.

In summary, our study shows a potential of ^{14}C chronologies and age-depth models to provide highly resolved and reliable chronologies.

[1] C.B. Ramsey, Quaternary Science Reviews 27 (2008) 42
[2] https://c14.arch.ox.ac.uk

[1] *GADAM Centre of Excellence, Silesian University of Technology, Gliwice, Poland*

RADIOCARBON ANALYSES OF AEROSOL COMPONENTS

A PREPARATIVE 2D-CHROMATOGRAPHY METHOD

S. Fahrni[1], H.W. Gäggeler[1,2], M. Ruff[1,2], S. Szidat[1], L. Wacker

Oxalic acid and other small dicarboxylic acids in carbonaceous aerosols have received much attention recently. Biogenic and fossil emissions as well as wood burning are thought to contribute precursors for the secondary formation of dicarboxylic acids [1]. Nevertheless, sources of those compounds in aerosols are subject to speculations. In order to gain further insight into sources and formation processes of dicarboxylic acids, a compound-specific radiocarbon measurement is the method of choice. In our approach, the separation of compounds is achieved through liquid chromatography and the radiocarbon measurement is conducted with accelerator mass spectrometry. As the carbon amounts needed for such ^{14}C measurements lie in the low microgram range, very high amounts of aerosols on air filters are still needed.

An anion chromatography column (IonPac AS 11HC, Dionex) was used in a 30 min hydroxide gradient run to separate oxalate roughly from other inorganic and organic anions, as for example humic-like substances. Tests with artificial solutions of certified oxalic acid ^{14}C reference materials (IAEA C7 and NIST OX-2 [2]) containing sulphate, malonic, maleic, malic and succinic acid and humic acid were performed to simulate real samples and possible contaminations (Fig. 1, top). Fractions of the desired peaks were collected in Teflon (PFA) vials and dried at 40°C under a stream of nitrogen.

The dried residue was then re-dissolved in 25 µl of water, injected into the high pressure liquid chromatograph (HPLC) and separated within 15 min (Fig. 1, bottom) on an Acclaim OA column in an isocratic run (eluent: aqueous HCl, 5mM, pH 2.3). The oxalic acid fractions were dried and re-dissolved in H_2O and put into baked-out quartz tubes for subsequent drying and combustion for gaseous ^{14}C measurements.

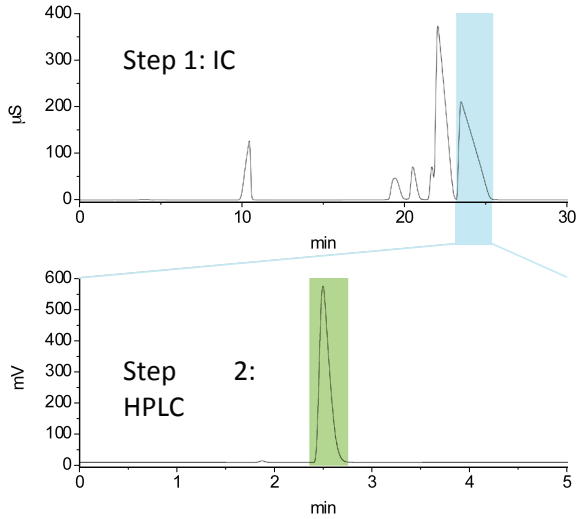

Fig. 1: *Top: Ion chromatography run with humic acid, different dicarboxylic acids, sulphate and oxalic acid ^{14}C reference material (blue). Bottom: HPLC chromatogram of the fraction collected with IC. The green fraction was collected for a subsequent ^{14}C measurement.*

The first cleaning step using the ion chromatography (IC) column removes the main matrix components like humic acid, malonic, maleic, malic and succinic acid with sulphate from oxalic acid. Only this allows then to access pure oxalic acid in a second HPLC step. The overall yield of the procedure is about 50%. ^{14}C measurements of the processed samples with the gas ion source of MICADAS confirm a good agreement of the measured values with the nominal values of the used reference materials. This indicates a complete separation of oxalic acid from other compounds.

[1] M. Legrand et al., J. Geophys. Res. 112 (2007) D23S0

[1] *Chemistry and Biochemistry, University of Bern*
[2] *Paul Scherrer Institut, Villigen*

APPLICATIONS IN GEOLOGY

Alpine glacier and rock glacier activity

Alpine glaciers in the Jura Mountains

Glaciations in the Kackar Mountains (NE Turkey)

Glaciations in the Dedegöl Mountains (Turkey)

Pleistocene glaciations in the subtropical Andes

Comparing ^{14}C and ^{10}Be exposure dating results

Large mass movements in the Alps

A tool to reconstruct rock fall history?

Testing dual-cosmogenic isotope burial dating

A new view of Alpine erosion

Erosion rates in the Hörnli area

Erosion rates from the eastern Altiplano

^{10}Be based denudation rates in foreland basins

Denudation rates from fault footwalls

Building stones in Hattusha (Hittite Empire)

^{36}Cl production in limestones and dolomites

ALPINE GLACIER AND ROCK GLACIER ACTIVITY

^{10}Be dating of events at the end of the Lateglacial

S. Ivy-Ochs[1], H. Kerschner[2], M. Maisch[3], M. Christl, P.W. Kubik, C. Schlüchter[4]

Glacier advances in the Alps related to Younger Dryas cooling led to the deposition of Egesen stadial moraines. Moraines of the earliest and most extended advance, the Egesen maximum, stabilized at 12.2±1.0 ka based on ^{10}Be exposure dating at the Schönferwall (Tyrol, Austria) and the Julier Pass outer moraine (eastern Switzerland). Final stabilization of moraines at the end of the Egesen stadial was at 11.3±0.9 ka as shown by ^{10}Be data from four sites across the Alps. From west to east the sites are Piano del Praiet (northwestern Italy), Grosser Aletschgletscher (central Switzerland), Julier Pass inner moraine (eastern Switzerland), and Val Viola (northeastern Italy). ^{10}Be data from the Kartell site (northern Tyrol, Austria) indicate that in the earliest Holocene, glaciers in the northernmost mountain ranges advanced at around 10.8±1.1 ka.

In more sheltered, drier regions rock glacier activity dominated as shown, for example, at Julier Pass and Larstig valley (Tyrol, Austria). New ^{10}Be dates presented here for two rock glaciers in Larstig valley (Fig. 1) indicate the cessation of rock glacier activity and final stabilization no later than 10.5±0.8 ka. The rock glaciers moved from the talus slope on the left-hand side of the valley into an ice-free valley after the Egesen glacier had melted back from its maximum extent. Thus the earliest time for onset of rock glacier activity is around 12 - 11.6 ka. The size and morphology of the Larstig rock glaciers supports one continuous period of activity which, based on an estimated average creep velocity of 0.5 m a^{-1}, lasted from 500 to 1500 years.

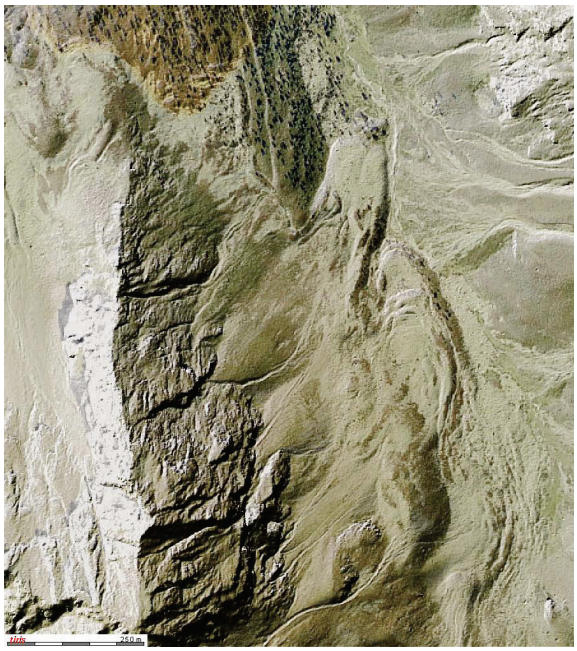

Fig. 1: *Orthophoto draped on laser scan image of ^{10}Be dated rock glaciers in Larstigtal, Austria (Orthophoto/DEM: © Land Tirol - tiris). Left lateral Egesen moraines are seen at the top center. Scale bar in lower left corner is 250 m.*

The sum of the data indicates that the earliest Holocene (between 11.6 and about 10.5 ka) was still strongly affected by the cold climatic conditions of the Younger Dryas and the Preboreal oscillation, with the intervening warming phase having had led to rapid downwasting of Egesen glaciers [1].

[1] S. Ivy-Ochs et al. Quat. Sci. Rev. 28 (2009) 2137

[1] *also Geography, University of Zurich*
[2] *Geography, University of Innsbruck, Austria*
[3] *Geography, University of Zurich*
[4] *Geology, University of Bern*

ALPINE GLACIERS IN THE JURA MOUNTAINS

Constraining the timing with ^{10}Be exposure dating

A. Graf[1], N. Akcar[1], S. Ivy-Ochs[2], P.W. Kubik, C. Schlüchter[1]

The Jura Mountains are formed by a succession of anticlines and synclines separated from the Alps by a perialpine basin, the Swiss Midlands. The bedrock of the Jura Mountains is dominated by limestone and marl. However, erratic boulders of Alpine lithology (mainly granites and gneisses) are found on some of the anticlines of the Jura Mountains. The very existence and their spatial distribution suggest that Alpine ice reached into this mountain chain at least twice. To better constrain the timing and extent of Alpine glacier advances, surface exposure dating was applied to erratic boulders of Alpine origin along three S-N transects (two are shown in Fig. 1).

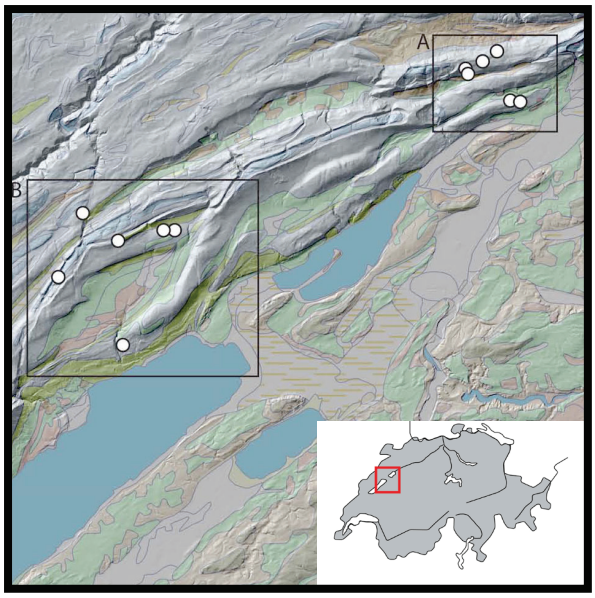

Fig.1: *Region of Jura Mountains where sampled Alpine lithology boulders (white circles) are located (approx. width of map area 50 km).*

The obtained exposure ages suggest that the remotest boulders were deposited during a pre-Last Glacial Maximum advance that took place no later than about 160,000 year ago. The ages of the erratic boulders deposited on the lower part of the first anticline suggest that Last Glacial Maximum Alpine ice retreated form the Jura Mountains some 19 ka ago. The exposure ages also indicate that some Last Glacial Maximum boulders may have been reworked from erratic material brought earlier to the Swiss Midlands and Jura Mountains.

Fig. 2: *This erratic boulder was deposited more than 160,000 years ago. Hammer for scale.*

[1] A. Graf et al., Quat. Int. 28 (2007) 2137
[2] A. Graf, dissertation, University of Bern (2008)

[1]*Geology, University of Bern*
[2]*also Geography, University of Zurich*

GLACIATIONS IN THE KAÇKAR MOUNTAINS (NE TURKEY)

Field and cosmogenic exposure dating evidence

N. Akçar[1], S. Ivy-Ochs[2], V. Yavuz[3], P.W. Kubik, C. Schlüchter[1]

The evidences of Quaternary paleoglaciations in the Kavron [1, 2] and Verçenik [3] valleys, which are located in the Eastern Black Sea Mountains, are studied in detail (Fig. 1). In order to construct the chronology of the paleoglacial activities in the region, 45 samples from erratic granitic boulders and glacially abraded bedrock were collected for surface exposure dating with ^{10}Be.

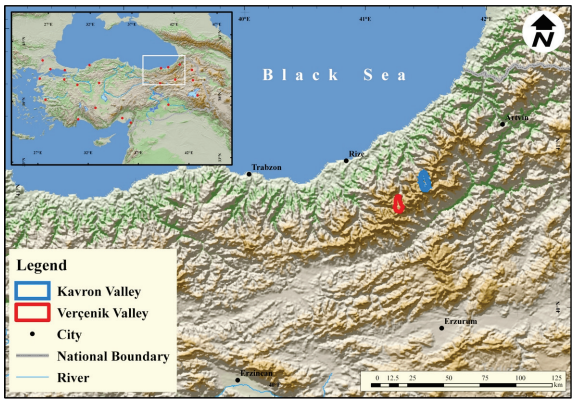

Fig. 1: *Location map of the study area.*

Exposure ages indicate that the Last Glacial Maximum (LGM) advance of paleoglaciers occurred before about 21 ka (Fig. 2). This advance continued until around 20 ka, after which paleoglaciers receded. Subsequent to this retreat, paleoglaciers in the Kaçkar Mountains most probably separated into smaller glaciers that were restricted to the tributary valleys (Fig. 2). A Lateglacial (most probably Younger Dryas) advance took place around 11 to 10 ka and produced terminal moraines (Fig. 2). Little Ice Age (LIA) moraines appear to be absent in all sites. Several snow-avalanche ridges were distinguished [2]. ^{10}Be exposure ages from five granitic boulders vary ranging from around 7 to 2 ka. These ages show that these events occurred during the Holocene and are therefore not linked to glacier fluctuations (Fig. 2).

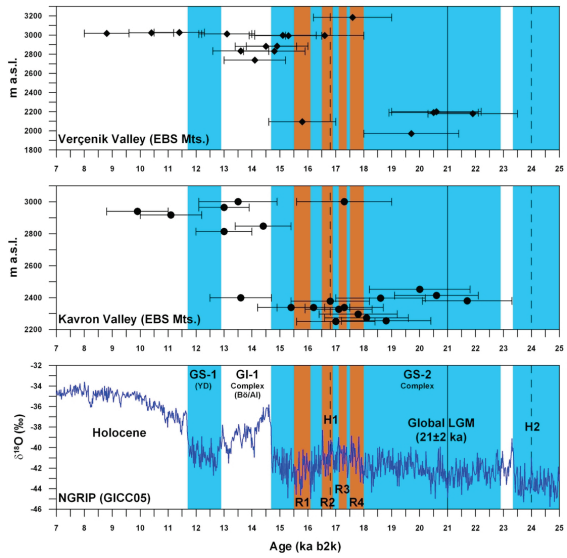

Fig. 2: *Surface exposure ages from the Kaçkar Mountains plotted against NGRIP (GICC05) ice core records, Heinrich events and four major red layers (R4, R3, R2, R1) deposited 18-15.5 ka in the northwestern Black Sea Basin [1, 2, 3].*

The LGM advance of paleoglaciers appears in the Kaçkar Mountains to correlate well with other exposure age data sets from Anatolia, the European Alps, Central Apennines (Italy) and the Greek Mountains. The Younger Dryas and the LIA cooling still remain to be studied in detail. Dry and cold climatic conditions during the LIA could explain the absence of glacier advance, as the conditions were not conducive for the build-up of ice.

[1] N. Akçar et al., Quat. Int. 164–165 (2007) 170
[2] N. Akçar et al., Quat. Int. 167–168 (2007) 4
[3] N. Akçar et al., J. Quat. Sci. 23/3 (2008) 273

[1] *Geology, University of Bern*
[2] *also Geography, University of Zurich*
[3] *Istanbul Technical University, Turkey*

GLACIATIONS IN THE DEDEGÖL MOUNTAINS (TURKEY)

Surface exposure dating of Late Pleistocene glacial deposits

C. Zahno[1], N. Akçar[1], V. Yavuz[2], P.W. Kubik, C. Schlüchter[1]

The Muslu Valley in the Dedegöl Mountains is situated on the interior side of the western central Taurus Mountains of SW Anatolia (Turkey), 2992 m above sea level. It represents the lower part of a formerly glaciated valley system of approx. 7.5 km in length (Fig. 1) [1].

Fig. 1: *Geomorphological evidence for the presence of the former Muslu Glacier: two tall lateral moraines (yellow line) and at the lower end of the first flat meadow, recessional terminal moraines (red line).*

We collected 25 surface samples from glacially transported boulders deposited on moraines and from bedrock for surface exposure dating with cosmogenic ^{10}Be and ^{26}Al. It is our objective to reconstruct a local chronology of glacier change and to explore its interrelationship with different terrestrial datasets of environmental change in central Anatolia. Surface exposure ages with cosmogenic ^{10}Be and ^{26}Al (Table 1) date a glacier expansion out of the Muslu Valley to 24.3±1.8 ka ago (1σ confidence interval) and give evidence for pronounced glacier advances prior to the global Last Glacial Maximum (21±2 ka). Deglaciation commenced no later than 17.7±1.4 ka ago. Superimposed climatic oscillations are indicated by glacier fluctuations dated to 19.8±1.6 ka and 13.9±2.3 ka, i.e. prior to the first major amelioration of climate.

Sample code	Corrected exposure age (ka)[a]		
	^{10}Be		^{26}Al
Bedrock, beyond palaeoglacier activity			
TRD-01	8.9 ± 1.0		n/a
TRD-02	41.2 ± 4.3		42.2 ± 4.9
Last glacial moraines			
(i) Deposited on subsidiary moraine ridge			
TRD-13A	15.9 ± 1.0	19.8±1.6[b]	n/a
TRD-13B	19.8 ± 1.6		n/a
(ii) Deposited on morphologically dominant lateral moraine ridges			
TRD-05[r]	23.6 ± 2.9		n/a
TRD-06[r]	14.7 ± 1.4		n/a
TRD-07A[r]	10.8 ± 1.1	16.4±1.7[b]	n/a
TRD-07B[r]	16.4 ± 1.7		n/a
TRD-08[r]	24.3 ± 1.8		n/a
TRD-12[l]	5.8 ± 0.4		n/a
(iii) Deposited on recessional moraines			
TRD-18A	12.7 ± 1.2	13.9±2.3[b]	n/a
TRD-18B	13.9 ± 2.3		n/a
Deposited in the transition into the sandur fan			
TRD-14	23.4 ± 3.0		n/a
TRD-21	17.7 ± 1.4		n/a
Ice-moulded bedrock			
TRD-09	10.9 ± 1.3		9.4 ± 1.2
TRD-10	11.7 ± 1.2		n/a
TRD-11	13.3 ± 1.5	13.3±1.5[b]	13.5 ± 2.0
TRD-11*	12.9 ± 1.6		16.4 ± 2.3
Adjacent palaeoglacier system			
TRD-03	13.4 ± 1.2		n/a

Tab. 1: *Snow, vegetation and erosion corrected ^{10}Be and ^{26}Al exposure ages from the Muslu Valley, with consideration of the temporal variations of the geomagnetic field. Broken down into geomorphological units.*

The Late Pleistocene glacier chronology from the western central Taurus Mountains, published lake level fluctuation data of palaeolake Konya and Lake Beyşehir, and nearby pollen data on the central Anatolian plateau reveal a conspicuous time correlation of palaeoenvironmental change.

[1] C. Zahno et al., J. Quatern. Sci. 24/8 (2009) 1016

[1] *Geology, University of Bern*
[2] *Istanbul Technical University, Turkey*

PLEISTOCENE GLACIATION IN THE SUBTROPICAL ANDES

Paleoclimate reconstruction and a calibration site for SED

J. Zech[1,2], R. Zech[2], P.W. Kubik, H. Veit[1]

In the semiarid subtropical Andes, glaciers react particularly sensitive to changes in precipitation. In order to reconstruct the temporal and spatial variability of the tropical circulation system during the Quaternary, we applied ^{10}Be surface exposure dating (SED) at Tres Lagunas (22°S, 65°W, 4500 m asl), NW Argentina (Fig. 1) [1].

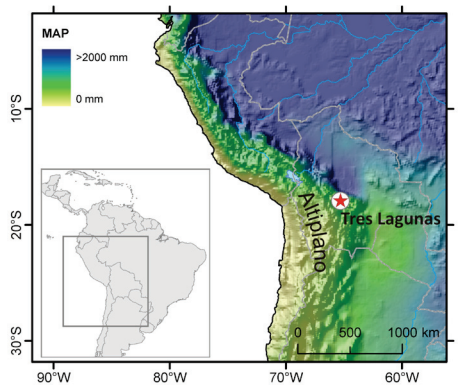

Fig. 1: *Geographic setting of the study area.*

The most extensive glaciation dates to ~122 ka and coincides with the Ouki (120-98 ka) Lake transgression phase on the Altiplano [1, 2]. Glaciers advanced again at ~22.2 ka and ~26.0 ka during the global Last Glacial Maximum and in phase with the Sajsi Lake transgression phase [2] (Fig. 2). Initial deglaciation resulted in the formation of a paleolake, dated to 20.2-18.8 cal. ka BP. A minor glacial readvance is documented by diamictic lake sediment deposits (18.8-18.6 cal. ka BP) and a lateral moraine (~17.0 ka). The most prominent moraine dates to ~13.9 ka, which coincides with the end of the Tauca Lake transgression phase. A minor glacial readvance, dated to ~11.3 ka, correlates with the Coipasa Lake transgression phase. Our chronology reveals major reorganizations of the tropical circulations system: (i) an intensification of the monsoonal circulation in response to North Atlantic cooling during Heinrich event I (H-I) and the Younger Dryas (YD), and (ii) increased precipitation in response to cold sea surface temperatures (SST) in the eastern tropical Pacific (Fig. 2) and sustained La Niña-like conditions.

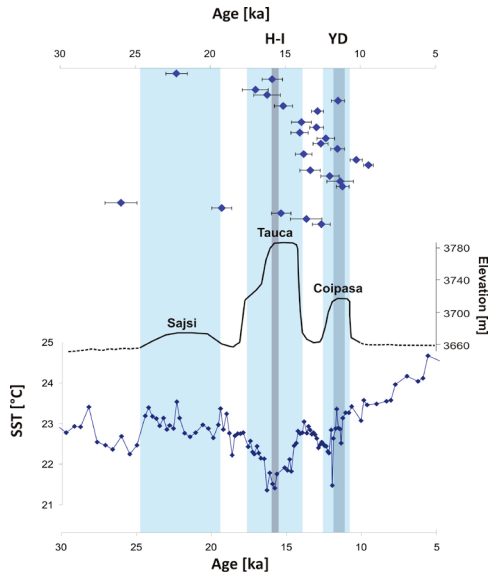

Fig. 2: *Exposure ages plotted against the lake transgression phases on the Altiplano [2] and SST in the eastern tropical Pacific [4].*

Additionally, Tres Lagunas has great potential to be the world's highest calibration site for SED. The preliminary reference production rate calculated with the scaling model of Lifton et al. [3] is 4.38±0.26 atoms/g/a and agrees closely with the global mean production rate of 4.65±0.12 atoms/g/a.

[1] J. Zech et al., Palaeo3, 284 (2009) 180
[2] C. Placzek et al., GSA Bull. 118 (2006) 515
[3] N. Lifton et al., Earth Planet. Sci. Lett. 239 (2005) 140
[4] M. Kienast et al., Nature 443 (2006) 846

[1] *Geography, University of Bern*
[2] *Geological Science, Brown University, USA*

COMPARING ^{14}C AND ^{10}Be EXPOSURE DATING RESULTS

Application of dating techniques in the Alpine environment

F. Favilli[1], M. Egli[1], D. Brandova[1], S. Ivy-Ochs[2], P.W. Kubik, P. Cherubini[3], W. Haeberli[1]

We have combined several dating techniques to elucidate signals of Alpine landscape evolution during the late Pleistocene and early Holocene in an Alpine valley in Trentino (northern Italy).

Attention was focused on soils, considered as natural archives of past climatic events and large boulders located on the moraine crests, considered as evidence of former glacial extents. Soils developed on moraines have been sampled and treated with 10% H_2O_2 to mineralize the labile, active pool of the organic matter (OM) and to isolate a resistant old OM pool. This old OM pool was considered as a part of the first OM formed after glacier retreat and the exposition of the deposited landforms. The ^{14}C dating of these organic residues gave minimum ages for OM formation and, therefore, for an ice-free surface.

Large boulders in stable position located on the crest of the glacial sediments and in the vicinity of the studied soils (Fig. 1) [1] have been sampled and dated by means of surface exposure dating with ^{10}Be.

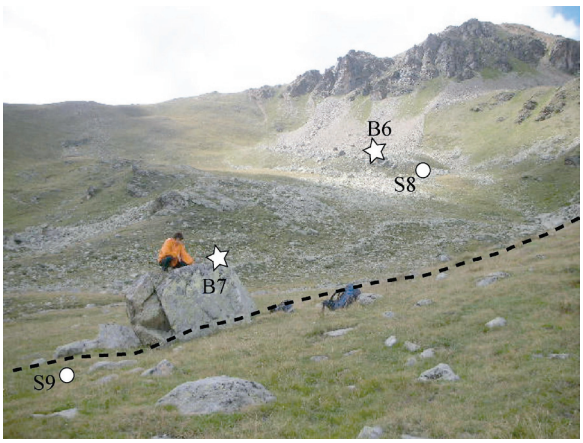

Fig. 1: *East-facing slope of the investigated area and location of the soils S8, S9 and of the boulders B6 and B7.*

The comparison between the results of the two absolute dating techniques was in a fairly good agreement, revealing the extent and the duration of the single stadials/interstadials which occurred in the investigated area. The oldest soil was sampled on the crest of the outermost lateral moraine in the investigated cirque. The ^{14}C age of the resistant OM pool referred to the Oldest Dryas chronozone, around 17.0 ka cal BP and it is consistent with the position of the soil itself. Most of the other dated soils referred to the Preboreal chronozone (c. 11.6 – 10.2 ka).They have developed on the moraines deposited during the Egesen stadial glacier readvance (12.9 – 11.6 ka yrs). The ^{10}Be ages of the boulders could define, between 2400 and 2100 m asl, the duration and spatial extent of the Egesen glaciers. The boulders' ages at the highest altitudes (> 2400 m asl) have revealed that the activities of local glaciers and rock glaciers have lasted until the onset of the Holocene climatic optimum (c. 9.0 ka yrs).

A combined approach can help in detecting crucial evidence and in avoiding misinterpretation of the ^{14}C ages. The ^{14}C ages of the soils referred to the warm phases of the Lateglacial, as the ^{10}Be ages of the boulders to the cold ones. Taken together, they can give a more complete view of the deglaciation process and provide indications about the time needed for the first OM accumulation and stabilization.

[1] F. Favilli et al., Geomorph. 112 (2009) 48

[1] *Geography, University of Zurich*
[2] *also Geography, University of Zurich*
[3] *Swiss Federal Inst. for Forest, Snow and Landscape Reseach (WSL), Birmensdorf*

LARGE MASS MOVEMENTS IN THE ALPS

Exposure dating with ^{10}Be and ^{36}Cl

S. Ivy-Ochs[1], H. Kerschner[2], V. Alfimov, P.W. Kubik, C. Schlüchter[3],

Absolute dating is required to decipher tectonic vs. climatic control on the magnitude-frequency distribution of slope instabilities in the Alps. Our contribution is to exposure date boulders and bedrock from numerous large landslides in the Alps with cosmogenic nuclides. For landslides in crystalline regions with abundant quartz ^{10}Be is utilized, while ^{36}Cl is used in areas underlain by calcareous rocks. Potential complications include pre-exposure of boulders, post-slide rock fall in the detachment area, and shielding of dated surfaces by soil or snow [1, 2]. Pre-exposure (exposure ages much older than ages of the rest of the boulders) occurs more frequently in landslide than in moraine boulders, reflecting the mode of movement of most slides.

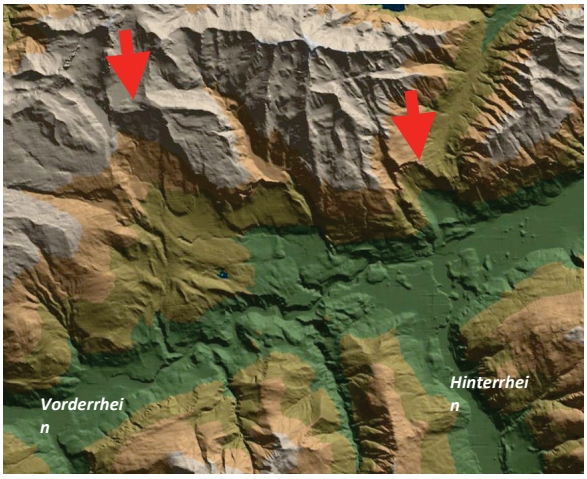

Fig. 1: *Shaded relief map of the confluence of the Vorderrhein and Hinterrhein rivers, from Atlas der Schweiz (based on DHM25). Red arrows seen in the center and center right, respectively, indicates detachment niches of the Flims (left) and Tamins landslides. Figure width approx. 20 km.*

In concert with radiocarbon dating, cosmogenic nuclide results have led to the abandonment of the hypothesis that most of the biggest landslides in the Alps took place right after the decay of the large valley glaciers at the end of the Last Glacial Maximum about 19 ka ago.

Fig. 1: *Photo of the accumulation (left center) and detachment (sharp ridge line) of the Köfels landslide (Tyrol, Austria). Photo: C. Prager.*

The ages of several of the largest landslides, Flims (volume 9-10 km^3), Kandertal, Köfels (volume 2-3 km^3), point to a focus of slope instability at the beginning of the Holocene. This is likely related to the marked climate change to significantly warmer and somewhat wetter conditions around 10 ka BP.

[1] S. Ivy-Ochs et al., Geomorph. 103 (2009) 104
[2] C. Prager et al., Geomorph. 103 (2009) 93

[1] *also Geography, University of Zürich*
[2] *Geography, University of Innsbruck, Austria*
[3] *Geology, University of Bern*

A TOOL TO RECONSTUCT ROCK FALL HISTORY?

Comparison of surface color and exposure ages at Aiguille du Midi (F)

R. Böhlert[1], S. Gruber[1], M. Egli[1], M. Maisch[1], D. Brandovà[1], S. Ivy-Ochs[2], P.W. Kubik, P. Deline[3], W. Haeberli[1]

To put into perspective modern observations of rock fall which may potentially be caused by permafrost thaw, information on past rock fall activity is required. Here we present exposure dating results for near vertical granite rock walls together with a first analysis of spectral signatures and their relation to the age of the surfaces dated [1].

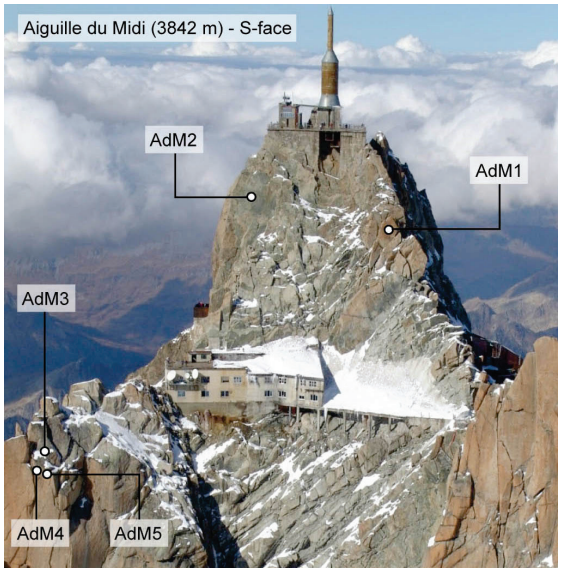

Fig. 1: *Sampling spots at Aiguille du Midi.*

We analyzed four samples from different sites near the summit of Aiguille du Midi in the Mont Blanc area using in situ produced ^{10}Be (Fig. 1). Assuming that intensively red colored parts in the rock wall were exposed to weathering over a longer time period, we chose the sampling sites on the basis of visually identifiable differences in color.

Results of ^{10}Be dating were corrected for topographic shielding. No correction was made for erosion or snow cover (slope angles were ≥ 79°). Spectral reflectance of each dated rock sample and of an additional piece of fresh rock was measured using a spectro-radiometer. Furthermore, the chemical composition of the samples was determined by X-ray fluorescence.

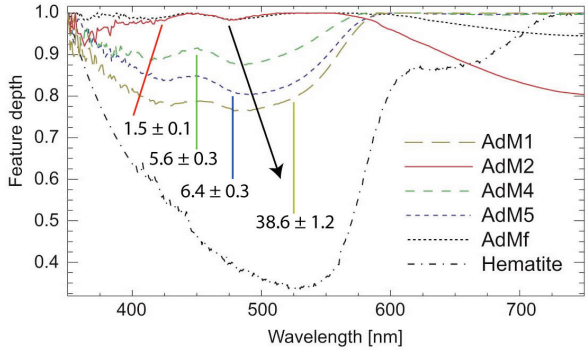

Fig. 2: *Continuum removed spectra and corresponding surface ^{10}Be exposure ages (ka). The arrow indicates the influence of the Fe-oxide content with age. AdMF = fresh, unweathered material.*

The rock surface exposure ages varied between less than 2000 years and almost 40,000 years, which is a remarkably high age (Fig. 2). We found a clear correlation between age and surface reflectance behavior in the range of ≈ 415-650 nm. These findings may be a first step towards a possibility of generating age distribution data in steep rock walls. The strong correlation between the two methods means that at least in Late Quaternary-aged high alpine surfaces (with comparable lithology) the redness is a direct indication of exposure time to weathering. Dating of rock walls therefore may be a tool to help to reconstruct rock fall activity history.

[1] R. Böhlert et al., Proc. Ninth Internat. Conf. on Permafrost (2008) 143

[1] *Geography, University of Zurich*
[2] *also Geography, University of Zurich*
[3] *Laboratoire EDYTEM, University of Savoy, France*

TESTING DUAL-COSMOGENIC ISOTOPE BURIAL DATING

Dating of Plio-Pleistocene sediments from the Lower Rhine Embayment

A. Dehnert[1], O. Kracht[1], F. Preusser[1], N. Akçar[1], H.A. Kemna[2], P.W. Kubik, C. Schlüchter[1]

The dating of terrestrial sediments over long time periods is often very imprecise and sometimes even impossible using available methods. The method of burial dating with *in situ* produced cosmogenic nuclides, however, is applicable to quartz bearing sediments and has the potential to improve the general dating issue in the Quaternary. Burial dating utilizes the different decay rates of previously produced cosmogenic nuclides to identify the duration of burial and dates the time since nuclide production has been significantly lowered or even ceased. Using ^{10}Be and ^{26}Al, this dating method has a useful range of a few 100 ka up to 5 Ma.

Being an area of subsidence, the Lower Rhine Embayment (LRE) in north-western Germany represents one of the most complete archives of Cenozoic continental and shallow marine deposits in Europe. It forms the north-western part of the European rift system extending throughout the European continent from south to north. Marine sedimentation prevailed over most of the LRE during the Neogene followed by fluvial deposition by the Rhine, Meuse and smaller Belgian rivers from the end of the Miocene. For this dating test, two sites have been selected (Fig. 1). The 'Weilerswist' site (WW) in the south of the LRE comprises the Pliocene Kieseloolite Formation and the Middle Pleistocene Upper Terrace Formation. The 'Hoher Stall' site (HS), c. 75 km to the north-west of WW, involves the Early Pleistocene Waalre Formation and again the Upper Terrace formation. At WW, the sampled depth profile ranges from 3 to 37 m below the surface, while at HS the sampled profile reaches only 16 m below the surface. The samples were processed in Berne and measured with the ETH TANDEM AMS facility.

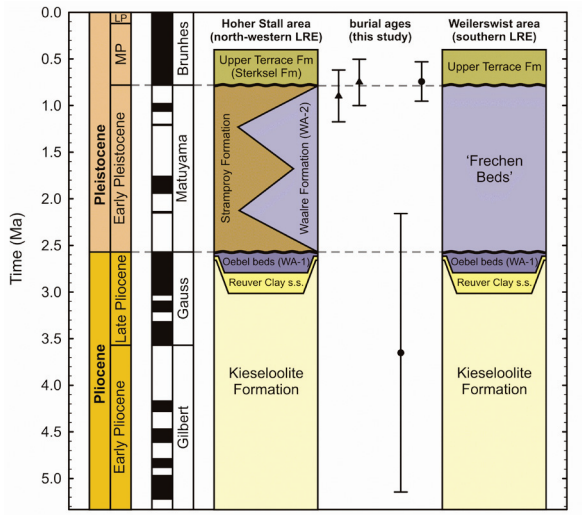

Fig. 1: *Generalized overview of lithostratigraphic sequences studied in the areas of the Lower Rhine Embayment, Germany. Triangles represent obtained burial ages from the 'Hoher Stall' site, while filled circles show dating results from 'Weilerswist'.*

A coupled iterative modeling-parameter estimation approach was developed and used to identify the unknown parameters of interest (e.g. burial age, on-site terrace erosion rate, and inheritance nuclide concentration). This optimization approach yields the first numerical deposition ages of the sampled sediment sequences. These ages are evaluated as reliable, as they reproduce the existing chronological framework of the LRE. The additionally performed sensitivity analysis showed a major improvement potential, when sampling shallower material (e.g. 3-5 m profile depth).

[1] *Geology, University of Bern*
[2] *Geology and Mineralogy, University of Cologne, Germany*

A NEW VIEW OF ALPINE EROSION

^{10}Be-derived rates of stochastic and diffusive erosion in the Alps

K.P. Norton[1], F. von Blanckenburg[2], P.W. Kubik

Denudation rates of small tributary valleys in the upper Rhone valley of the Swiss Central Alps vary by more than an order of magnitude within a very small distance (tens of km). Morphometric data indicate that two distinct erosion processes operate in these steep mountain valleys. We determined the rates of these processes using cosmogenic ^{10}Be in pooled soil and stream sediment samples. Denudation in deep, glacially scoured valleys is characterized by rapid, non-uniform processes, such as debris flows and rock falls (Fig. 1).

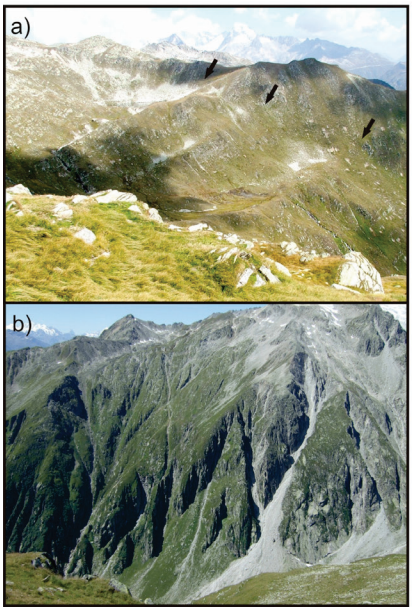

Fig. 1: *a) Soil mantled slopes with faults (indicated by arrows). b) Glacially scoured basins with alternating debris flows and soil mantled slopes.*

In these steep valleys denudation rates are 760-2100 mm/ky (Fig. 2). In those basins which show minimal previous glacial modification denudation rates are low (60-560 mm/ky). The denudation rate in each basin represents a binary mixture between the rapid, non-uniform processes, and soil creep. The soil production rate measured with cosmogenic ^{10}Be in soil samples averages at 60 mm/ky (Fig. 2).

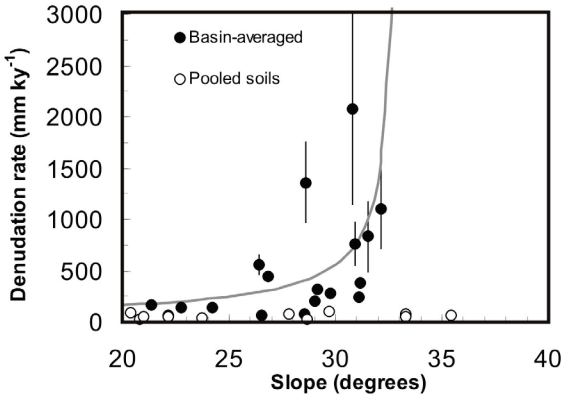

Fig. 2: *Denudation rates plotted against mean hill-slope for both basin-averaged sediment samples (filled circles) and amalgamated soil samples (open circles).*

Mixing calculations suggest that the debris flows and rock falls are occurring at rates up to 3000-7000 mm/ky. These very high rates occur in the absence of baselevel lowering, since the tributaries drain into the Rhone trunk stream upstream of a knickzone. The flux-weighted spatial average of denudation rates for the upper Rhone valley is 1400 mm/ky, which is similar to rock uplift rates determined in this area from leveling. The pace and location of erosion processes are determined by the oscillation between a glacial and a non-glacial state, preventing the landscape from reaching equilibrium.

[1] K.P. Norton, F. von Blanckenburg and P.W. Kubik, Earth Surface Processes and Landforms (2010) in press

[1] *Geology, University of Bern*
[2] *German Geoscience Research Center GFZ, Potsdam, Germany*

EROSION RATES IN THE HÖRNLI AREA

Cosmogenic catchment-wide denudation rates in the Hörnli area

F. Kober[1], S. Ivy-Ochs[2], L. Abbühl[3], M. Dürst[3], F. Schlunegger[3], P.W. Kubik

Although the landscape of the Hörnli region in NE Switzerland would, at first glance, imply that landscape processes and process rates must be different between the fluvially and glacially overprinted landform parts, there is no strong evidence for this argument in geomorphic parameters such as relief, slope, hypsometry or catchment size. It is also difficult to differentiate the two landscape types based on spatially averaged catchment-wide denudation rates obtained with cosmogenic ^{10}Be.

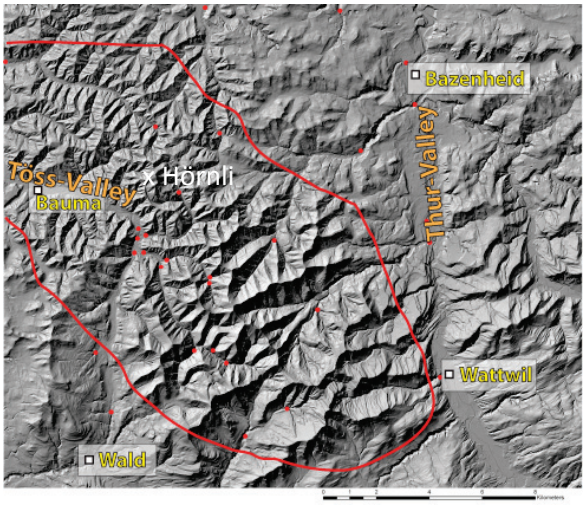

Fig. 1: *The Hörnli region in NE Switzerland. The fluvially shaped landscape is within the red line, outside is glacially modified landscape. Red points indicate sampling sites for cosmogenic nuclides*

While glacially overprinted catchments (glaciated during the Last Glacial Maximum between 28 and 19 ka) tend to have lower average slopes and are at lower mean elevations, other parameters fail to show correlations. Slope-area plots suggest partial rejuvenation for glacially modified catchments, i.e., incision into accumulation planes (terraces) in the lower river courses. This is also in accordance with observed knickpoints which are beyond the commonly lithologically controlled channel steps (Nagelfluh benches) that are observed everywhere. Spatially averaged ^{10}Be catchment-wide denudation rates vary between 30-2000 mm/ky with a tendency towards lower values in catchments with a glacial overprint, though this is not always the case.

One possibility is that glacially overprinted catchments with smoother topographies and abundant glacial deposits in their lower reaches protect the landscape against faster erosion rates. Another option would be that glacially sourced sediments of the catchment after having been exposed for nearly 20,000 years have relatively higher cosmogenic nuclide concentrations thus lower denudation rates. In contrast, the fluvial catchments which have steeper slopes that reach to higher elevations than the glaciated catchments are controlled by more active processes. These include shallow landsliding, rock falls, debris flows (also reflected in limited soil development) which promote shorter residence time in the catchment, hence higher denudation rates.

As such it is suggested, that the remnants of the glacial overprinting, i.e., sculpting of landforms and deposition of glacial deposits, has a profound impact on present day landscape denudation rates. Further investigation will shed light on these first results.

[1] *Geology, ETHZ*
[2] *also Geography, University of Zurich*
[3] *Geology, University of Bern*

EROSION RATES FROM THE EASTERN ALTIPLANO

Studying erosional processes by using *in situ* ^{10}Be and ^{26}Al

K. Hippe[1], F. Kober[1], G. Zeilinger[2], S. Ivy-Ochs[3], P.W. Kubik, C. Maden[1], R. Wieler[1]

The Andes Mountains are a key area for studying the interactions between climate, erosion and tectonics on topographic evolution at the orogen scale. However, to test the various geodynamic models the erosional history of the mountains must be quantified independently. While absolute erosion rates are known for the Eastern and Western Cordillera, few data exists on erosional processes and rates on the large, internally drained, high-elevation Altiplano plateau. We investigate the Late Quaternary erosional history of the eastern Altiplano, Bolivia, based on paired terrestrial cosmogenic nuclide analyses (^{10}Be and ^{26}Al).

Fig. 1: *Sampling site on the eastern Altiplano, view upstream towards east. The landscape typically shows a smooth and flat relief. Channels are often temporarily waterless.*

The eastern margin of the Bolivian Altiplano is a flat, low-relief landscape with erosion dominated by diffusive hillslope and eolian processes. Low precipitation with a strong interannual variability causes episodic fluvial transport of sediment in often small, ephemeral channels. Fig. 1 gives an impression of the geomorphology in the sampling area.

For 13 river sediment samples collected from catchments along the Altiplano margin, catchment wide denudation rates have been derived from ^{10}Be and ^{26}Al concentrations. Based on ^{10}Be, these are very low, < 30 mm/kyr. ^{26}Al data indicate also low, though slightly higher single-catchment wide denudation rates. In combination with ^{10}Be, this suggests a complex exposure history with a significant component of sediment storage.

Results agree with geomorphological observations of (a) very low slopes, (b) low relief and (c) transient river channels that might account for locally and/or temporarily ineffective erosional and transport processes on the eastern Altiplano. Inter-catchment comparison shows a positive correlation between catchment wide denudation rates and geomorphometric catchment parameters, but also further influence by lithology and anthropogenic interferences.

The slow and complex erosion transport processes on the Altiplano differ significantly from those of the neighboring Rio La Paz basin and the Eastern Cordillera, which also corresponds to dramatic changes of geomorphological parameters across the drainage divide.

[1] *Geology, ETHZ*
[2] *Geosciences, University of Potsdam, Germany*
[3] *also Geography, University of Zürich*

^{10}Be-BASED DENUDATION RATES IN FORELAND BASINS

Assessing the effects of sediment storage on TCN concentrations

H. Wittmann[1], F. v. Blanckenburg[1], J.L. Guyot[2], L. Maurice[3], P.W. Kubik

Terrestrial cosmogenic nuclides (TCN) in detrital material are routinely used to determine mountain erosion and weathering rates. Our research however focuses on the complex, non-steady state settings of depositional floodplains, where TCN concentrations and respective denudation rates inherited from a sediment-providing area may change during storage in these basins. For this purpose, we designed a nuclide-based mixing model that is floodplain depth- and also residence time-dependent, so that changes in nuclide concentrations due to deep floodplain burial or long-term sediment storage are predicted. The model was tested in several river systems, such as the large (70'000 km^2) Beni basin in Bolivia, which is a foreland basin with vast flooded areas and enormous deposition of sediment eroded in the Andes [1].

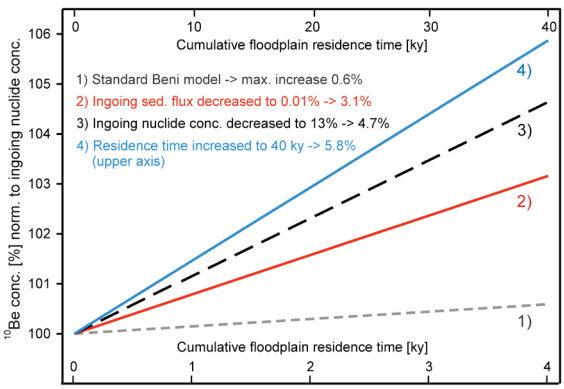

Fig. 1: *Beni River model results.*

Floodplain sediment residence times are ≈4 kyr [2] as the Beni is a rapidly migrating river (≈15 m/yr) [3] with a modern Andean sediment load of 220 Mt/yr entering the floodplain [1]. For these parameters, our model [4] predicts a ^{10}Be concentration change of only 0.6% (see Fig. 1), an increase that is not resolvable analytically. Our model results suggest that long-lived TCN concentrations inherited from the source areas are not changed during floodplain storage. ^{10}Be measurements in the Beni floodplain relative to the nuclide concentration measured at the Andean outlet (see Fig. 2) confirm these predictions. Resulting calculated basin-wide denudation rates are at any point in the floodplain very similar to the denudation rate of the Andean part of the basin [5], suggesting that cosmogenic nuclides are the method of choice for tracing denudation signals over long floodplain distances despite sediment storage. In other words, samples taken at the floodplain outlet provide spatially- and temporally-integrated rates of Andean erosion processes.

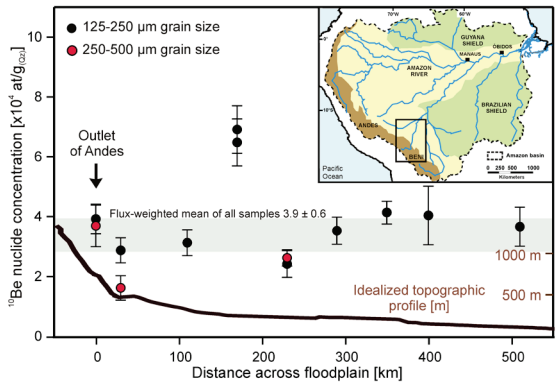

Fig. 2: *Beni River nuclide concentration data in lowlands (see topographical profile) is similar to those measured at Andean outlet.*

[1] J.L. Guyot et al., IAHS Publication (1996) 55
[2] A. Dosseto et al., EPSL 248 (2006) 759
[3] E. Gautier et al., ESPL 32 (2007) 230
[4] H. Wittmann and F. von Blanckenburg, Geomorphology 109 (2009) 246
[5] H. Wittmann et al., EPSL 288 (2009) 463

[1] *Mineralogy, University of Hannover (now GFZ Potsdam), Germany*
[2] *IRD, Lago Sul, Brazil*
[3] *IRD/ LMTG, University of Toulouse, France*

DENUDATION RATES FROM FAULT FOOTWALLS

Decoupling of erosion and fault activity

A. Densmore[1], R. Hetzel[2], S. Ivy-Ochs[3], W. Krugh[4], N. Dawers[5], P.W. Kubik

We test the spatial correspondence between rock uplift in active normal fault footwalls and catchment-averaged denudation rates using cosmogenic radionuclide (CRN) [1]. We focus on two faults: the single-segment Sweetwater fault (18 km long) in Montana (USA), with rock uplift rates of 40-100 mm kyr^{-1}; and the Wassuk fault (130 km long) in Nevada USA), with a rock uplift rate of ~900-1100 mm kyr^{-1}. For the Sweetwater fault, footwall relief is largely inherited, and denudation rates are only partly reflective of fault displacement (Fig. 1A). For the Wassuk fault, all inherited topography has been removed by erosion, but denudation rates show little along-strike consistency (Fig. 1B).

In the early stages of fault growth, CRN-derived denudation rates reflect inherited pre-faulting relief, with an overprint of fault-controlled erosion. Later rates are decoupled from fault displacement through stochastic landsliding events, and longer-term measures of denudation may provide a better record of spatial variations in rock uplift (Fig. 1B).

Our results raise an intriguing question: if CRN-derived denudation rates are partly decoupled from fault displacement at the onset of fault growth due to inherited topography, and are decoupled later due to mass wasting, are such rates ever properly reflective of underlying rock uplift rates? A major issue is the temporal variation in slip rates across the earthquake cycle compared with the time interval over which the CRN-derived rates are averaged. The CRN integration time for the Wassuk Range samples is 1-6 kyrs, comparable to the recurrence interval of large Holocene earthquakes. Because the CRN-derived rates are not sampled over repeated earthquakes, they are unlikely to show a simple relationship to rock uplift rates averaged over longer time scales, even in the absence of stochastic erosion.

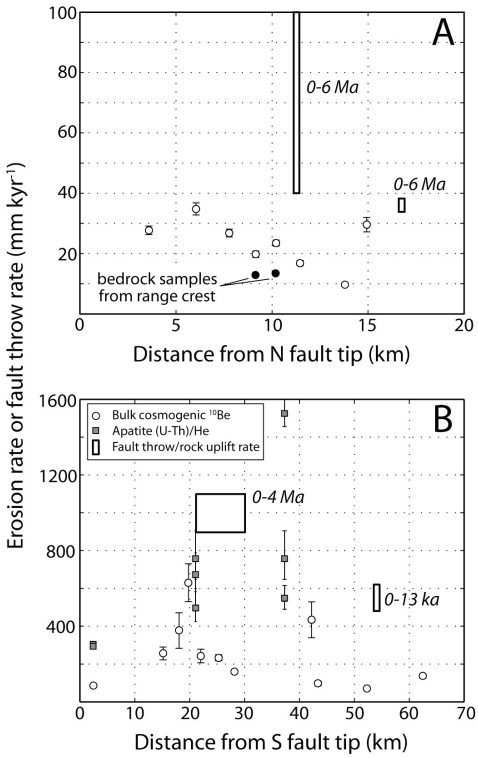

Fig. 1: *^{10}Be-derived denudation rates in the (A) Sweetwater footwall with minimum footwall rock uplift rates since 6 Ma (boxes). Catchment-averaged rates (o), bedrock rates (•) (B) Wassuk Range with (1) fault throw rate since ~13 ka (narrow box), (2) long-term footwall rock uplift rate since 4 Ma (large box), and (3) long-term denudation rates estimated from Apatite/He samples (squares).*

[1] A. Densmore et al., Geology 37 (2009) 1139

[1] *Geography, Durham University, Great Britain*
[2] *Geology-Paleontology, University of Münster, Germany*
[3] *also Geography, University of Zurich*
[4] *Geology, University of Wyoming, USA*
[5] *Earth and Environmental Sciences, Tulane University, USA*

BUILDING STONES IN HATTUSHA (HITTITE EMPIRE)

First results from cosmogenic ^{36}Cl

N. Akçar[1], S. Ivy-Ochs[2], V. Alfimov, İ.Ö. Yılmaz[3], A. Schachner[4], D. Altıner[3], V. Yavuz[5], C. Schlüchter[1]

Hattusha (Boğazköy, Turkey) was the capital of the Hittite Empire which lasted from about 1650/1600 to 1200 BC. At Yenicekale, Hittite masons flattened the summit of an outcropping limestone knoll to form an artificial platform as the foundation for a building. Next, they built a circuit wall along the lateral precipices of the flattened bedrock platform. We have measured ^{36}Cl in one sample from the limestone bedrock platform and two samples from limestone building blocks of the circuit wall (Fig. 1) [1].

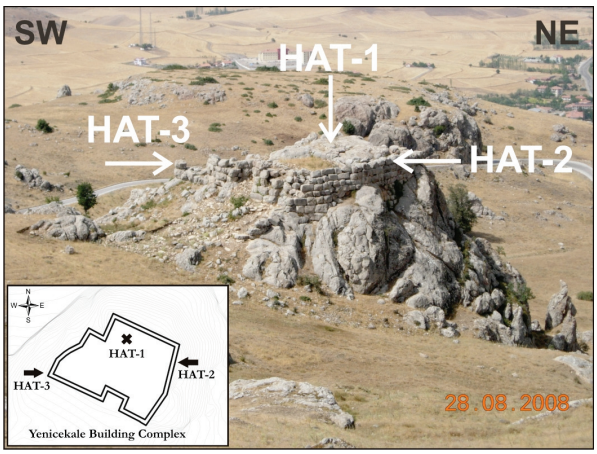

Fig. 1: *Sampling locations at Yenicekale.*

Our results show that the sampled surfaces contain significant inherited cosmogenic ^{36}Cl and we cannot directly determine exposure ages for the building complex based on these three samples. In contrast, we were able to determine how much rock was removed from the platform during flattening by modeling the variation of ^{36}Cl production with depth using the results from the bedrock sample (Fig. 2). We conclude that the Hittite masons removed only around 3 m from the top of the limestone bedrock knoll. This means that they did not gain enough rock from this flattening to make the structure which stood on top of the knoll. In agreement with this, the first results of our detailed microfacies analysis indicate that many of the building blocks are not of the same limestone facies as the underlying bedrock and must have been quarried elsewhere.

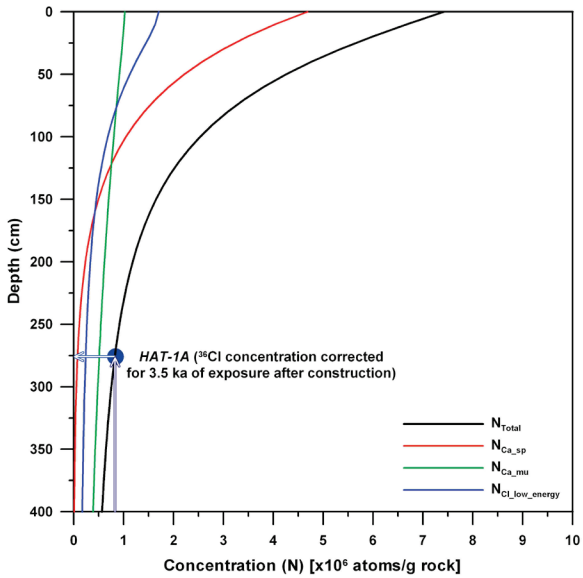

Fig. 2: *Variation of ^{36}Cl concentration with depth for bedrock sample HAT-1A at Yenicekale based on an infinite exposure (more than several Ma) with constant erosion at a rate of 5 mm/ka.*

[1] N. Akçar et al., Quat. Geochron. 4 (2009) 533

[1] *Geology, University of Bern*
[2] *also Geography, University of Zurich*
[3] *Middle East Technical University, Ankara, Turkey*
[4] *German Archaeological Institute, Istanbul, Turkey*
[5] *Istanbul Technical University, Turkey*

^{36}Cl PRODUCTION IN LIMESTONES AND DOLOMITES

Chlorine-rich or subsurface samples have more uncertainties

V. Alfimov, S. Ivy-Ochs[1]

We have evaluated the available ^{36}Cl production rate calibrations from Ca by fast neutron spallation and concluded that the production rate of Stone et al. [1] (P_{sp} = 48.8±1.7 atoms ^{36}Cl /g_Ca/yr) should be used for ^{36}Cl calculations in limestone and dolomite. The usefulness of the other available production rates is greatly reduced because of the assumptions made to calculate the non-negligible production of ^{36}Cl from stable chlorine by thermal neutrons (^{35}Cl(n,γ)^{36}Cl). The samples used by Stone et al. had negligible concentrations of chlorine making the calculations independent of those assumptions. Figure 1 shows the relative contribution of thermal neutron capture. It is also a handy diagram for the geologist to estimate the thermal neutron effect before measuring major and trace elements.

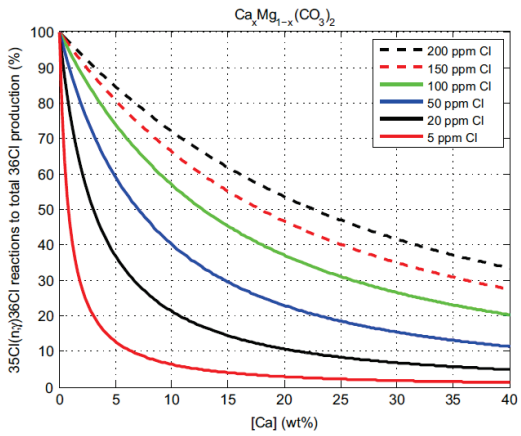

Fig. 1: *The contribution of ^{35}Cl(n,γ)^{36}Cl reactions to the total ^{36}Cl production as a function of Ca content in $Ca_xMg_{1-x}(CO_3)_2$ for 5–200 ppm Cl at sea-level and high geomagnetic latitude*

The presently accepted ^{36}Cl production rate from thermal neutrons [2] is based on the thermal neutron flux that was derived by fitting all 3 production processes (Ca spallation, muon capture on Ca and thermal neutron capture by ^{35}Cl). Based on the measurements of thermal neutron fluxes by Liu et al. [4], we developed a new and independently calibrated production parameter for thermal and epithermal neutrons (Pepi = 760±150 neutrons/g_air/yr) [3]. The high uncertainty, however, reduces its usefulness for chlorine-rich samples.

Currently, two different stopped muon production rates [1, 4] are available. There is no good reason to prefer one over the other. This results in an increased uncertainty of ^{36}Cl production with depth (Fig. 2).

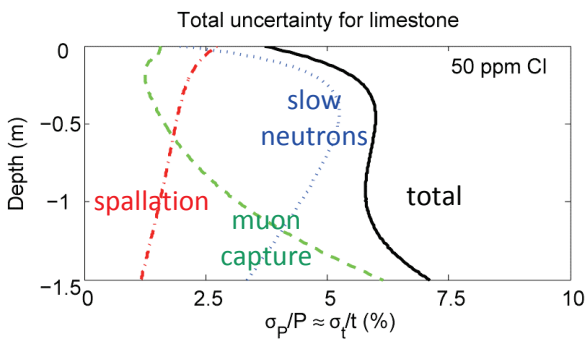

Fig. 2: *The relative uncertainty in calculated ^{36}Cl production as a function of depth in limestone from Ca spallation [1], muon capture on Ca [3, 4, 5] and our low-energy neutron capture calculation (50 ppm Cl), no erosion, and an exposure of <50kyr.*

[1] J. Stone et al., Geochim. Cosmochim. Acta 62 (3) (1998) 433

[2] F.M. Phillips et al., Chem. Geology 175 (3–4) (2001) 689

[3] V. Alfimov and S. Ivy-Ochs, Quat. Geochron. 4 (2009) 462

[4] B. Liu et al., Water Resources Res. 30 (1994) 3115

[5] B. Heisinger et al, Earth and Planet. Sci. Lett. 200 (3–4) (2002) 357

[1] *also Geography, University of Zurich*

ICE AND OCEAN SEDIMENTS

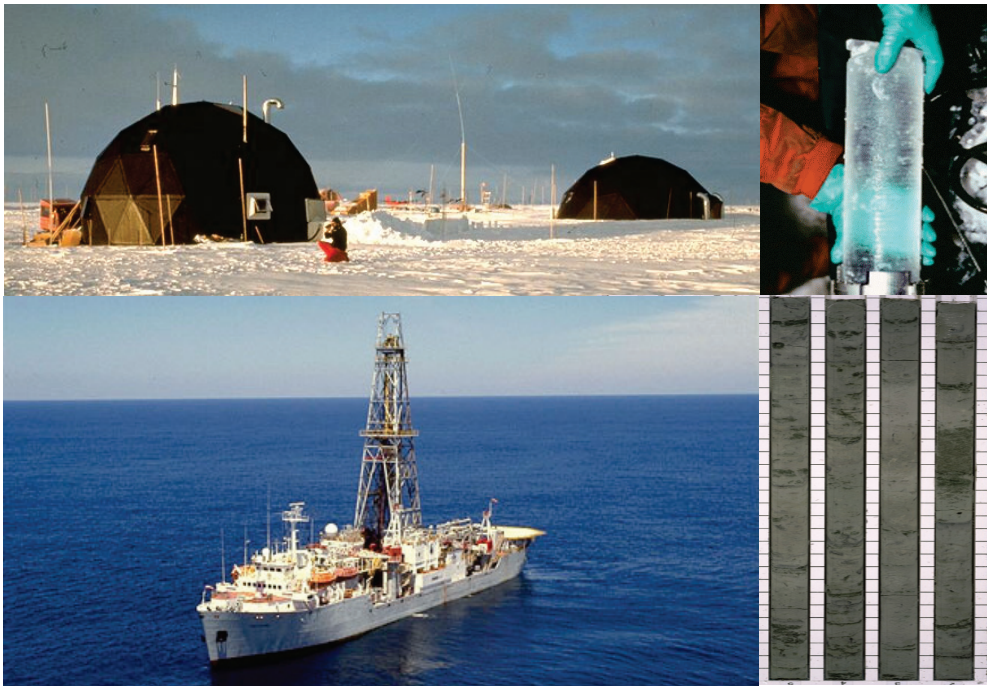

Past and future solar activity

Solar irradiance since the Maunder Minimum

^{36}Cl in permafrost ice from Sibiria

Carrier free ^{10}Be/^{9}Be measurements at the TANDY

^{231}Pa/^{230}Th off West Africa

PAST AND FUTURE SOLAR ACTIVITY

Potential of ^{10}Be to constrain solar dynamo theories

J. Abreu[1], F. Steinhilber[1], J. Beer[1], M. Mann[1], M. Christl, P.W. Kubik

Our knowledge of solar activity was until recently mainly based on the sunspot record, which has been observed since 1610, shortly after the telescope was invented. Cosmogenic radionuclides such as ^{10}Be measured in ice cores can be used to trace back changes in the open magnetic field of the Sun for many thousands of years revealing unprecedented information on the history of solar activity. Fig. 1 shows the solar modulation potential ϕ, a measure of the solar open magnetic field, reconstructed from ^{10}Be in the GRIP ice core [1]. This record extends back for almost 10'000 years showing many grand maxima and minima.

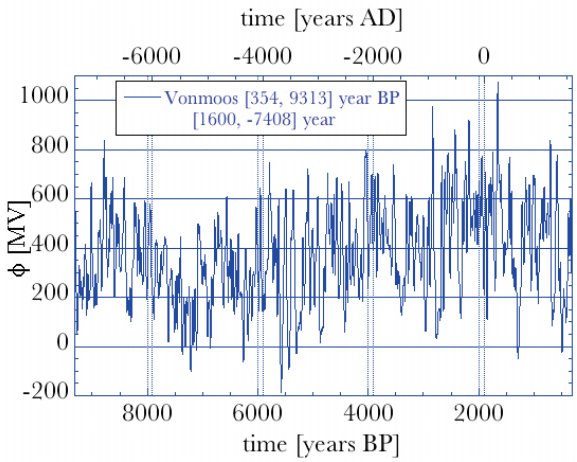

Fig. 1: *Time series for the solar modulation potential ϕ reconstructed from the ^{10}Be data in the GRIP ice core.*

We have used the information contained in that record to answer the question: can we predict the next grand minimum in solar activity?

Fig. 2 shows the distribution of the variable m (waiting time between grand minima). The question above can be answered by fitting appropriate statistical distributions to **m**. We found that the best fit is provided by a gamma distribution. Based on this distribution we computed the life expectancy of **m.** As a result, we expect a grand minimum in solar activity to occur around the year 2100 AD [2].

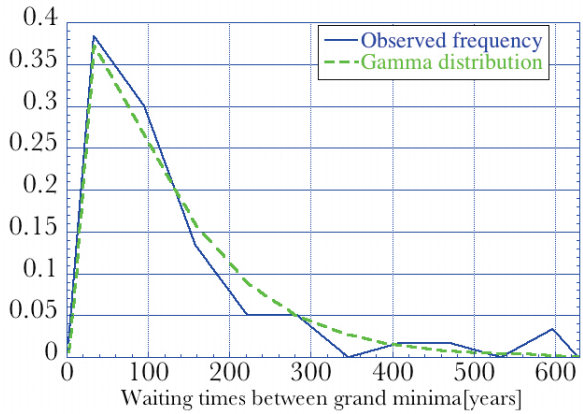

Fig. 2: *Binned distribution for waiting times between grand minima. Superimposed is the fitted gamma distribution (green).*

The origin of the solar activity is ascribed to a hydrodynamic dynamo operating at the base of the convection zone. The understanding of the processes taking place below the solar surface is mainly inferred from theoretical models. The record of solar activity (Fig. 1) provides a number of constraints that a realistic solar dynamo model must fulfill. Some examples are:

(i) Spectral analysis reveals significant periodicities around 2300 y (Hallstatt), 980 y (Eddy), 207 y (de Vries) and 90 y (Gleissberg),

(ii) Grand minima tend to occur in clusters,

(iii) The distribution of grand minima follows a gamma distribution (Fig. 2).

[1] M. Vonmoos, J. Beer and R. Muscheler, J. Geophys. Res. 111 (2006) A10105
[2] J. Abreu et al, Astrophys. J. (2010) subm.

[1] *Swiss Federal Institute of Aquatic Science and Technology, Dübendorf*

SOLAR IRRADIANCE SINCE THE MAUNDER MINIMUM

^{10}Be from ice cores provides the key to past solar irradiance

F. Steinhilber[1], J. Abreu[1], J. Beer[1], M. Mann[1], M. Christl, P.W. Kubik

The Sun is a variable star that drives the climate system of Earth. From the sunspot record (Fig. 1a) it is known that solar activity was generally lower during the 17th and 18th century than today. In particular, the period 1645-1715 (Maunder Minimum) is characterized by an almost complete absence of sunspots, i.e. low solar activity. This period is part of the so-called Little Ice Age, a period of cold climate conditions lasting from about 1350 to 1850. It raises the question of the role of solar influence in past, present, and future climate changes. When talking about solar activity we mean here the total solar irradiance (TSI), also known as solar constant.

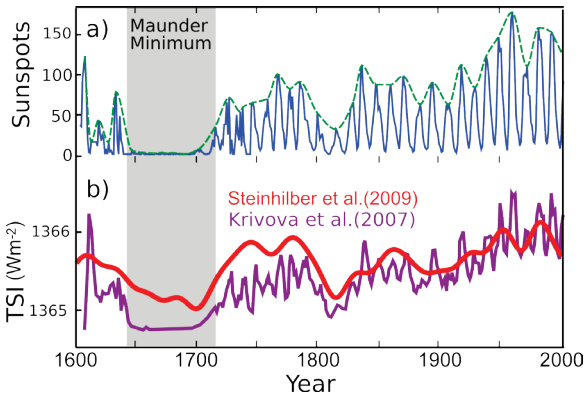

Fig. 1: *a) 400-year long record of group sunspot numbers. b) Comparison of TSI reconstructions [1, 3].*

In order to establish the relationship between TSI variability and past climate changes, first, it has to be known how much TSI has changed in the past, and second, how the Earth climate system has responded to such changes.

The response of the climate system can be obtained with climate models using TSI as input. Due to atmospheric disturbances, measurements of TSI are only possible with space-based instruments. Such measurements have only begun in 1978, and thus reconstructions are needed for periods prior to this time. We used the cosmogenic radionuclide ^{10}Be from polar ice cores to reconstruct TSI [1].

^{10}Be is a proxy for cosmic ray intensity, which is modulated by solar activity, i.e. the open solar magnetic field. The stronger the open magnetic field, the fewer cosmic rays can reach the Earth leading to a lower ^{10}Be production. By combining the physical relation-ship between ^{10}Be, cosmic ray intensity, and the open magnetic field [1] with a recent calibration between TSI and the open magnetic field [2] we obtained TSI for the past 9300 years. Our result (Fig. 1b) is compared with a sunspot-based reconstruction [3].

The long-term behavior of both curves is very similar, but there are differences. First, using sunspots allows a modeling of the 11-year cycle variation in TSI, which has not been possible with the smoothed ^{10}Be data used in our work. But we hope to do this in future applying our model to annually resolved ^{10}Be data. Second, the sunspot-based models are restricted to the past 400 years of sunspot observations. Our model, however, allows reconstructing TSI at least for 10,000 years back in time, if radionuclide records for ^{10}Be or ^{14}C exist.

[1] F. Steinhilber, J. Beer and C. Fröhlich, Geophys. Res. Lett. 36 (2009) L19704
[2] C. Fröhlich, Astron. & Astrophys. 501 (2009) L27
[3] N.A. Krivova, L. Balmaceda and S.K. Solanki, Astron. & Astrophys. 467 (2007) 335

[1] *Swiss Federal Institute of Aquatic Science and Technology, Dübendorf*

^{36}Cl IN PERMAFROST ICE FROM SIBERIA

Can the ^{36}Cl/Cl ratio be used for an absolute chronology of permafrost?

A. Blinov[1], V. Alfimov, J. Beer[2], D. Gilichinsky[3], L. Schirrmeister[4]

The potential of permafrost as a natural archive makes the development of a permafrost chronology an essential objective of geological, climatological and paleoecological studies. The recently proposed method [1] to use the long-lived cosmogenic radionuclide chlorine-36 (^{36}Cl) for this purpose could offer an absolute dating range of up to one million years, far beyond the fifty-sixty thousand years for radiocarbon.

We have measured ^{36}Cl and chloride (Cl^-) concentrations in samples from different horizons of Quaternary permafrost collected from the west and the north coasts of Cape Svyatoy Nos and Oyogos Yar, and on the southern coast of Bol'shoy Lyakhovsky Island (northeastern Siberia). During fieldwork a volume of 2 l of the initial sample was melted and shipped to a laboratory for follow-up analysis. Chloride concentrations were measured in filtered aliquots using ion chromatography. Measurements of ^{36}Cl/Cl ratios were carried out at the TANDEM facility. The ^{36}Cl/Cl ratios in 32 samples ranged from $2.4 \cdot 10^{-14}$ to $1.4 \cdot 10^{-12}$ [2].

The chloride concentrations and ^{36}Cl/Cl ratios in permafrost both exceed the values measured for modern snow and river water. Nonetheless, excluding several extreme values, the ^{36}Cl/Cl ratios provided a local permafrost chronology which is shown in Fig. 1. The general concordance of the determined ages with geological expectations and alternative chronological methods supports the potential power of the proposed dating method. At the same time, the large observed change in ratios from higher to lower values during the transition from Last Glacial Maximum to Holocene climatic conditions remains still unexplained. Our initial assumption that the ^{36}Cl/Cl ratio, which is averaged by nature over a thousand-year interval of constant climatic conditions and fixed in the permafrost ice, is insensitive to changes in the supply of surface water. However, this assumption could be violated by eroded dust or sea-salt aerosol input that may have altered the local balance.

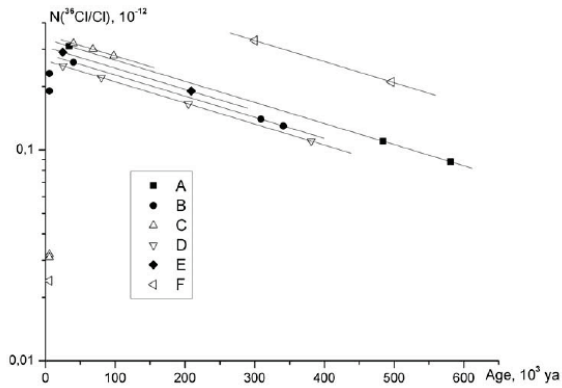

Fig. 1: *Local permafrost chronologies: site A, Cape Svyatoy Nos; site B, Bol'shoy Lyakhovsky Island; site C, Oyogos Yar coast; site D, Khaptashinsky Yar; site E, Allaikha River; site F, Bol'shoy Khomus Yuryakh River.*

Further ^{36}Cl/C time series measurements of modern precipitation and fossil permafrost ice are needed to possibly make the proposed dating method into a practical tool with a clear protocol.

[1] D.A. Gilichinsky et al., Quat. Sci. Rev. 26 (2007) 1547.

[2] A.V. Blinov et al., Geochem. Geophys. Geosyst. 10 (2009) Q0AA03.

[1] *St. Petersburg Polytechnic University, Russia*
[2] *Swiss Federal Institute of Aquatic Science and Technology, Dübendorf*
[3] *Institute of Soil Science, Russia*
[4] *Alfred Wegener Institute, Germany*

CARRIER FREE $^{10}Be/^{9}Be$ MEASUREMENTS AT THE TANDY

The $^{10}Be/^{9}Be$ signature of the last geomagnetic field reversal

J. Lachner, M. Christl

Marine sediments can be used to reconstruct ^{10}Be production changes caused by variations of the geomagnetic field strength. Here we use the authigenic $^{10}Be/^{9}Be$ ratio as a proxy for geomagnetic paleointensity. The global signature of an excursion or a magnetic field reversal seen in the $^{10}Be/^{9}Be$ ratio can be used to connect the chronologies of ice cores, marine and terrestrial sediments.

Fig. 1: *ODP Sites sampled for the project.*

Five sediment cores from the ODP drilling program (Fig. 1) were selected for sampling (Sites 769: Sulu Sea, 983: North Atlantic, 1021: Outer Delgada Fan, 1063: Bermuda Rise, 1090: Southern Ocean). Primary selection criteria were a broad geographical distribution, the availability of good magneto-stratigraphic data, and a relatively high sedimentation rate.

The direct measurement of the natural $^{10}Be/^{9}Be$ ratio in the sediments (without the addition of ^{9}Be carrier material) was performed on the compact 0.6 MV accelerator TANDY. The new method simplifies the determination of the $^{10}Be/^{9}Be$ ratio in natural samples, because only a single measurement is required.

One challenge of the carrier-free AMS method is to avoid any contamination of the samples with stable ^{9}Be during the chemical preparation, and in particular during the leaching procedure that tries to attack only the authigenic Be of the sediments and should leave the detrital Be untouched. Chemistry blank samples, which monitor the possible contamination with ^{9}Be and ^{10}Be during chemical processing, were produced together with every sample series (i.e. 8 samples + 1 blank). Currently, the full process blanks produce currents of only few tens of pA, while samples from marine sediments have several hundreds of pA. ^{10}Be introduced during chemistry and target preparation is negligible.

First results (Fig. 2) from ODP Site 1021 (blue dot in Fig. 1) show a $^{10}Be/^{9}Be$ peak at the depth where the last magnetic field reversal (Brunhes/Matuyama reversal about 780 kyr ago) was recorded in the magneto-stratigraphic data [1].

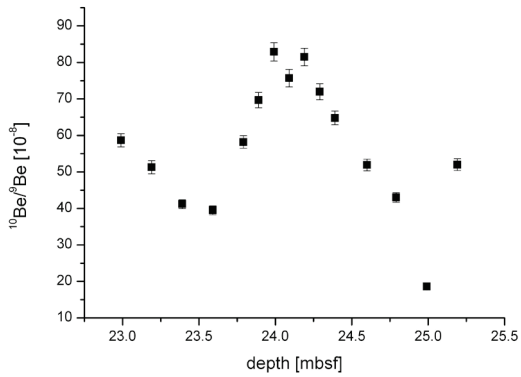

Fig. 2: *Preliminary data from Site 1021, where the Brunhes-Matuyama reversal is expected at about 24 mbsf (meter below sea floor).*

[1] M. Lyle, I. Koizumi and C. Richter, Proc. of ODP, Initial Reports 167 (1997)

^{231}Pa/^{230}Th OFF WEST AFRICA

A proxy for water-mass upwelling

M. Christl, A. Hofmann[1], J. Lippold[1]

Recently, it has been shown that femtogram amounts of ^{231}Pa can be precisely determined with the compact AMS system TANDY [1]. Here we show the first ^{231}Pa profile of core GeoB3722 measured with this facility (Fig. 1).

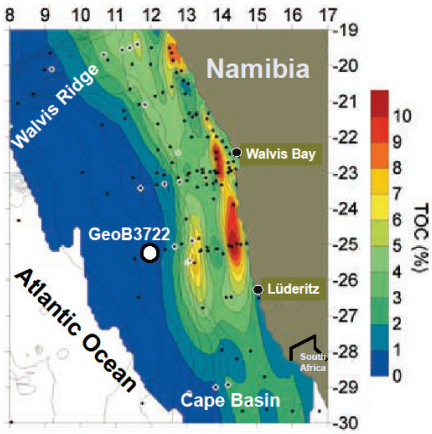

Fig. 1: *Location of core GeoB3722, TOC: Total Organic Carbon concentration in the core tops.*

Measured ^{231}Pa/^{230}Th activity ratios (Fig. 2) can be separated into two parts: a glacial part with high ratios (mostly around the production ratio of 0.093, red line) and a Holocene part with consistently low ratios.

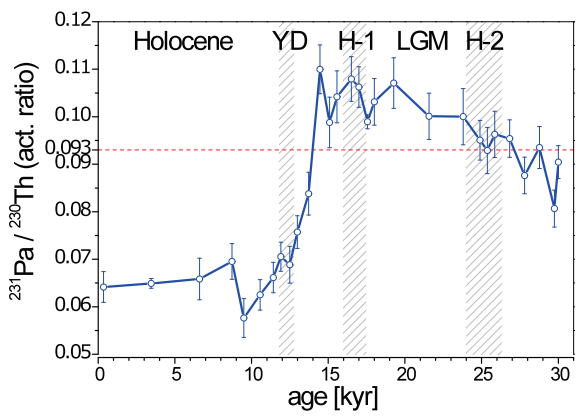

Fig. 2: *^{231}Pa/^{230}Th off West Africa over the past 30 ka, YD: Younger Dryas, H-1, H-2: Heinrich Events, LGM: Last Glacial Maximum.*

The combination of ^{231}Pa/^{230}Th with other proxies from the same site (Fig. 3) leads to the following scenario [2]: During the Holocene GeoB37222 is located in an open ocean area showing a characteristic ^{231}Pa/^{230}Th signature of North Atlantic Deep Water. During glacial times the site was dominated by southern waters. Strong glacial trade winds enhanced coastal upwelling and shifted or extended the upwelling cells to the west. Total particle flux increased and led to an enhanced glacial ^{231}Pa deposition. Imprints of glacial Atlantic Ocean circulation shutdowns (Heinrich Events) were not found.

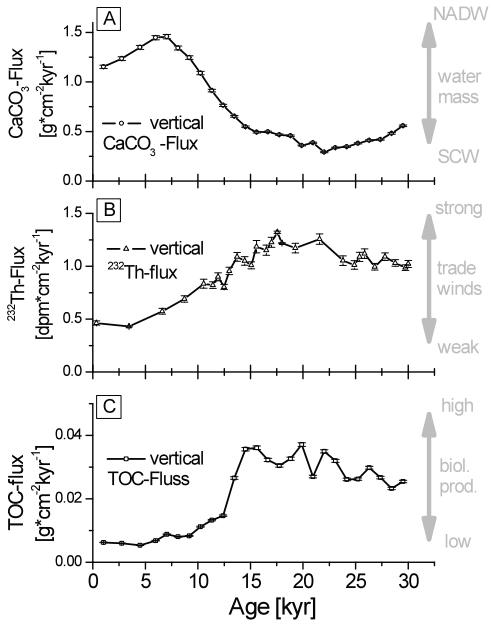

Fig. 3: *Reconstruction of water masses (A), trade winds (B), and bioproductivity (C).*

[1] M. Christl et al., Nucl. Instr. & Meth. B 262 (2007) 379

[2] M. Christl et al., Nucl. Instr. & Meth. B 268 (2010) 1159

[1] *Heidelberg Academy of Sciences, Germany*

ENVIRONMENTAL MONITORING

^{14}C as tracer of fossil fuel CO_2

Iodine-129 in the environment

Oceanic transport of radioactive waste

Determination of plutonium using AMS

Plutonium isotopes from a nuclear test site

^{14}C AS TRACER OF FOSSIL FUEL CO_2

Comparison of high-precision gas counting and AMS

B. Kromer[1,2], I. Levin[2], S. Lindauer[1,2], L. Wacker, A. Synal

^{14}C is an ideal tracer to monitor and quantify the contribution of fossil fuel in atmospheric CO_2, because fossil carbon is ^{14}C free, and hence the dynamical range is large. However, disentangling natural and anthropogenic components in the carbon cycle requires high precision in ^{14}C analyses, which is still best met economically with the radiometric technique (decay counting in gas proportional counters). On the other hand, AMS would be highly attractive because of small sample size and fast, high-volume throughput. In an extensive inter-comparison we measured duplicates of CO_2 gas samples obtained in our global atmospheric ^{14}C sampling program [1] both with gas counting and AMS using the MICADAS machine. The CO_2 gas for two AMS graphite targets was taken from the 10L gas sample used for gas counting.

We compared $^{14}CO_2$ time series from three sites, Neumayer station in Antarctica (Fig. 1) Jungfraujoch in the Swiss Alps (Fig. 2) and Schauinsland (Black Forest, Germany).

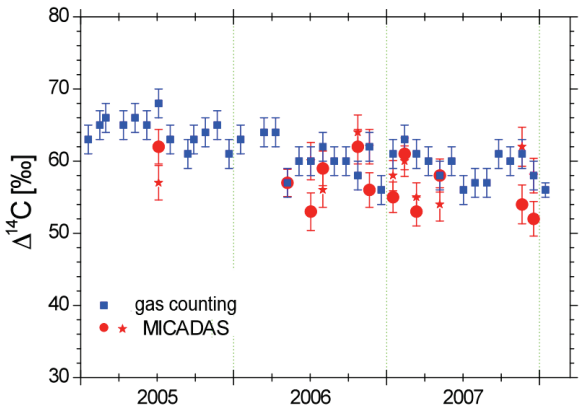

Fig. 1: *Comparison of $\Delta^{14}C$ in duplicate samples measured by gas counting (blue) and AMS (red) for Neumayer (Antarctica). For AMS we obtained two graphite targets (red circles and stars).*

The amplitude in the annual cycle of ^{14}C at these clean-air sites is small ($\Delta^{14}C$ ca. 5 ‰) and superimposed on a general decline due to the emission of fossil fuel (Suess effect). Hence, they are an ideal test bed for this study. The results of the two techniques agree well in the shape of the seasonal cycle. The two AMS targets of each gas counting sample are within the quoted error (2 - 2.5 ‰). However, we observe a slight offset of 3 ‰ in the absolute level of the two techniques, which will be investigated further. Sub-standards (e.g. IAEA-C6) do not show this offset.

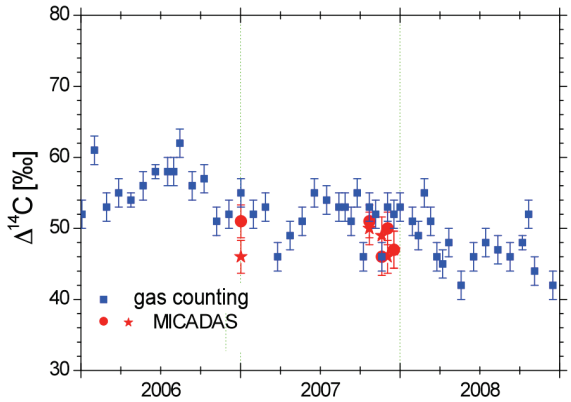

Fig. 2: *Same as Fig. 1, but for the Jungfraujoch site.*

The $\delta^{13}C$ values obtained by IRMS (precision ±0.03 ‰) compare well with those obtained with AMS (mean difference 0.8 ‰). The variance of the differences (1.6 ‰) is compatible with the quoted AMS $\delta^{13}C$ uncertainties.

[1] I. Levin et al., Tellus B 62(1) (2010) 26

[1] *Heidelberg Academy of Sciences, Germany*
[2] *Environmental Physics, University of Heidelberg, Germany*

IODINE-129 IN THE ENVIRONMENT

A 1000-fold disequilibrium around the world

A. Daraoui[1], L. Tosch[1], M. Gorny[1], D. Jakob[1], R. Sachse[1], R. Michel[1], V. Alfimov, H.-A. Synal

Atmospheric nuclear weapons tests, nuclear accidents, and emissions from reprocessing plants have changed the natural abundances of ^{129}I ($T_{1/2}$=15.7 Ma) in a drastic manner. ^{129}I is in disequilibrium in all environmental compartments of Western Europe, mainly as a consequence of the releases from the European reprocessing plants. ^{129}I from precipitation accumulates in soils, is transported by surface water, infiltrates ground-water and makes its way into the biosphere. To date, the radioecology of ^{129}I is not completely understood.

Concentrations of ^{127}I and ^{129}I were investigated in soils and water samples from Germany, Chile and Ukraine, and from the North Sea. ^{129}I was determined by AMS and ^{127}I by ICP-MS. For detailed descriptions of sampling procedures, preparations and results see [1, 2, 3].

The deposition density of ^{129}I in the soils from Bavaria has a geometric mean value of (109 × $1.5^{\pm1}$) mBq m^{-2}. The dominant sources here are the reprocessing plants of La Hague and Sellafield and not the Chernobyl fallout. The ^{129}I/^{127}I isotopic ratios range from 10^{-10} to 10^{-7}, which is 100 to 1000 times higher than the ratios observed in the samples from Chile. The ^{129}I integral deposition densities in Chile are between 0.3 and 2 mBq m^{-2}. In these soils, the observed ^{129}I/^{127}I ratios are about 10^{-12}. This value is consistent with results from marine sediments representing the pre-nuclear equilibrium ratios.

With ^{129}I a retrospective dosimetry of the ^{131}I exposure after the Chernobyl accident becomes possible for the highly contaminated zone in the Ukraine. Calculations based on ^{129}I measurements showed that in 35 villages in Contamination Zone II the geometric mean thyroid doses were (1.9 × $3.2^{\pm1}$) Gy for 5-year-old children and (0.45 × $3.2^{\pm1}$) Gy for adults, respectively.

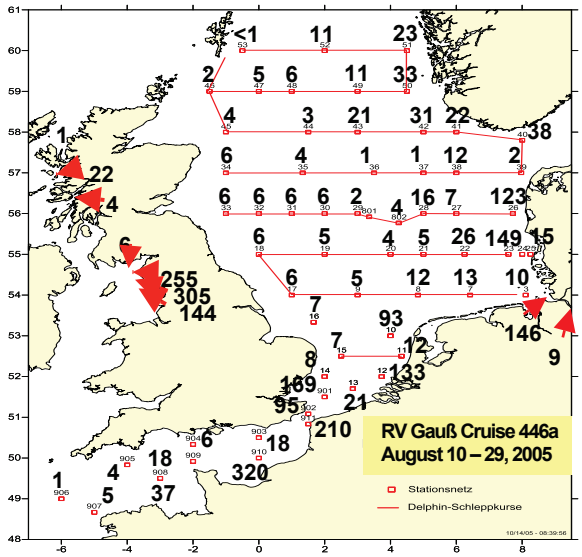

***Fig. 1**: ^{129}I/^{127}I ratios in units of 10^{-8} in the surface waters of the North Sea.*

The ^{127}I concentrations in seawater of the North Sea are relatively constant with (39 ± 4) ng g^{-1}. The observed ^{129}I/^{127}I isotopic ratios range between $4{\cdot}10^{-9}$ and $3{\cdot}10^{-6}$ with the highest ratios seen in the English Channel east of La Hague. The emissions from La Hague can be traced through the English Channel and subsequently the North Sea. These results and those of our earlier studies show the disequilibrium of ^{129}I in the environmental compartments.

[1] H. Nies et al., Vorhaben StSch 4481, BSH, Hamburg, 2009

[2] R. Michel et al., 41. Jahrestagung d. Fachverband f. Strahlenschutz, Alpbach (2009) 155-160

[3] A. Daraoui et al., 41. Jahrestagung d. Fachverband f. Strahlenschutz, Alpbach (2009) 167-172 and 193-198

[1] *Center for Radiation Protection and Radioecology, University of Hannover, Germany*

OCEANIC TRANSPORT OF RADIOACTIVE WASTE

Iodine-129 as a benchmark for global circulation models

S. Orre[1], J.N. Smith[2], V. Alfimov, M. Bentsen[1]

In a new study radioactive waste material from Sellafield and La Hague is used to shed light on ocean currents in the Nordic Seas, the Arctic Ocean, and the Atlantic Ocean, and to test the performance of an ocean model in this region.

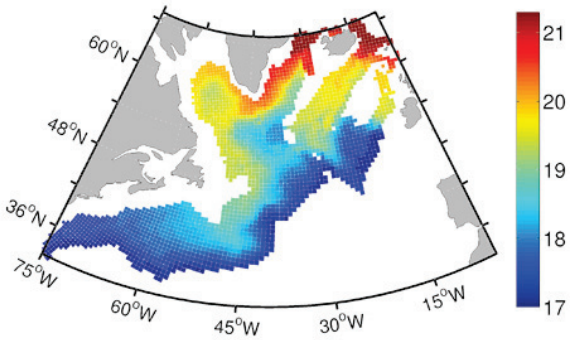

Fig. 1: *Iodine-129 in deep layers of the Atlantic Ocean: The map shows the simulated concentration of ^{129}I (the logarithm of number of ^{129}I atoms per liter sea-water) in the deep layers of the Atlantic Ocean.*

European nuclear reprocessing plants have discharged radioactive waste into the sea since the early 1950s. The waste material is swept away by ocean currents and can be observed both in sea-ice and sea-water in the Arctic Ocean and at the bottom of the Atlantic Ocean. While discharges of most radioactive species have been reduced the last two decades, discharges of Iodine-129 from Sellafield (UK) and La Hague (France) greatly increased during the 1990s. Naturally occurring concentration of ^{129}I is insignificant compared to the concentration in the sea after being contaminated by discharges from Sellafield and La Hague [1].

The radioactive waste material from these sources has proven to be useful to infer details of ocean pathways and their timescales. The observed propagation of ^{129}I from its sources and into the Arctic Ocean and the North Atlantic provides a valuable benchmark which ocean models can be tested against.

We have fed an ocean model with the historical release rates of ^{129}I from the reprocessing plants and simulated the subsequent transport by ocean currents. The results of this study were published in [1] and represent a unique direct comparison of observed and modeled levels of ^{129}I in the Arctic and Atlantic Oceans. The ocean model developed at the Nansen Center and the Bjerknes Centre shows impressive skills in predicting the magnitude and time history of ^{129}I in the ocean. In particular, the time development of ^{129}I distribution in deep layers of the Labrador Sea (south-west of Greenland) is fairly accurately captured by the model, thus indicating that the model is able to predict the formation of dense waters ventilating the global oceans.

The validation of the model with a limited number of observations produces a more complex picture of the oceanic pathways and timescales of ^{129}I. This model and its successors could be used to monitor future radioactive releases from Sellafield and La Hague and also predict the impact of accidental releases of radioactive or toxic waste in the ocean.

This work is a part of the project Arctic Radioactive Contamination, financed by the Research Council of Norway.

[1] S. Orre et al., Env. Fluid Mech. (2009) doi: 10.1007/s10652-009-9138-3

[1] *Nansen Environmental and Remote Sensing Center & Bjerknes Centre for Climate Research, Bergen, Norway*

[2] *Bedford Institute of Oceanography, Dartmouth, Canada*

DETERMINATION OF PLUTONIUM USING AMS

A method to identify the origin of a contamination

T. Bisinger[1], R. Michel[1], L. Wacker, M. Christl, H.-A. Synal

Plutonium is present in the environment as a consequence of atmospheric nuclear weapons testing, reprocessing of nuclear fuel and accidents in nuclear facilities. AMS allows the determination of $^{240}Pu/^{239}Pu$ isotopic ratios as well as the detection of ^{241}Pu. Thereby a reliable distinction of different plutonium sources in the environment is possible. Advantages of AMS are also short analysis times and high sensitivity.

Samples from the highly contaminated areas near Chernobyl, from the North Sea, from the Irish Sea, from Germany and from the Bikini atoll were investigated. Soil samples were dissolved using hydrofluoric and nitric acid. Sediment samples were leached with aqua regia. In water samples plutonium was co-precipitated using ferrous hydroxide. For all matrices, plutonium was then chemically separated from the bulk material using extraction chromatography. ^{242}Pu was used as a chemical yield tracer [1].

Fig. 1: *Chernobyl nuclear power plant.*

The measured $^{240}Pu/^{239}Pu$ isotopic ratios provide information on the origin of the plutonium. Plutonium emitted in the Chernobyl accident can thus be distinguished from the plutonium of the global fallout or other sources. The lowest isotopic ratios, which are typical for Pu emitted in atmospheric nuclear weapons tests, were found in samples from Germany (Fig. 2). Water samples from the Scottish north coast and sediment samples from the Irish Sea show the typical isotopic ratio of the Sellafield reprocessing facility. One of these samples with an exceptionally low isotopic ratio (0.08) is contaminated by the Dounreay reprocessing facility.

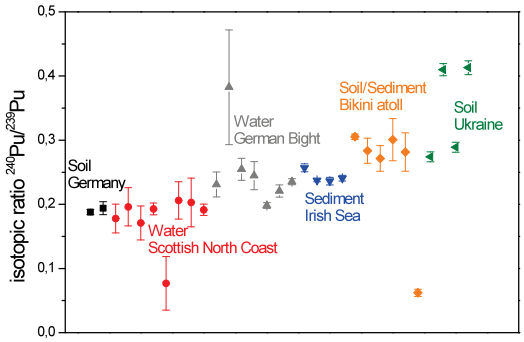

Fig. 2: *Isotopic ratios of the analyzed samples.*

Water samples from the German Bight show an enhanced isotopic ratio. These samples were either contaminated by the effluents of the La Hague reprocessing facility or by Pu from Chernobyl, which is transported downriver.

Samples from Bikini Island and from the Bravo crater have high isotopic ratios (~ 0.3) due to high-yield nuclear weapons tests (*Bravo*). One sediment sample from the lagoon has a low isotopic ratio (0.06) due to contamination by low-yield tests (*Able, Baker*).

The highest ratios were found in samples from the Ukraine. Those samples were directly contaminated by the Chernobyl accident.

[1] T. Bisinger et al., Nucl. Instr. & Meth. B (2009) in press

[1] *Center for Radiation Protection and Radioecology, University of Hannover, Germany*

PLUTONIUM ISOTOPES FROM A NUCLEAR TEST SITE

First measurements of ^{244}Pu at the TANDY

J. Lachner, M. Christl, H.-A. Synal, T. Bisinger [1], R. Michel [1]

The main source of Pu in the environment is the fallout from atmospheric nuclear weapons tests. Environmental contamination with plutonium can be identified from its isotopic composition.

Between 1946 and 1958 the Bikini atoll had been used for nuclear bomb testing and is since then heavily contaminated by local fallout. We determined atom ratios of the isotopes ^{239}Pu, ^{240}Pu, ^{241}Pu and ^{244}Pu in sediments and soils from the atoll (Fig. 1) using the 0.6 MV TANDY AMS system.

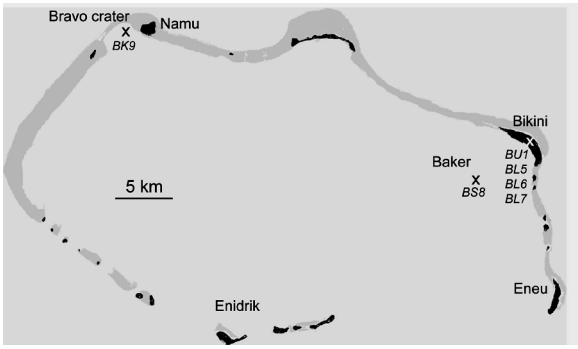

Fig. 1: *Sample locations at Bikini atoll.*

All examined samples deviate significantly from the isotopic signature of the global fallout. The large variations in the isotopic composition (Fig. 2) can be ascribed to the high or low yields of single tests and to mixing of sediments containing fallout from different tests. The variations in the ^{244}Pu/^{239}Pu ratio are more distinct than in the ^{240}Pu/^{239}Pu ratio of the same samples.

At the main island, Bikini, ^{240}Pu/^{239}Pu atom ratios of 0.28 - 0.32 were observed. This agrees with the expectation of heavy contamination of the region by local fallout from the Castle Bravo test [1] with a high explosive yield of 15 MT TNT equivalent. ^{240}Pu/^{239}Pu and ^{244}Pu/^{239}Pu ratios measured in sample BK9 from the crater of the Bravo test are lower than those from the single, high yield detonation Ivy Mike [2]. This indicates a mixture of material from the early high yield tests Bravo and Romeo (11 MT TNT eq.) with material from later explosions with lower yields at exactly the same site [3].

The sample (BS8) from the seafloor of the lagoon near the sunken ship Saratoga indicates isotopic ratios that show the signature of a low yield explosion, the plutonium implosion weapon Baker.

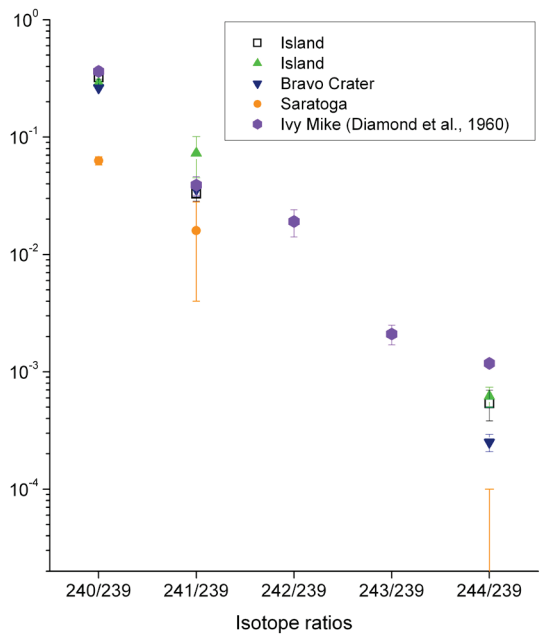

Fig. 2: *Measured Pu isotopic ratios (^{241}Pu/^{239}Pu is decay corrected). Ratios from the Ivy Mike explosion [2] are shown for comparison.*

[1] Y. Muramatsu et al., Sci. Total Environ. 278 (2001) 151
[2] H. Diamond et al., Phys. Rev. 119(6) (1960) 2000
[3] US Dept. of Energy, Nuclear Tests July 1945 through September 1992 (2000)

[1] *Center for Radiation Protection and Radioecology, University of Hannover, Germany*

BIOMEDICAL APPLICATIONS

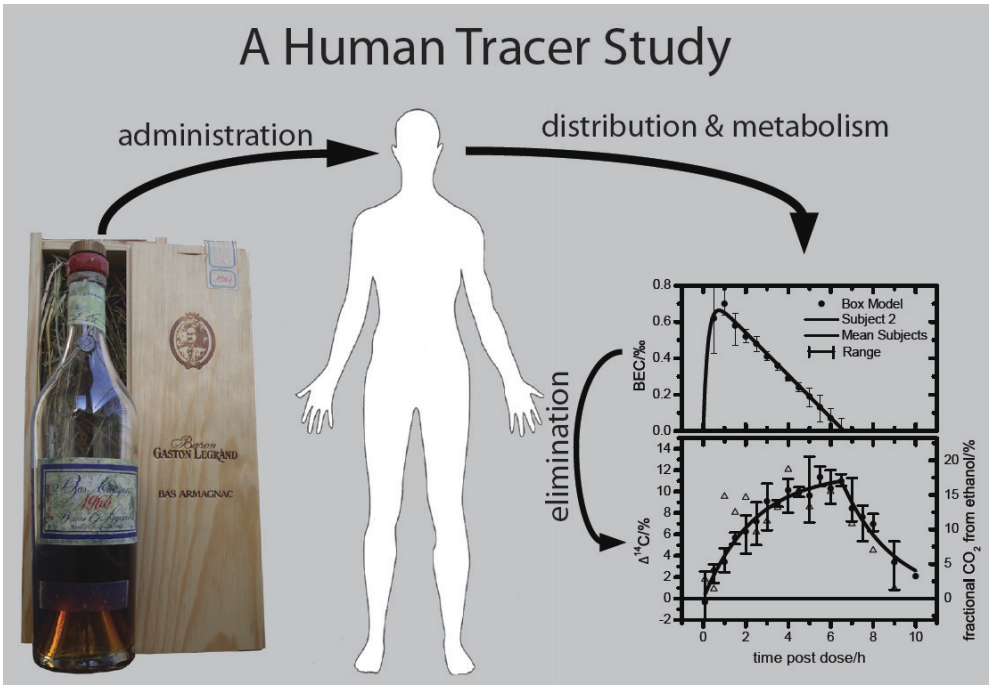

Bomb peak dating of French brandy

Tracing ethanol metabolism with a 1964 brandy

Isotopic labeling of a sheep skeleton

BOMB PEAK DATING OF FRENCH BRANDY

Bomb-test produced ^{14}C was used to determine the age of *Armagnac*

T. Schulze-König, M. Němec[1], L. Wacker, H.-A. Synal

Nuclear bomb testing in the late 1950s and early 1960s resulted in a doubling of the radiocarbon concentration in atmosphere. Because of the nuclear test ban treaty in 1963, the radiocarbon concentration in the atmosphere declined with a half-life of about 10 years. This behavior can be followed in comestibles, amongst others in wine ethanol as shown in Fig. 1. It can thus also be used to verify the age of brandies and wines of the last 45 years.

The radiocarbon concentrations of seven French brandies of the *Armagnac*, type (Fig. 2) from four different brands have been measured (Tab. 1). Aliquots of 10 µl were taken, combusted in an elemental analyzer and graphitized for AMS analysis. In a second step, ethanol was extracted via distillation from two bottles (ID 1 and ID 6) and analyzed. Radiocarbon concentrations in ethanol did not differ significantly from those in total carbon.

Based on the calibration curve published by Martin and Thibault [1] for wine from the Armagnac region, three bottles showed large differences between expected and measured ratios, e.g. in Fig. 1. The corresponding vintages and measured ages are shown in Tab. 1.

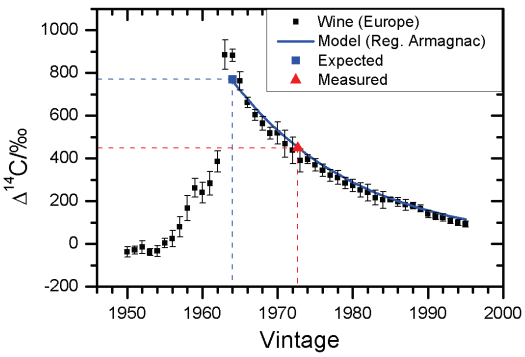

Fig. 1: *Measured ^{14}C concentrations in wine ethanol and a model curve for the Armagnac region versus vintage [1]. The expected and the measured $\Delta^{14}C$ values for sample 2 are shown.*

Fig. 2: *Analyzed bottle of Baron Gaston Legrand (1964).*

Dating brandies is based on two assumptions: first, the brandy is of single vintage; second, addition of carbon containing supplements is limited. Both assumptions are apparently supported by producer regulations for *Armagnac*, which prohibits mixing of vintages and limits addition of sugar. The latter may cause alteration by maximal 5 pMC (1-2 years). Other carbon sources like leftovers in the barrel may also influence the carbon content by 5 pMC. Neither the French exporter nor the association of Armagnac producers could present conclusive reasons for the depletion in ^{14}C. It seems that mislabeling occurs.

ID	Brand	Vintage (label)	Vintage (measure
1	B. de Saint-Feux	1964	1964
2	B. G. Legrand	1964	1973
3	B. G. Legrand	1965	1976
4	B. G. Legrand	1964	1965
5	Dom. de Cepede	1970	1975
6	Labiette Castille	1964	1972
7	Labiette Castille	1967	1970

Tab. 1: *Analyzed bottles of Armagnac brandy.*

[1] G.J. Martin and J.N. Thibault, Radiocarbon 37 (1995) 943

[1] *also Chemistry and Biochemistry, University of Bern*

TRACING ETHANOL METABOLISM WITH A 1964 BRANDY

Radiocarbon AMS with a novel analysis kit for exhaled air

T. Schulze-König, M. Christl, L. Wacker, H.-A. Synal

Radiocarbon has a still underutilized potential as a powerful tracer for metabolism studies in humans. Organic substances and their metabolic pathways can be traced in vivo with radiocarbon enriched above natural levels. Quantification of low tracer concentrations, however, requires an efficient analytic technique with AMS being the method of choice [1]. To simplify the analysis of exhaled human air, we developed a kit to measure radiocarbon directly in CO_2. We used the gas interface of the MICADAS AMS instrument to overcome the obstacle of time-consuming sample preparation.

The applicability of the novel method could be shown in a tracer study using a comestible (i.e. a brandy of 1964 vintage). Due to atmospheric nuclear bomb testing at that time [2] this brandy is enriched in ^{14}C by about 70% compared to today's atmospheric radiocarbon levels.

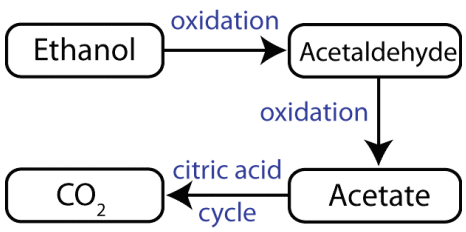

Fig. 1: *Path of ethanol metabolism as studied in this project.*

Five male subjects received a single oral dose of approximately 150 ml of brandy with an activity of 10 Bq each. Breath test samples were then taken in 30 min. intervals. The samples were analyzed with respect to their ethanol concentration and their $^{14}CO_2/^{12}CO_2$ ratio to determine the blood ethanol concentration (BEC) and the rate of totally metabolized ethanol, respectively (Fig. 1).

Our results show that the $^{14}CO_2/^{12}CO_2$ ratio increased steadily (Fig. 2 bottom) during ethanol degradation (Fig. 2 top) and almost reached a plateau 5.5 – 6.5 h postdose. When ethanol degradation was finished (about 6.5 h postdose), $^{14}CO_2/^{12}CO_2$ ratios began to decrease sharply. At this time, about 15 % of the CO_2 in the exhaled air has its origin in the labeled ethanol. The shape of the measured curves can be modeled using a two-box model.

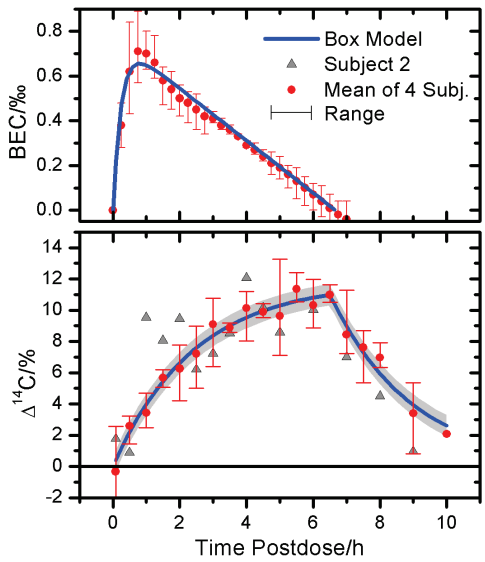

Fig. 2: *Blood ethanol concentration BEC (top) and radiocarbon concentration in exhaled air (bottom) versus time.*

This pilot study demonstrated that the combination of both the novel and easy-to-use analysis kit for exhaled air and the enormous sensitivity of AMS has the potential to initiate a new class of metabolic investigations in humans, nutrition and pharmacokinetics, and for pharmaceutical phenotype tests.

[1] S.S. Hah, J. Biomed. Sci. 16 (2009) 14
[2] Q. Hua and M. Barbetti, Radiocarbon 46 (2004) 1273

ISOTOPIC LABELING OF A SHEEP SKELETON

Bone calcium metabolism in a sheep is traced using ^{41}Ca and ^{86}Sr

T. Schulze-König, J. Irrgeher[1], A. Liesegang[2], G. Kuhn[3], T. Prohaska[1], T. Walczyk[4], H.-A. Synal

Sensitive techniques for assessing changes in bone metabolism are needed for the evaluation of novel strategies for osteoporosis prevention and treatment. Existing limitations can be potentially overcome by the use of ^{41}Ca or ^{86}Sr as bone calcium tracers. Following administration, both isotope tracers are partially incorporated into the bone matrix. After a labeling period of a few months, when most of the tracer has been cleared from compartments other than bone, excreted tracer material in urine originates mainly from bone and is supposed to reflect the bone Ca metabolism.

We designed a study to examine the incorporation of ^{41}Ca into bone of different type and structure. Similarities and dissimilarities in Sr and Ca dynamics were to be observed to evaluate the potential of Sr as surrogate tracer. A two year-old female domestic sheep was labeled intravenously with a single dose of ^{41}Ca (2.85 kBq) and ^{86}Sr (40 mg). Overall 28 urine samples were taken over a time span of six months. Finally, the sheep was sacrificed and bone samples were taken (Fig. 1).

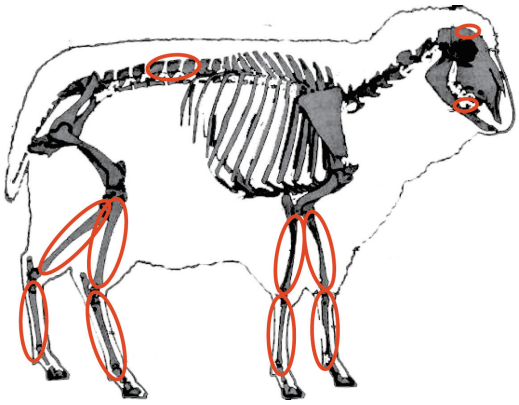

Fig. 1: *Skeleton of a sheep with bone sampling sites indicated in red.*

^{41}Ca/^{40}Ca ratios were measured with the 0.6 MV AMS system TANDY. Separation of ^{41}K by energy loss analysis is impossible at 1.7 MeV. Instead, ^{41}K interferences are suppressed by chemical Ca separation and element specific ionization. Samples are prepared as CaF_2 and ionized as CaF_3^-.

So far, the ^{41}Ca/^{40}Ca ratios of two urine samples were measured. One sample, 12 h post-dose, had a ^{41}Ca/^{40}Ca ratio of $1.14(2)\cdot10^{-7}$, the other, from a pool lasting 175 to 183 days post-dose, was $4.6(3)\cdot10^{-10}$. Currently measured ratios of unlabeled urine are at the level of $7\cdot10^{-12}$, which is well below the labeled urine samples. The results show that a long-term Ca pool of the sheep was successfully labeled with ^{41}Ca.

^{86}Sr/^{88}Sr ratios were measured in a bone sample (Fig. 2) using MC-ICP-MS. Compared to unlabeled bone, certain areas (epiphysis and diaphysis) were significantly enriched in ^{86}Sr but showed indications for differences in tracer deposition rates.

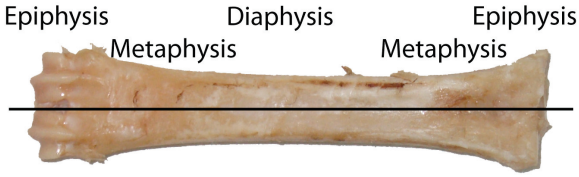

Fig 2: *Bone sample (Metatarsus). The black line indicates the cutting plane for spatially resolved isotope analysis of tracer deposition.*

Differences in the physiological behavior of both tracers will be explored by measuring the tracer concentrations in urine at different points in time and in bone at different positions.

[1] *Analytical Chemistry, BOKU, Austria*
[2] *Animal Nutrition, University of Zurich*
[3] *Biomechanics, ETHZ*
[4] *Chemistry and Biochemistry, NUS, Singapore*

MATERIALS SCIENCES

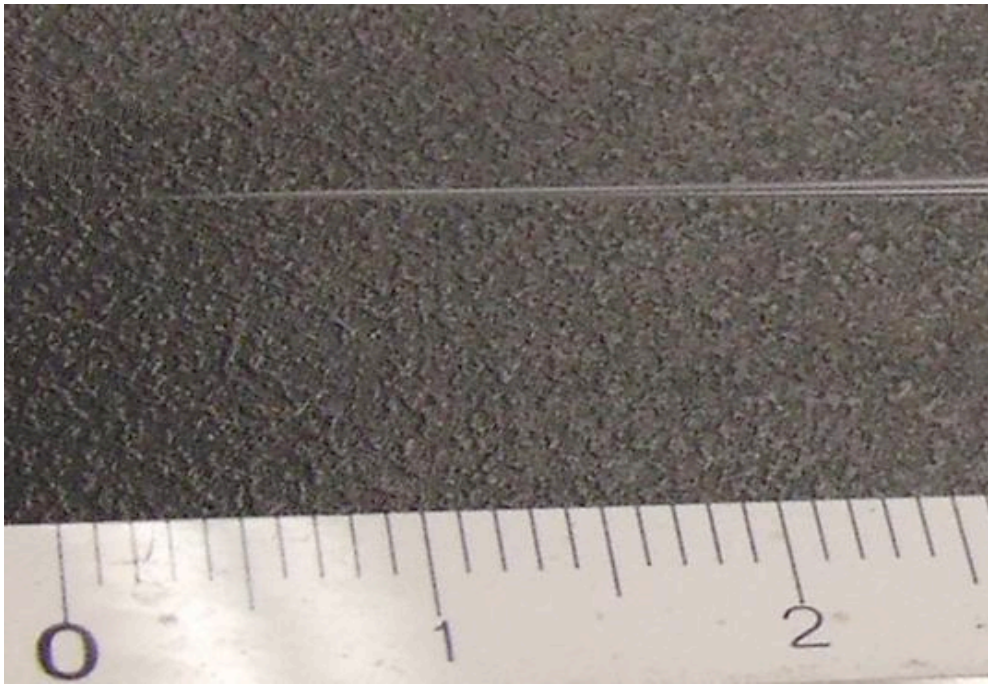

Capillary microprobe

Simultaneous RBS and PIXE

A new set-up for Helium PIXE

New high temperature irradiation set-up

Analysis of PLD-grown ion-conductive films

Converting polycrystals into single crystals

CAPILLARY MICROPROBE

Glass capillary focuses ion beam

M. Simon, M. Döbeli, J. Bourquin, R. Gruber, A. Herrmann, S. Roost, W. Wiederkehr

At the Laboratory of Ion Beam Physics small glass capillaries (Fig. 1) are being developed to extract a focused MeV ion beam. The beam is used as a raster ion probe for typical applications such as STIM (Scanning Transmission Ion Microscopy) or PIXE (Particle Induced X-ray Emission).

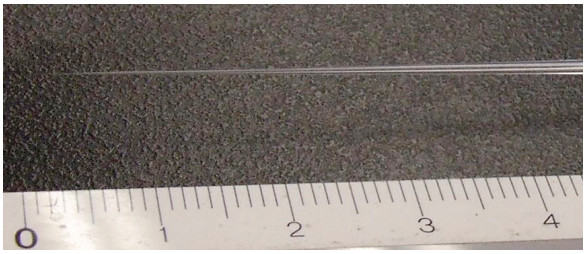

Fig. 1: *Tip of an in-house produced capillary. The inlet diameter is 0.86 mm and the outlet diameter is about 2 microns.*

Test runs with in-house produced capillaries have shown that ion beams can be extracted without significant energy loss if the capillary is of sufficiently regular conical shape. About 70% of all extracted particles have full energy, as shown in Fig. 2. We measured a so-called focusing factor, that is, the ratio of the number of transmitted particles to the number of incident particles divided by the geometric ratio of exit and entrance areas of the capillary, and obtained values of up to 120. The mechanism which leads to this effect is still unknown but is currently being investigated. It is assumed that either a charge build-up on the inner walls of the capillary and/or surface channeling is responsible for the focusing effect.

The above mentioned applications can be made as beam-in-air measurements because the outlet diameter of the capillaries is so small that the ion beam can be extracted into air without thin foils or special differential pumping. This enables the routine analysis of samples which cannot be brought into vacuum.

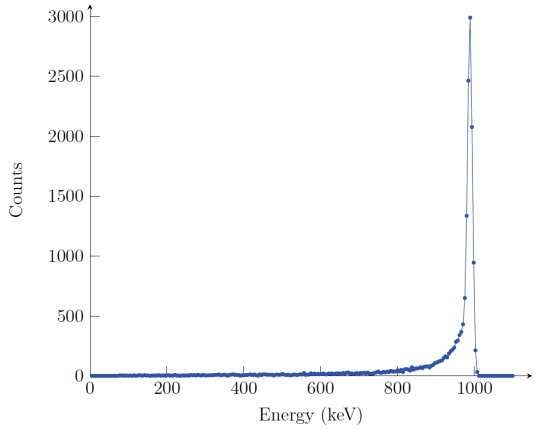

Fig. 2: *Energy spectrum of a 1 MeV proton beam which was transmitted through one of the capillaries with an outlet diameter of about 2 microns.*

The development led to the design of a new goniometer (Fig. 3) for the end of the beam line with which it will be possible to adjust the capillary to the ion beam.

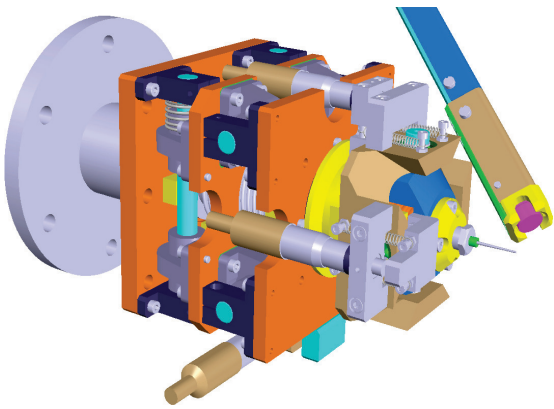

Fig. 3: *Design drawing of the new goniometer for the end of the beam line. At the capillary tip an in-house modified Silicon Drift Detector for PIXE measurements is shown.*

SIMULTANEOUS RBS AND PIXE

Neighboring elements are discriminated by X-ray emission

M. Döbeli, S. Heiroth[1]

There are a few important materials such as Yttria Stabilized Zirconia (YSZ) or phase change alloys (Ge-Sb-Te or Ag-In-Sb-Te) for which the precise composition is difficult to determine because of the entangled isotopic patterns of the constituents. During the past two decades we have developed high resolution spectrometers (Time-of-Flight and gas ionization detectors) that allow in many cases to resolve the individual isotopes by Heavy Ion Backscattering (HIBS) or high energy RBS.

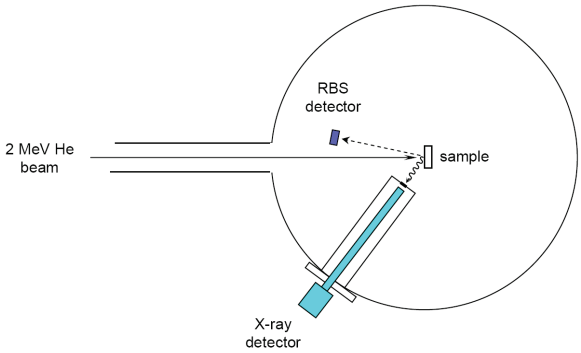

Fig. 1: *Schematic experimental set-up for simultaneous RBS/PIXE analysis.*

However, there are still elements that are extremely hard to separate by this technique if their masses are very close and if the heavier component is the more abundant one (e.g. YSZ). In these specific cases, we have started to acquire PIXE (Particle Induced X-ray Emission) spectra in addition to RBS measurements (Fig. 1). Fig. 2 shows an example for a complete stoichiometric analysis of a thin YSZ layer grown by PLD (Pulsed Laser Deposition). While the oxygen content is accurately determined by RBS the Y/Zr ratio is extracted from the PIXE spectrum. Since in all the envisaged cases neighboring elements have to be distinguished, the characteristic X-ray energies are very similar and exact quantification is simplified by this reason [1].

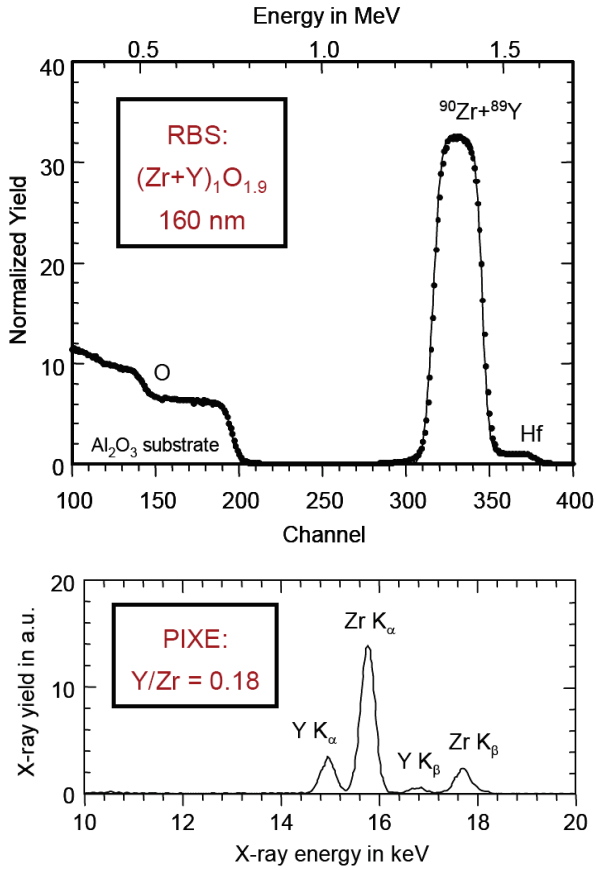

Fig. 2: *RBS/PIXE analysis of a 160 nm YSZ layer.*

In the same way, small admixtures of iron in cobalt oxide as well as Co/Ni and Gd/Ce ratios have been successfully determined in thin film and bulk samples.

[1] M. Döbeli, J. Phys.: Condens. Matter 20 (2008) 264010

[1] *Paul Scherrer Institut, Villigen*

A NEW SET-UP FOR HELIUM PIXE

To look through gold with characteristic X-rays

M. Döbeli, M. Simon, A. Herrmann

PIXE (Particle Induced X-ray Emission) is one of the standard techniques of ion beam analysis. It is the analogon to EDX (Energy Dispersive X-ray analysis) performed with electron microprobes. The incident beam particles (normally MeV protons) eject inner-shell electrons from the target atoms which results in the emission of characteristic X-rays.

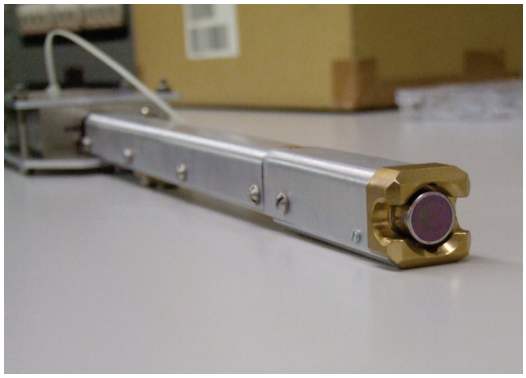

Fig. 1: *Modified Silicon Drift Diode Detector (originally by AMPTEK).*

In principle, all elements heavier than C can be detected with a suitable X-ray detector. However, due to the complete absence of primary bremsstrahlung the sensitivity of PIXE is enhanced by about a factor of 100 compared to EDX and is of the order of ppm for most elements.

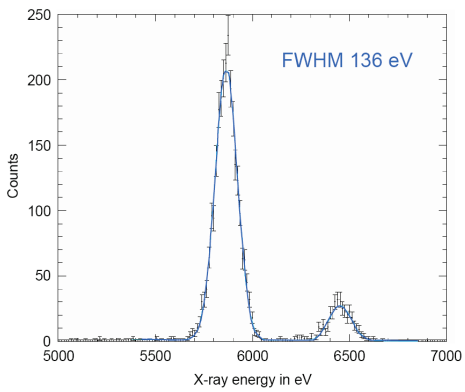

Fig. 2: *The energy resolution of the X-ray detector for ^{55}Mn K_α X-rays is 136 eV.*

At our laboratory a modified Silicon Drift Diode (SDD) X-ray detector has been attached to the RBS chamber which makes PIXE possible also at this experimental end-station (Fig. 1 and 2). In several tests with a number of thin layer samples we have proven that PIXE can be successfully performed by using the standard 2 MeV ^{4}He RBS beam instead of 3 MeV protons routinely used for PIXE at most other ion beam laboratories.

The significant reduction in bremsstrahlung background allows even to look at light elements through a thick layer of gold, as depicted in Fig. 3.

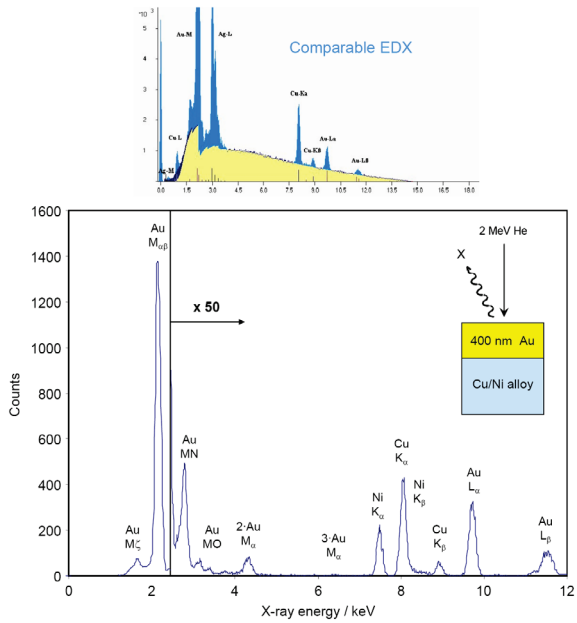

Fig. 3: *Bottom: ^{4}He PIXE analysis of a Cu/Ni alloy covered by 400 nm of gold. The spectrum on top demonstrates the tremendous improvement in background suppression of this technique relative to standard EDX.*

NEW HIGH TEMPERATURE IRRADIATION SET-UP

Investigation of He irradiation effects in ODS at elevated temperature

M.A. Pouchon [1], T. Rebac[1], W. Hoffelner[1], M. Döbeli

Ferritic oxide dispersion strengthened (ODS) steels are promising candidates for high temperature applications in future nuclear reactor systems.

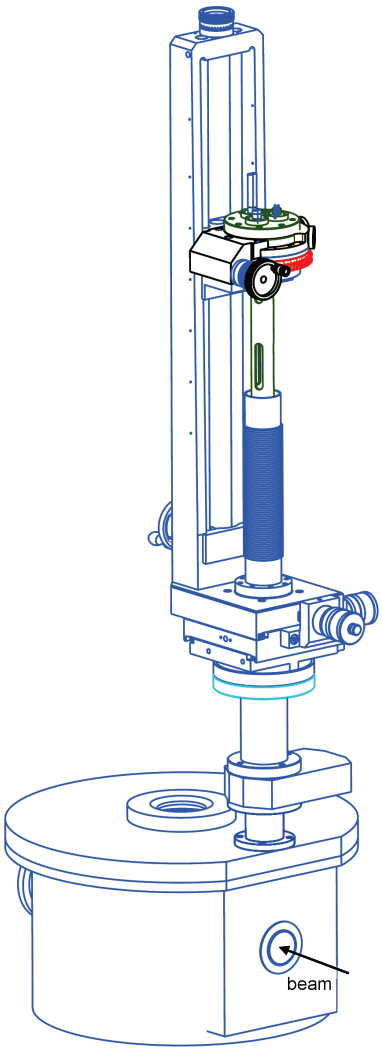

Fig. 1: *Drawing of the 3-axes translation stage mounted on the irradiation chamber.*

The applicability of ODS steels in a nuclear reactor environment has to be carefully investigated. Besides the classical exposures, such as temperature, mechanical load and chemical environment, the irradiation can also modify the material. Irradiation hardening, irradiation creep and swelling are classical properties to be tested in this context [1].

For this purpose a high temperature thermostat has been developed at the Laboratory for Nuclear Materials (LNM) at the Paul Scherrer Institut. The oven is mounted on a 3-axes translation stage for exact transfer and positioning of the samples (Fig. 1). This device is used at LIP for irradiation of ODS steel (PM2000) samples with ^{4}He of energies between 1 and 2 MeV to generate an almost evenly damaged surface layer of 2.5 µm. An irradiated ODS surface is shown in Fig. 2. From experiment to experiment the sample temperature during irradiation was gradually increased from room temperature up to a maximum of 700 °C. An oven for use at even higher temperatures is under construction.

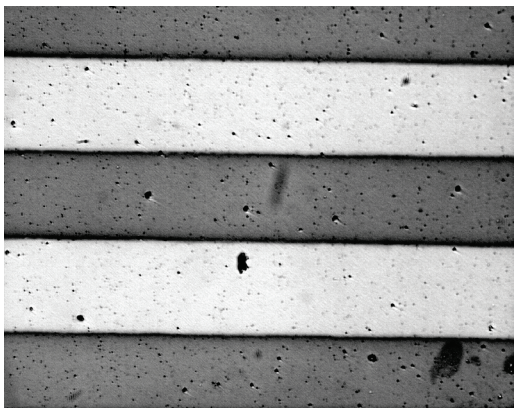

Fig. 2: *Irradiated ODS surface under the optical microscope. The sample was covered during the experiment by a Ni mesh to produce implanted and non-implanted regions.*

[1] M.A. Pouchon et al., Journal of Nuclear Materials 352 (2006) 57

[1] *Paul Scherrer Institut, Villigen*

ANALYSIS OF PLD-GROWN ION-CONDUCTIVE FILMS

Well-defined solid electrolyte layers for micro-solid oxide fuel cells

M. Döbeli, S. Heiroth[1], T. Lippert[1]

Pulsed Laser Deposition (PLD) is a powerful technique for the growth of ceramic thin films (Fig. 1). Dense, gas impermeable sub-µm layers of Y_2O_3:ZrO_2 (YSZ) and Gd_2O_3:CeO_2 (CGO), which are attractive as solid electrolyte in micro-solid oxide fuel cells, can be obtained with comprehensive microstructural control [1, 2].

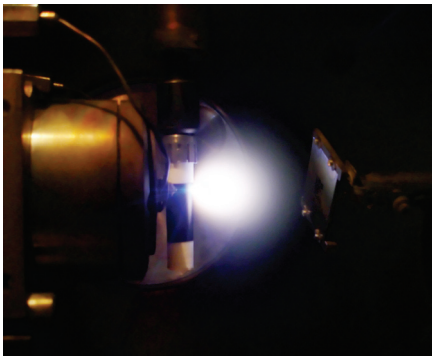

Fig. 1: *Thin film growth by PLD. View into the deposition chamber.*

Accurate analysis of the film stoichiometry is essential for two reasons: a) for an optimization of the film growth parameters, and b) because the defect chemistry, which determines the electrical transport properties, depends directly on the dopant concentration and the lattice oxygen content.

Standard 2 MeV ^{4}He RBS allows an efficient determination of the cation to oxygen ratio in YSZ (Yttria Stabilized Zirconia) and CGO (Cer-Gadolinium Oxide) layers. However, the similar atomic masses of Y and Zr respectively Gd and Ce prevent a separation of these elements. The mass resolution in the high Z elemental range can be enhanced by the use of higher projectile energies. 5 MeV ^{4}He RBS spectra allow a quantification of the Ce:Gd ratio (Fig. 2). In some cases (like YSZ) an additional particle-induced X-ray emission (PIXE) spectrum enables the determination of elemental ratios that are difficult to separate by RBS.

For films on heavy substrates and thick layers containing heavy elements the exact analysis of the oxygen content by RBS is impeded by the large low-energy background. In these cases the oxygen stoichiometry can be measured precisely by HI-ERDA (Heavy Ion Elastic Recoil Detection Analysis) using suitable oxide standards.

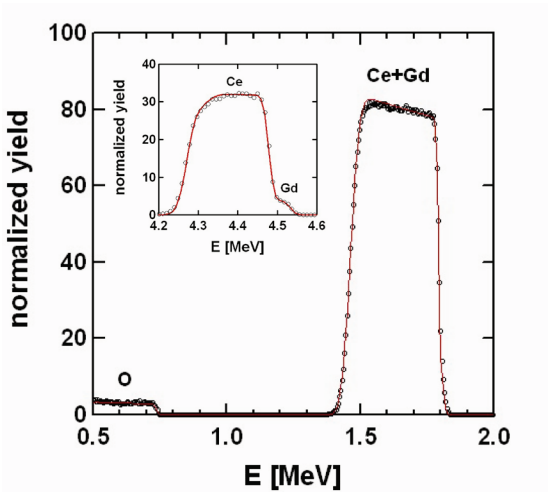

Fig. 2: *^{4}He RBS spectra of a 350 nm thick CGO layer at projectile energies of a) 2 MeV and b) 5 MeV (inset).*

By a combination of these techniques it has been shown that with optimized parameters of the PLD process, the chemical composition of the laser ablation target can be retained upon transfer to the substrate.

[1] S. Heiroth et al., Appl. Phys. A **93** (2008) 639

[2] S. Heiroth et al., J. Eur. Ceram. Soc. **30** (2010) 489

[1] *Paul Scherrer Institut, Villigen*

CONVERTING POLYCRYSTALS INTO SINGLE CRYSTALS

Selectively induced grain growth by high energy ion bombardment

M. Seita[1], R. Spolenak[1], M. Döbeli

The micro- and nanostructure of metal films is of increasing technical importance. In this project, the texture evolution of thin metal films by ion bombardment is investigated. Au or Ag layers deposited on silicon are irradiated at liquid nitrogen temperature by self-ions with an energy of a few MeV. The incident beam is set to an angle of 35° towards the sample surface normal, corresponding to the <110> channeling direction. The evolution of the microstructure and the grain orientation is characterized by EBSD (Electron Backscatter Diffraction) or TEM (Transmission Electron Microscopy).

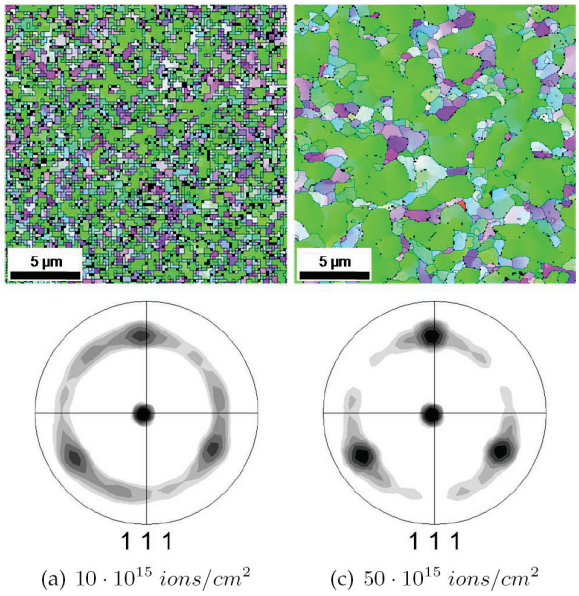

Fig. 1: *EBSD maps of a 500 nm silver film after self-ion irradiation at 3.5 MeV. The pole figures show a progressive sharpening of the in-plane texture induced by the ion-beam. For high fluences we can see a bi-modal grain size distribution caused by the selective grain growth process.*

Both, Ag and Au film show a significant grain growth during ion bombardment and an important change of the crystal texture. Figures 1 and 2 compare the effects in silver and gold films, respectively. More details can be found in reference [1].

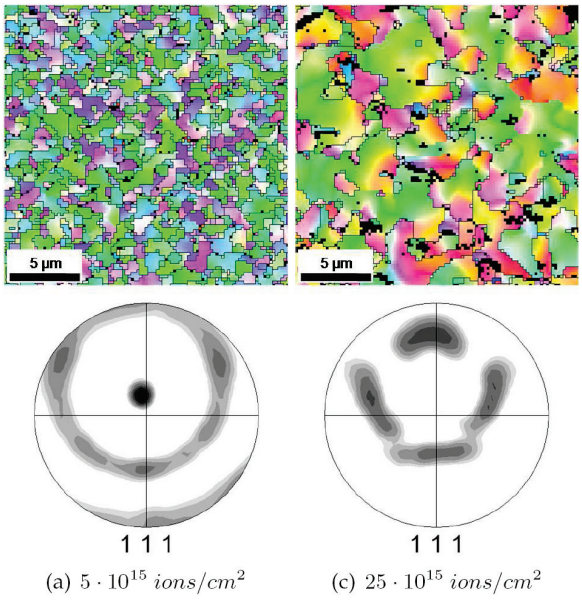

Fig. 2: *EBSD maps of a 500 nm gold film after self-ion irradiation at 7 MeV. The pole figures show a progressive tilt of the out-of-plane texture toward the (100) crystal direction. No selective grain growth can be distinguished from the pole figures. The in-plane grain maps show color gradients within single grains, which are representative of the continuous crystal rotations.*

As a possible explanation, it is supposed that upon irradiation a subset of grains oriented for ion channeling is growing significantly at the expense of the remaining grains.

[1] M. Dietiker et al., Acta Mater. 57 (2009) 4009

[1] *Dept. Materials, ETHZ*

EDUCATION

Learning by playing with your own samples

Development of new lab equipment

LEARNING BY PLAYING WITH YOUR OWN ^{14}C SAMPLES

Summary of school projects performed in the laboratory

I. Hajdas, G. Bonani, S. Iglesias, R. Monnier, M. Maurer, H.-A. Synal, C. Vockenhuber, L. Wacker

The Laboratory of Ion Beam Physics promotes outreach for the public and actively relates research applications to subjects of everyday life. In particular, we provide grammar school students (Gymnasium) the opportunity to come in contact with modern science and learn about ^{14}C dating directly in our laboratory. Usually, we oversee individual projects, which are designed as internships for interested pupils in small groups and which typically last about one week.

Fig. 1: *Grammar school students operate the graphitization line in the sample preparation laboratory.*

In 2009, for the third time a project with students from the Kantonsschule Olten took place. Two pupils prepared wood samples taken from a supporting beam of the historic watermill "Hayozmueli" in St. Ursen (FR), Switzerland. Six consecutive sections were sampled from the tree log, each comprising 5 annual rings (Fig 2). The obtained radiocarbon age sequence was matched with the radiocarbon calibration curve Intcal04 by exploiting the age information of the tree itself. Using a special model of the OxCAL4.0 calibration program [1], the age of the last ring of the log could be determined to be within the interval 1649-1660 AD (Fig.3).

Fig. 2: *Tree log from a 17th century watermill sampled for ^{14}C dating.*

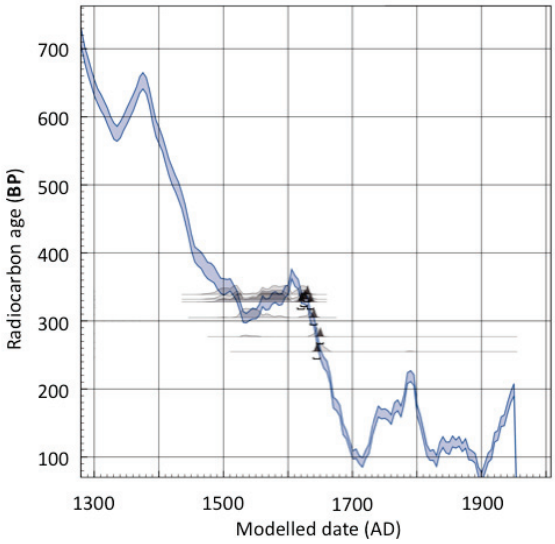

Fig. 3: *Wiggle matching of the measured age sequence with the Intcal04 calibration curve using the OxCAL4.0 calibration program.*

Such educational projects are very instructive for pupils. They provide the full range of challenges in radiocarbon dating and the opportunity for a first-hand experience in active research.

[1] https://c14.arch.ox.ac.uk

DEVELOPMENT OF NEW LAB EQUIPMENT

Apprenticeship at the Laboratory of Ion Beam Physics

L. Wacker, J. Bourquin, J, Metzger, R. Walser, H.-A. Synal

The Laboratory of Beam Physics is actively involved in the ETHZ apprentice program to educate physics laboratory assistants. Apprentices are integrated into the laboratory operations and training is provided covering the full spectrum of technical skills and expertise anticipated from physics laboratory assistants. They learn how to use CAD programs, to design mechanical components, to layout electronic circuit boards, to assemble electrical or electronic devices, and to coordinate the production of mechanical components with the workshops or manufacture simple mechanical parts themselves. We attach great importance to give them a chance to design individual technical instruments and complete operations before they leave our laboratory or finish their education. Depending on their skills, instruments of various degrees of complexity can be made. Of course, the success of these projects depends greatly on the supervision by the senior technical staff of the laboratory and the guidance of the scientist who defines the specifications of the instruments to be built.

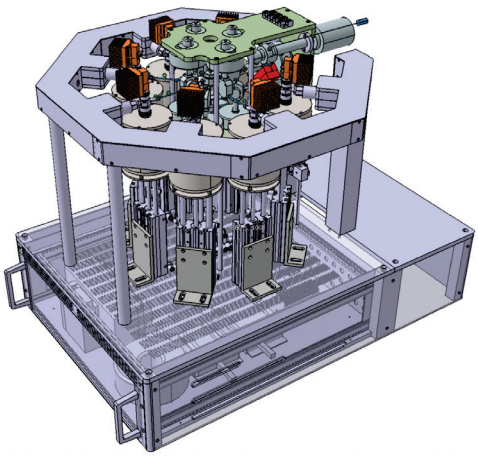

Fig. 1: *The fully automated graphitization equipment (AGE) automatically traps CO_2 from an elemental analyzer and converts it to graphite.*

Last year, the apprentices were responsible for a series of new equipment required to be used at the MICADAS system (Fig. 1, 2).

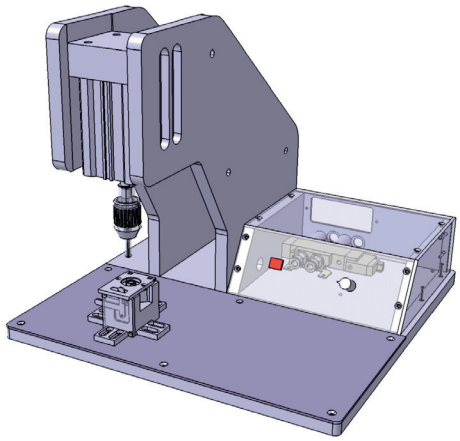

Fig. 2: *The new pneumatic sample press is an important tool to produce sputter targets for high-precision measurements efficiently.*

Also our latest instrumental developments for the gas ion source at the MICADAS facility were strongly influenced by new ideas and work from the apprentices (Fig. 3).

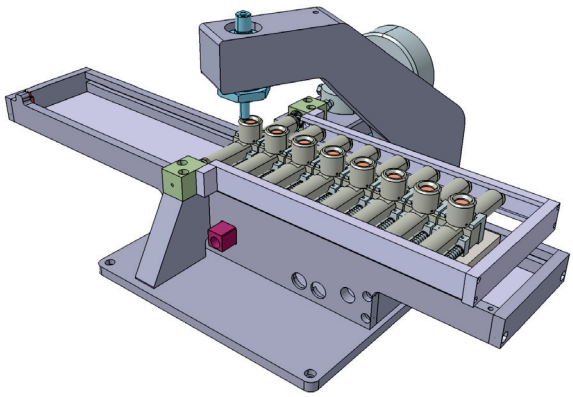

Fig. 3: *The new sample changer for CO_2 samples in gas ampoules allows for the first time autonomous AMS measurements with a gas ion source.*

PUBLICATIONS

L.M. Abbühl, N. Akcar, S. Strasky, A. Graf, S. Ivy-Ochs and C. Schlüchter
A zero-exposure time test on an erratic boulder: evaluating the problem of pre-exposure in surface exposure dating
Quaternary Science Journal **58/1** (2009) 1-11

N. Akçar, S. Ivy-Ochs, V. Alfimov, I.Ö. Yilmaz, A. Schachner, D. AltIner, V. Yavuz and C. Schlüchter
First results on determination of cosmogenic ^{36}Cl in limestone from the Yenicekale complex in the Hittite capital of Hattusha (Turkey)
Quaternary Geochronology **4** (2009) 533-540

V. Alfimov and S. Ivy-Ochs
How well do we understand production of ^{36}Cl in limestone and dolomite?
Quaternary Geochronology **4** (2009) 462-474

A.M. Berggren, J. Beer, G. Possnert, A. Aldahan, P.W. Kubik, M. Christl, S.J. Johnsen, J. Abreu and B.M. Vinther
A 600-year annual ^{10}Be record from the NGRIP ice core, Greenland
Geophysical Research Letters **36** (2009) L11801, doi:10.1029/2009GL038004

A. Blinov, V. Alfimov, J. Beer, D. Gilichinsky, L. Schirrmeister, A. Kholodov, P. Nikolskiy, T. Opel, D. Tikhomirov and S. Wetterich
Ratio of ^{36}Cl/Cl in ground ice of east Siberia and its application for chronometry
Geochemistry, Geophysics, Geosystems **10** (2009) doi:10.1029/2009GC002548

E. Boaretto, R. Barkai, A. Gopher, F. Berna, P.W. Kubik and S. Weiner
Specialized flint procurement strategies for hand axes, scrapers and blades in the late Lower Paleolithic: A ^{10}Be study at Qesem Cave, Israel
Human Evolution **24** (2009) 1-12

S. Canulescu, C.N. Borca, M. Döbeli, P. Schaaf, T. Lippert and A. Wokaun
Processing and properties of thin manganite films
In: Magnetic Properties of Solids, ed. K.B. Tamayo, Nova Science Publishers (2009)

A.L. Densmore, R. Hetzel, S. Ivy-Ochs, W.C. Krugh, N. Dawers and P.W. Kubik
Spatial variations in catchment-averaged denudation rates from normal fault footwalls
Geology **37** (2009) 1139-1142

L. Di Nicola, S. Strasky, C. Schlüchter, M.C. Salvatore, N. Akçar, P.W. Kubik, M. Christl, H.U. Kasper, R. Wieler and C. Baroni
Multiple cosmogenic nuclides document complex Pleistocene exposure history of glacial drifts in Terra Nova Bay (northern Victoria Land, Antarctica)
Quaternary Research **71** (2009) 83-92

I. Dillmann, C. Domingo-Pardo, M. Heil, F. Kappeler, A. Wallner, O. Forstner, R. Golser, W. Kutschera, A. Priller, P. Steier, A. Mengoni, R. Gallino, M. Paul and C. Vockenhuber
Determination of the stellar (n,γ) cross section of Ca-40 with accelerator mass spectrometry
Physical Review C **79** (2009) Doi 10.1103/Physrevc.79.065805

F. Favilli, M. Egli, D. Brandova, S. Ivy-Ochs, P.W. Kubik, P. Cherubini, A. Mirabella, G. Sartori, D. Giaccai and W. Haeberli
Combined use of relative and absolute dating techniques for detecting signals of Alpine landscape evolution during the late Pleistocene and early Holocene
Geomorphology **112** (2009) 48-66

T.G. Fisher, N. Waterson, T.V. Lowell and I. Hajdas
Deglaciation ages and meltwater routing in the Fort McMurray region, northeastern Alberta and northwestern Saskatchewan, Canada
Quaternary Science Reviews **28** (2009) 1608-1624

M. Frank, D. Porcelli, P. Andersson, M. Baskaran, G. Björk, P.W. Kubik, B. Hattendorf and D. Guenther
The dissolved beryllium isotope composition of the Arctic Ocean
Geochimica et Cosmochimica Acta **73** (2009) 6114-6133

G. Gennari, F. Tamburini, D. Ariztegui, I. Hajdas and S. Spezzaferri
Geochemical evidence for high-resolution variations during deposition of the Holocene S1 sapropel on the Cretan Ridge, eastern Mediterranean
Palaeogeography, Palaeoclimatology, Palaeoecology **273** (2009) 239-248

B. Giaccio, F. Marra, I. Hajdas, D.B. Karner, P.R. Renne and A. Sposato
Ar-40/Ar-39 and C-14 geochronology of the Albano maar deposits: Implications for defining the age and eruptive style of the most recent explosive activity at Colli Albani Volcanic District, Central Italy
Journal of Volcanology and Geothermal Research **185** (2009) 203-213

M.M. Goethals, R. Hetzel, S. Niedermann, H. Wittmann, C.R. Fenton, P.W. Kubik, M. Christl and F. von Blanckenburg
An improved experimental determination of cosmogenic $^{10}Be/^{21}Ne$ and $^{26}Al/^{21}Ne$ production ratios in quartz
Earth and Planetary Science Letters **284** (2009) 187-198

I. Hajdas
Applications of radiocarbon dating method
Radiocarbon **51** (2009) 79-90

I. Hajdas and G. Bonani
Radiocarbon dating and chronology of the Late-Glacial and Early Holocene
in: Reconstruction of Upper Palaeolithic and Early Mesolithic natural environments, Office et musee cantonal d'archeologie de Neuchatel, N. Thew, P. Hadorn and G.R. Coope (2009)

I. Hajdas, P. Della Casa, M. Egli, U. Hugi, S. van Willigen and M. Worle
Proceedings of the 5th International Symposium on Radiocarbon and Archaeology Vol 51, Nr 2, 2009 Preface
Radiocarbon **51** (2009) V-Vii

I. Hajdas, A. Michczynski, G. Bonani, L. Wacker and H. Furrer
Dating bones near the limit of the radiocarbon dating method: study case mammoth from Niederweningen, ZH, Switzerland
Radiocarbon **51** (2009) 675-680

U. Heikkila, J. Beer, J. Feichter, V. Alfimov, H.-A. Synal, U. Schotterer, A. Eichler, M. Schwikowski and L. Thompson
Cl-36 bomb peak: comparison of modeled and measured data
Atmospheric Chemistry and Physics **9** (2009) 4145-4156

K. Heine, A.U. Reuther, H.U. Thieke, R. Schulz, N. Schlaak and P.W. Kubik
Timing of Weichselian ice marginal positions in Brandenburg (northeastern Germany) using cosmogenic in situ ^{10}Be
Zeitschrift für Geomorphologie **53** (2009) 433-454

K. Hippe, F. Kober, H. Baur, M. Ruff, L. Wacker and R. Wieler
The current performance of the in situ ^{14}C extraction line at ETH
Quaternary Geochronology **4** (2009) 493-500

S. Ivy-Ochs, H. Kerschner, M. Maisch, M. Christl, P.W. Kubik and C. Schlüchter
Latest Pleistocene and Holocene glacier variations in the European Alps
Quaternary Science Reviews **28** (2009) 2137-2149

S. Ivy-Ochs, A. v. Poschinger, H.-A. Synal and M. Maisch
Surface exposure dating of the Flims landslide, Graubünden, Switzerland
Geomorphology **103** (2009) 104-112

T.M. Jenk, S. Szidat, D. Bolius, M. Sigl, H.W. Gäggeler, L. Wacker, M. Ruff, C. Barbante, C.F. Boutron and M. Schwikowski
A novel radiocarbon dating technique applied to an ice core from the Alps indicating late Pleistocene ages
Journal of Geophysical Research-Atmospheres **114** (2009) Doi 10.1029/2009jd011860

F. Kober, S. Ivy-Ochs, G. Zeilinger, F. Schlunegger, P.W. Kubik, H. Baur and R. Wieler
Complex multiple cosmogenic nuclide concentration and histories in the arid Rio Lluta catchment, northern Chile
Earth Surface Processes and Landforms **34** (2009) 398-412

S. Kraft-Bermuth, V.A. Andrianov, A. Bleile, A. Echler, P. Egelhof, A. Kiseleva, O. Kiselev, H.J. Meier, J.P. Meier, A. Shrivastava, M. Weber, R. Golser, W. Kutschera, A. Priller, P. Steier and C. Vockenhuber
Calorimetric low temperature detectors for low-energetic heavy ions and their application in accelerator mass spectrometry
Review of Scientific Instruments **80** (2009) 103304-1 - 103304-9

A.M. Kreuzer, C. von Rohden, R. Friedrich, Z.Y. Chen, J.S. Shi, I. Hajdas, R. Kipfer and W. Aeschbach-Hertig
A record of temperature and monsoon intensity over the past 40 kyr from groundwater in the North China Plain
Chemical Geology **259** (2009) 168-180

J. Kuhlemann, M. Milivojevic, I. Krumrei and P.W. Kubik
Last glaciation of the Sara Range (Balkan peninsula): Increasing dryness from the LGM to the Holocene
Austrian Journal of Earth Sciences **102** (2009) 146-158

J. Lippold, J. Grützner, D. Winter, Y. Lahaye, A. Mangini and M. Christl
Does sedimentary $^{231}Pa/^{230}Th$ from the Bermuda Rise monitor past Atlantic meridional overturning circulation?
Geophysical Research Letters **36** (2009) doi:10.1029/2009GL038068

T.V. Lowell, T.G. Fisher, I. Hajdas, K. Glover, H. Loope and T. Henry
Radiocarbon deglaciation chronology of the Thunder Bay, Ontario area and implications for ice sheet retreat patterns
Quaternary Science Reviews **28** (2009) 1597-1607

M. Mallepell, M. Döbeli and M. Suter
Annular gas ionization detector for low energy heavy ion backscattering spectrometry
Nuclear Instruments and Methods B **267** (2009) 1193-1198

I. Marozau, A. Shkabko, G. Dinescu, M. Döbeli, T. Lippert, D. Logvinovich, M. Mallepell, C.W. Schneider, A. Weidenkaff and A. Wokaun
Pulsed laser deposition and characterization of nitrogen-substituted $SrTiO_3$ thin films
Applied Surface Science **255** (2009) 5252-5255

I. Marozau, A. Shkabko, M. Döbeli, T. Lippert, D. Logvinovich, M. Mallepell, C. Schneider, A. Weidenkaff and A. Wokaun
Optical properties of nitrogen-substituted strontium titanate thin films prepared by pulsed laser deposition
Materials **2** (2009) 1388-1401

P.I. Moreno, M.R. Kaplan, J.P. Francois, R. Villa-Martinez, C.M. Moy, C.R. Stern and P.W. Kubik
Renewed glacial activity during the Antarctic Cold Reversal and persistence of cold conditions until 11.5 ka in southwestern Patagonia
Geology **37** (2009) 375-378

S. Orre, J.N. Smith, V. Alfimov and M. Bentsen
Simulating transport of ^{129}I and idealized tracers in the northern North Atlantic Ocean
Environmental Fluid Mechanics (2009) DOI: 10.1007/s10652-009-9138-3

C. Prager, S. Ivy-Ochs, M. Ostermann, H.-A. Synal and G. Patzelt
Geology and radiometric ^{14}C-, ^{36}Cl- and Th-/U-dating of the Fernpass rockslide (Tyrol, Austria)
Geomorphology **103** (2009) 93-103

P.J. Reimer, M.G.L. Baillie, E. Bard, A. Bayliss, J.W. Beck, P.G. Blackwell, C.B. Ramsey, C.E. Buck, G.S. Burr, R.L. Edwards, M. Friedrich, P.M. Grootes, T.P. Guilderson, I. Hajdas, T.J. Heaton, A.G. Hogg, K.A. Hughen, K.F. Kaiser, B. Kromer, F.G. McCormac, S.W. Manning, R.W. Reimer, D.A. Richards, J.R. Southon, S. Talamo, C.S.M. Turney, J. van der Plicht and C.E. Weyhenmeye
Intcal09 and Marine09 Radiocarbon Age Calibration Curves, 0-50,000 Years Cal BP
Radiocarbon **51** (2009) 1111-1150

D. Schumann, J. Neuhausen, J. Eikenberg, M. Ruthi, M. Wohlmuther, P.W. Kubik, H.-A. Synal, V. Alfimov, G. Korschinek, G. Rugel and T. Faestermann
Radiochemical analysis of a copper beam dump irradiated with high-energetic protons
Radiochimica Acta **97** (2009) 123-131

A. Shkabko, M.H. Aguirre, I. Marozau, M. Döbeli, M. Mallepell, T. Lippert and A. Weidenkaff
Characterization and properties of microwave plasma-treated $SrTiO_3$
Materials Chemistry and Physics **115** (2009) 86-92

R.H. Smittenberg, I. Hajdas, L. Wacker and S.M. Bernasconi
Soil organic geochemistry and carbon dynamics of an alpine chronosequence
Geochimica Et Cosmochimica Acta **73** (2009) A1242-A1242

F. Simmen, T. Lippert, P. Novák, B. Neuenschwander, M. Döbeli, M. Mallepell and A. Wokaun
Influence of the substrate material on the properties of pulsed laser deposited thin $Li_{1+x}Mn_2O_{4-\delta}$ films
Applied Surface Science **255** (2009) 5303-5306

S. Strasky, L. Di Nicola, C. Baroni, M.C. Salvatore, H. Baur, P.W. Kubik, C. Schlüchter and R. Wieler
Surface exposure ages imply multiple low-amplitude Pleistocene variations in East Antarctic Ice Sheet, Ricker Hills, Victoria Land
Antarctic Science **21** (2009) 59-69

S. Strasky, A. Graf, Z. Zhao, P.W. Kubik, H. Baur, C. Schlüchter and R. Wieler
Late Glacial ice advances in southeast Tibet
Journal of Asian Earth Sciences **34** (2009) 458-465

S. Szidat, M. Ruff, N. Perron, L. Wacker, H.-A. Synal, M. Hallquist, A.S. Shannigrahi, K.E. Yttri, C. Dye and D. Simpson
Fossil and non-fossil sources of organic carbon (OC) and elemental carbon (EC) in Goteborg, Sweden
Atmospheric Chemistry and Physics **9** (2009) 1521-1535

S. van Willigen, I. Hajdas and G. Bonani
New Radiocarbon Dates for the Early Neolithic of the Western Mediterranean
Radiocarbon **51** (2009) 831-838

C. Vockenhuber, L.E. Erikson, L. Buchmann, U. Greife, U. Hager, D.A. Hutcheon, M. Lamey, P. Machule, D. Ottewell, C. Ruiz and G. Ruprecht
A transmission time-of-flight system for particle identification at a recoil mass separator at low energies
Nuclear Instruments and Methods B **603** (2009) 372-378

H. Wittmann, F. von Blanckenburg, J.L. Guyot, L. Maurice and P.W. Kubik
From source to sink: Preserving the cosmogenic ^{10}Be-derived denudation rate signal of the Bolivian Andes in sediment of the Beni and Mamoré foreland basins
Earth and Planetary Science Letters (2009) 463-474

C. Zahno, N. Akçar, V. Yavuz, P.W. Kubik and C. Schlüchter
Surface exposure dating of Late Pleistocene glaciations at the Dedegöl Mountains (Lake Beysehir, SW Turkey)
Journal of Quaternary Science **24** (2009) 1016-1028

J. Zech, R. Zech, P.W. Kubik and H. Veit
Glacier and climate reconstruction at Tres Lagunas, NW Argentina, based on ^{10}Be surface exposure dating and lake sediment analyses
Palaeogeography, Palaeoclimatology, Palaeoecology 284 (2009) 180-190

R. Zech, M. Zech, P.W. Kubik, K. Kharki and W. Zech
Deglaciation and landscape history around Annapurna, Nepal, based on Be-10 surface exposure dating
Quaternary Science Reviews **28** (2009) 1106-1118

INVITED TALKS

N. Akcar, V. Alfimov and S. Ivy-Ochs
Sampling in Turkey 2008
Zurich, Switzerland, April 1, 2009, Seminar Series Ion Beam Physics

V. Alfimov
AMS for long-lived radionuclides
Risø-Roskilde, Denmark, November 16-20, 2009, Workshop on Radioanalytical Chemistry for Radioecology and Waste Management (RadWorkshop)

Evaluation of Cl-36 production rates
Zurich, Switzerland, December 9, 2009, Seminar Series Ion Beam Physics

M. Christl
Actinide measurements with a small accelerator - recent developments and applications in environmental sciences
Berne, Switzerland, February 2, 2009, Seminar at Dept. for Chemistry and Biochemistry, University of Bern

Beschleunigermassenspektrometrie und Klimarekonstruktion
Cologne, Germany, February 12, 2009, Seminar at the University of Cologne

M. Döbeli
IBA with high resolution gas ionization detectors
Cambridge, England, September 8, 2009, 19th International Conference on Ion Beam Analysis

I. Hajdas
Radiocarbon dating calibration and applications
Anzonico, Switzerland, September 1, 2009, International Geochronology Summer School

I. Hajdas, S. Ivy-Ochs and F. Preusser
How to correctly report geochronological data
Berne, Switzerland, January 24, 2009, CH-QUAT Meeting

S. Ivy-Ochs
Surface exposure dating of giant landslides in the Alps
Zurich, Switzerland, March 17, 2009, Engineering Geology Seminar Series, ETH Zurich

Deciphering landslide histories with surface exposure dating
Padua, Italy, May 19, 2009, Geology Seminar Series, University of Padua

Surface exposure dating with cosmogenic nuclides
Anzonico, Switzerland, September 3, 2009, International Geochronology Summer School

Cosmogenic nuclides in archeology
Zurich, Switzerland, November 4, 2009, Archeology Seminar Series, University of Zurich

Holocene climate change in the Alps
New York, USA, November 12, 2009, Workshop on Holocene Climate Change, Columbia University

Glaciations of the Alps
Zurich, Switzerland, December 7, 2009, Seminar Earth Sciences, ETH Zurich

J. Lachner
Plutonium Isotope auf dem Bikini-Atoll
Zurich, Switzerland, October 14, 2009, Seminar Series Ion Beam Physics

T. Schulze-König
Armagnac zum Frühstück: Alkohol und Stoffwechsel
Zurich, Switzerland, October 28, 2009, Seminar Series Ion Beam Physics

M. Simon
PIXE mittels Mikro-Kapillare
Zurich, Switzerland, May 20, 2009, Seminar Series Ion Beam Physics

M. Suter
How can we build better instruments for Accelerator Mass Spectrometry?
Seville, Spain, January 15, 2009, Seminar at Centro Nacional de Aceleradores (CNA)

How can we build better instruments for Accelerator Mass Spectrometry?
Aix-en-Provence, France, February 2, 2009, Seminar at CEREGE, Europôle Méditerranéen de l'Arbois

Gas ionization chambers (IC)-principles and recent developments
Seville, Spain, March 10-12, 2009, Course at Centro Nacional de Aceleradores (CNA)

Are universal compact AMS facilities a competitive alternative to larger tandem accelerators?
Kona, Hawaii, May 31 – June 5, 2009, 20th International Radiocarbon Conference

Developments of compact AMS facilities- scientific and technical challenges
Beijing, China, June 24, 2009, Seminar School of Physics, Peking University

Developments of compact AMS facilities - scientific and technical challenges
Beijing, China, June 25, 2009, Seminar China Institute of Atomic Energy

Accelerator Mass Spectrometry: instrumental developments and the wide range of applications
Beijing, China, June 26, 2009, Seminar School of Environmental Sciences, Peking University

Challenging developments in 3 decades of Accelerator Mass Spectrometry: from large particle accelerators to table size instruments
Bremen, Germany, August 31 – September 4, 2009, 18th International Mass Spectrometry Conference

Physics of Accelerator Mass Spectrometry
Vienna, Austria, December 3, 2009, Seminar at VERA Laboratory, University of Vienna

H.-A. Synal
Accelerator Mass Spectrometry (AMS) measurement technique after 30 years: possibilities and limitations of low energy systems
Heidelberg, Germany, April 16, 2009, Colloquium Max-Planck-Institute for Nuclear Physics

New and improved AMS facilities
Venice, Italy, June 10, 2009, HIAT'09

Introduction to AMS: basics concepts and ideas
Huelva - La Rabida, Spain, July 6, 2009, International Scientific Meeting on Nuclear Physics

Low energy limits of AMS
Huelva - La Rabida, Spain, July 7, 2009, International Scientific Meeting on Nuclear Physics

Ion optics and design of AMS systems
Huelva - La Rabida, Spain, July 8, 2009, International Scientific Meeting on Nuclear Physics

Applications of AMS measurements
Huelva - La Rabida, Spain, July 9, 2009, International Scientific Meeting on Nuclear Physics

New and future perspectives of ion beam physics
Villigen, Switzerland, October 1, 2009, Colloquium at Paul Scherrer Institut

New and future perspectives of Accelerator Mass Spectrometry
Berne, Switzerland, November 5, 2009, Colloquium at Institute of Chemistry, University of Bern

C. Vockenhuber
Measurements for ^{44}Ti at TRIUMF-ISAC, ^{40}Ca(α, γ)^{44}Ti and future RIB experiments
Garching, Germany, January 15, 2009, Ti-44 Workshop at Max-Planck-Institute for Extraterrestrial Physics

Long-lived radionuclides in nuclear astrophysics
Frankfurt, Germany, October 12, 2009, NuPECC Long Range Plan 2010 Scoping Workshop

L. Wacker
MICADAS: What can be done with a mini radiocarbon dating system?
Sweden, Lund, May 15, 2009, Seminar at Lund University

TALKS AND POSTERS

N. Akçar, S. Ivy-Ochs, İ.Ö.Yılmaz, V. Alfimov, A. Schachner, D. Altıner, V. Yavuz and C. Schlüchter
Determining the origin of building stones in the Hittite capital of Hattusha
Berne, Switzerland, January 24, 2009, CH-QUAT meeting

N. Akçar, S. Ivy-Ochs, P. Deline, P.W. Kubik and C. Schlüchter
^{10}Be production rate from 1717 AD rock avalanche in Val Ferret (Mont Blanc Massif, Italy)
Davos, Switzerland, June 21-26, 2009, Goldschmidt Conference

N. Akçar, V. Yavuz, S. Ivy-Ochs, C. Zahno, M. Christl, P.W. Kubik and C. Schlüchter
Chronology of the Quaternary glaciations of the southern Black Sea coast and paleoclimatic interpretations
Ankara, Turkey, October 5-6, 2009, 2nd International Symposium on the Geology of the Black Sea Region

V. Alfimov, S. Ivy-Ochs
The systematics of the ^{36}Cl production rate calculations in limestone
Germany, Hamburg, March 2-6, 2009, DPG Conference

The systematics of ^{36}Cl production rate calculations in limestone and dolomite
Davos, Switzerland, June 21-26, 2009, Goldschmidt Conference

C. Baroni, L. Di Nicola, S. Strasky, M.C. Salvatore, C. Schlüchter, P.W. Kubik and R. Wieler
Cenozoic glacial history in northern Victoria Land (Antarctica): geomorphological evidences and exposure ages
Melbourne, Australia, July 6-11, 2009, VII International Geomorphologic Congress

A. Birkholz, R. Smittenberg, I. Hajdas, L. Wacker, J. Bakke and S. Bernasconi
Reconstruction of European soil carbon build-up and dynamics using compound-specific radiocarbon analysis from lake sediments
Bremen, Germany, November 6-11, 2009, 24th International Meeting on Organic Geochemistry (IMOG)

M. Christl
Carrier-free Be-10/Be-9 measurements at low energies
Hamburg, Germany, March 2-6, 2009, DPG Conference

Water mass properties and circulation in the Cape Basin – a multi proxy approach
Davos, Switzerland, June 21-26, 2009, Goldschmidt Conference

L. Di Nicola, C. Baroni, S. Strasky, M.C. Salvatore, C. Schlüchter, N. Akcar, P.W. Kubik and R. Wieler
Cenozoic landscape evolution in Terra Nova Bay region: new evidence from multiple comogenic nuclides
Vienna, Austria, April 19-25, 2009, European Geophysical Union Conference

F. Favilli, M. Egli, D. Brandova, S. Ivy-Ochs, P.W. Kubik, P. Cherubini, A. Mirabella, G. Sartori, D. Giaccai, and W. Haeberli
Combined use of relative and numerical dating techniques for detecting signals of Alpine landscape evolution during the late Pleistocene and early Holocene in Val di Rabbi (Trentino, northern Italy)
Vienna, Austria, April 19-25, 2009, European Geophysical Union Conference

I. Hajdas, D. Michczynska, G. Bonani, M. Maurer and L. Wacker
Closed tubes preparation of graphite for high-precision AMS radiocarbon analysis
Vienna, Austria, April 19-25, 2009, European Geophysical Union Conference

I. Hajdas, A. Michczyński
Comparison of lake sediments age-depth model based on the high resolution ^{14}C datings with varve chronology
Kona, Hawaii, May 31 – June 5, 2009, 20th International Radiocarbon Conference

I. Hajdas, D. Michczynska, G. Bonani, M. Maurer and L. Wacker
Closed tubes preparation of graphite for high-precision AMS radiocarbon analysis
Kona, Hawaii, May 31 – June 5, 2009, 20th International Radiocarbon Conference

K. Hippe, F. Kober, G. Zeilinger, S. Ivy-Ochs, P.W. Kubik and R. Wieler
Short and long-term denudation rates at the Altiplano margin, La Paz region, Bolivia
Davos, Switzerland, June 21-26, 2009, Goldschmidt Conference

K. Hippe, F. Kober, G. Zeilinger, S. Ivy-Ochs, P.W. Kubik and R. Wieler
Quantifying rates of surface denudation at the eastern Altiplano margin, La Paz region, Bolivia
Neuchâtel, Switzerland, November 20-21, 2009, 7th Swiss Geoscience Meeting

S. Ivy-Ochs, N. Akçar, H. Kerschner, V. Alfimov, P.W. Kubik and C. Schlüchter
The timing of the last deglaciation in the European Alps
Ankara, Turkey, March 13-17, 2009, 62nd Geological Congress of Turkey

S. Ivy-Ochs, H. Kerschner, M. Maisch, M. Christl, P.W. Kubik and C. Schlüchter
^{10}Be surface exposure dating of rock glaciers in Larstigtal, Tyrol, Austria
Vienna, Austria, April 19-25, 2009, European Geophysical Union Conference

S. Ivy-Ochs, V. Alfimov and D. van Husen
Surface exposure dating of large landslides in the European Alps: Wildalpen (Styria, Austria)
Davos, Switzerland, June 21-26, 2009, Goldschmidt Conference

F. Kober, G. Zeilinger, S. Ivy-Ochs, A. Dolati, J. Smit, J.-P. Burg, A. Bahroudi, P.W. Kubik, H. Baur, R. Wieler and N. Haghipour
Temporal correlation of fluvial and alluvial sequences in the Makran Range, SE-Iran
Vienna, Austria, April 19-25, 2009, European Geophysical Union Conference

F. Kober, S. Ivy-Ochs, L. Abbühl, F. Schlunegger, O. Kracht, P.W. Kubik, H. Baur and R. Wieler
Denudation rates across the fluvially/glacially Hörnli landscape (Switzerland) during the late Pleistocene/Holocene
Vienna, Austria, April 19-25, 2009, European Geophysical Union Conference

F. Kober, V. Alfimov, S. Ivy-Ochs, P.W. Kubik and R. Wieler
An evaluation of the cosmogenic $^{21}Ne/^{10}Be$ ratio and the ^{21}Ne production rate in quartz
Davos, Switzerland, June 21-26, 2009, Goldschmidt Conference

F. Kober, L. Abbühl, M. Dürst, S. Ivy-Ochs, F. Schlunegger and P.W. Kubik
The shape versus the processes of a landform- the Hörnli region, NE Switzerland
Neuchatel, Switzerland, November 20-21, 2009, 7th Swiss Geoscience Meeting

J. Lachner
Suche nach schwersten primordialen Radionukliden
Hamburg, Germany, March 2-6, 2009, DPG Conference

Long-lived isomeric states in neutron-deficient thorium isotopes?
Bochum, Germany, March 19, 2009, DPG and EuNPC Conference Bochum

Direct search for primordial ^{244}Pu
Davos, Switzerland, June 21-26, 2009, Goldschmidt Conference

J. Lippold, M. Christl, A. Hofmann, G. Mollenhauer, S. Mulitza, S. Weyer and A. Mangini
The response of sedimentary ^{231}Pa/^{230}Th on particle flux - findings from the African margin
Davos, Switzerland, June 21-26, 2009, Goldschmidt Conference

S. Merchel, W. Bremser, V. Alfimov, M. Arnold, G. Aumaître, L. Benedetti, D.L. Bourlès, R. Braucher, M. Caffee, M. Christl, L.K. Fifield, R.C. Finkel, S.P.H.T. Freeman, A. Ruiz-Gomez, P.W. Kubik, D.H. Rood, K. Sasa, P. Steier, S.G. Tims, A. Wallner, K.M. Wilcken and S. Xu
^{10}Be and ^{36}Cl interlaboratory comparisons
Hamburg, Germany, March 2-6, 2009, DPG Conference

S. Merchel, W. Bremser, V. Alfimov, M. Arnold, G. Aumaître, L. Benedetti, D.L. Bourlès, R. Braucher, M. Caffee, M. Christl, L.K. Fifield, R.C. Finkel, S.P.H.T. Freeman, A. Ruiz-Gomez, P.W. Kubik, D.H. Rood, K. Sasa, P. Steier, S.G. Tims, A. Wallner, K.M. Wilcken and S. Xu
^{10}Be and ^{36}Cl interlaboratory comparisons: implications for terrestrial production rates?
Davos, Switzerland, June 21-26, 2009, Goldschmidt Conference

D. Michczyńska, I. Hajdas
Chronostratigraphic subdivision of the Late Glacial and the Holocene in Alaska
Kona, Hawaii, May 31 – June 5, 2009, 20th International Radiocarbon Conference

A.M. Müller
Design eines zusätzlichen Ablenkmagneten für das 600 kV ETH AMS System
Hamburg, Germany, March 21-26, 2009, DPG Conference

M. Ruff
Radiocarbon dating of small samples
Bremen, Deutschland, August 31 – September 4, 2009, 18th International Mass Spectrometry Conference

G.M.H. Ruiz, F. Negro, J. Babault, J. Foeken, F.M. Stuart, F. Kober and S. Ivy-Ochs
Tectono-thermal evolution of the Atlas system – SW Morocco
Vienna, Austria, April 19-25, 2009, European Geophysical Union Conference

T. Schulze-König
Increasing the dynamic range of radiocarbon AMS
Hamburg, Germany, March 2-6, 2009, DPG Conference

Developments for AMS in the biomedical field
Bremen, Germany, August 31 – September 4, 2009, 18th International Mass Spectrometry Conference

M. Simon
MeV Ion microscopy by means of microcapillaries
Zurich, Switzerland, June 4, 2009, Ph.D. Student Seminar ETH Zurich

R. Smittenberg, I. Hajdas, L. Wacker and S. Bernasconi
Soils organic carbon dynamics of an alpine chronosequence
Bremen, Germany, September 6-11, 2009, 24th International Meeting on Organic Geochemistry (IMOG)

M. Strobl, R. Hetzel, S. Ivy-Ochs, V. Alfimov, P.W. Kubik, C. Fassoulas and L. Palumbo
A long-term rock uplift rate for eastern Crete from exposure dating of marine terraces
Vienna, Austria, April 19-25, 2009, European Geophysical Union Conference

L. Tosch, R. Michel, H. Nies, H.-A. Synal and V. Alfimov
Iod-129 und andere anthropogene Radionuklide in der Nordsee
Hamburg, Germany, March 2-6, 2009, DPG Conference

C. Vockenhuber, V. Alfimov, A.M. Müller, M. Suter and H.-A. Synal
Energy loss and straggling measurements for AMS
Hamburg, Germany, March 2-6, 2009, DPG Conference

L. Wacker
MICADAS: a versatile radiocarbon dating system in routine operation
Hamburg, Germany, March 2-6, 2009, DPG Conference

How to measure small samples with a gas ion source
Kona, Hawaii, May 31 – June 5, 2009, 20th International Radiocarbon Conference

MICADAS: routine and high-precision radiocarbon dating
Kona, Hawaii, May 31 – June 5, 2009, 20th International Radiocarbon Conference

J. Zech, R. Zech, J.-H. May, P.W. Kubik and H. Veit
Heinrich I and younger Dryas glaciation in the Central Andes
San Francisco, USA, December 14-18, 2009, AGU Fall Meeting

G. Zeilinger, F. Kober, M.R. Strecker, S. Ivy-Ochs, P.W. Kubik and K. Hippe
Erosion rates in the Rio La Paz drainage basin: evidence for spatially and temporally variable erosion processes
Vienna, Austria, April 19-25, 2009, European Geophysical Union Conference

SEMINAR 'AKTUELLE THEMEN AUS DER BESCHLEUNIGERMASSEN-SPEKTROMETRIE UND DEREN ANWENDUNGEN'

Spring semester

18.02.2009
Friedhelm Steinhilber (EAWAG, Switzerland), *Rekonstruktion der solaren Aktivität*

25.02.2009
Bernd Heber (University of Kiel, Germany), *Solar and heliospheric modulation of cosmic rays*

11.03.2009
Janet Rethemeyer (AWI-Bremerhaven, Germany), *Compound-specific radiocarbon analysis -- analytical challenges and applications*

18.03.2009
Jörg Lippold (University of Heidelberg, Germany), *^{231}Pa ein Proxy für Ozeanzirkulation?*

01.04.2009
Vasily Alfimov, Naki Akçar and Susan Ivy-Ochs (ETH Zurich, Switzerland), *Sampling fault scarps in Turkey*

15.04.2009
Ralph Böhlert and Filippo Favilli (University of Zurich, Switzerland), *Reconstructing Lateglacial and early Holocene landscape history using different dating techniques - examples from eastern Switzerland and northern Italy*

22.04.2009
Berko Sierau (ETH Zurich, Switzerland), *In-situ measurements of atmospheric aerosols using Mass Spectrometry*

29.04.2009
Simon Fahrni (University of Bern, Switzerland), *Compound-specific radiocarbon measurements*

11.05.2009
Noemi Rebollo (INFN Ferrara, Italy), *Anatomically modern humans migrated out of Africa almost 50,000 years ago: Radiocarbon dating of the MP-UP transition in Kebara Cave, Israel*

13.05.2009
Peter Steier (University of Vienna, Austria), *AMS of ^{36}Cl with a 3MV Tandem*

20.05.2009
Marius Simon (ETH Zurich, Switzerland), *PIXE mittels Mikro-Kapillare*

27.05.2009
Jose Angel Abreu (EAWAG, Switzerland), *Principal Component Analysis (PCA) - Trennung von Klima und Produktion bei kosmogenen Radionukliden*

Fall semester

16.09.2009
Kristina Hippe (ETH Zurich, Switzerland), *Quantifying rates of surface denudation at the eastern Altiplano margin, La Paz region, Bolivia*

30.09.2009
Ola Kwiecien (ETH Zurich, Switzerland), *Revised chronology of the Black Sea sediments over the last 25,000 years*

07.10.2009
Martin Seiler (ETH Zurich, Switzerland), *Entwicklung eines neuen MICADAS-Stripperrohres: Betrachtungen zum Leitwert*

14.10.2009
Johannes Lachner (ETH Zurich, Switzerland), *Plutonium Isotope auf dem Bikini-Atoll*

21.10.2009
Axel Birkholz (ETH Zurich, Switzerland), *Compound specific radiocarbon analyses as a tool for the reconstruction of soil organic carbon build-up*

28.10.2009
Tim Schulze-König (ETH Zurich, Switzerland), *Armagnac zum Frühstück: Alkohol und Stoffwechsel*

11.11.2009
Toni Wallner (University of Vienna, Austria), *Anwendungen von AMS in der Astrophysik*

18.11.2009
Mathias Mann (EAWAG, Switzerland) and Ulrike van Raden (ETH Zurich, Switzerland), *Lacustrine sediments: high resolution archives for geomagnetic field behavior and paleoclimate*

25.11.2009
Andreas Dehnert (University of Bern, Switzerland), *Burial dating using the cosmogenic isotopes Be-10 and Al-26 - Feasibility studies for Pliocene to Pleistocene terrestrial sediments*

02.12.2009
Florian Kober (ETH Zurich, Switzerland), *Evaluation of Ne-21 production rates*

09.12.2009
Vasily Alfimov (ETH Zurich, Switzerland), *Evaluation of Cl-36 production rates*

16.12.2009
Heather Graven (ETH Zurich, Switzerland), *Recent observations of $\Delta^{14}C$ in atmospheric CO_2 from the Scripps CO_2 program*

THESES (INTERNAL)

Term papers

Daniela Frauchiger
Transmissionsmessungen für AMS Analysen am TANDY
ETH Zurich

Melchior Limacher
Untersuchung des Pulshöhendefektes in Gasionisationsdetektoren
ETH Zurich

Martin Seiler
Leitwertmessung am Stripperrohr
ETH Zurich

Doctoral theses

Marc Mallepell
Ringförmiger Gasionisationsdetektor für Schwerionen-Rückstreuanalyse
ETH Zurich, ETH Nr. 18394

Arnold Milenko Müller
Entwicklung von universellen AMS Anlagen bei tiefen Energien
ETH Zurich, ETH Nr. 18393

THESES (EXTERNAL)

Diploma/Master theses

Katharina Gückel
Analytik von ^{127}I und ^{129}I in Umweltproben
University of Hannover (Germany)

Jens Korntheuer
Analytik von ^{127}I und ^{129}I in Umweltproben
University of Hannover (Germany)

Jan Kuhlmann
Ermittlung der spätquartären Bewegungsrate der aktiven Las Penas-Überschiebung in der Präkordillere der Anden nahe Mendoza, Argentinien
University of Münster (Germany)

Marc Lücke
Kosmogenes ^{10}Be und ^{26}Al an Granit von alpinen Gipfeln des Goms, Schweizer Alpen
University of Hannover (Germany)

Doctoral theses

Jose Abreu
^{10}Be in polar ice cores and ^{14}C in tree rings: Separation of production and system effects, comparison with past climate changes and implications for solar activity
ETH Zurich, ETH-Nr. 18430

Andreas Dehnert
Burial dating using the cosmogenic isotopes ^{10}Be and ^{26}Al – Feasibility studies for Pliocene to Pleistocene terrestrial sediments
University of Bern (Switzerland)

Ivan Marozau
Pulsed laser deposition and characterisation of perovskite-type oxynitride thin films
ETH Zurich, ETH-Nr. 18328

Henning Meyer
Quantification and geochemical characterization of total mass fluxes in river catchments of the Rhenish Massif and the Black Forest, Germany
University of Münster (Germany)

Thomas Opel
Glacier and ground ice as archives of Late Holocene climate and environmental change in the Russian Arctic
University of Berlin (Germany)

Friedhelm Steinhilber
Reconstruction of solar activity during the Holocene using the cosmogenic radionuclide Beryllium-10

ETH Zurich, ETHZ-Nr. 18256

Conradin Zahno
Late Pleistocene glacier variations in western Turkey: chronology and palaeoclimate
University of Bern (Switzerland)

Jana Zech
^{10}Be surface exposure dating in the Central Andes
University of Bern (Switzerland)

COLLABORATIONS

Austria

Geology and Mass Movements, AlpS - Zentrum für Naturgefahren- und Riskomanagement GmbH, Innsbruck

Institute of Applied Geology, University of Natural Resources and Applied Life Sciences, Vienna

Institute of Geography, University of Innsbruck, Innsbruck

Institute of Geology, University of Innsbruck, Innsbruck

Institute for Geology, Vienna University of Technology, Vienna

Sediment Geology, Geological Survey of Austria, Vienna

VERA, Faculty of Physics, University of Vienna, Vienna

Canada

Marine Environmental Sciences Division, Bedford Institute of Oceanography, Dartmouth

TRIUMF, Vancouver

France

CEREGE, University of Aix-Marseille, Aix-en-Provence

Germany

Center for Radiation Protection and Radioecology, University of Hannover, Hannover

Department of Periglacial Research, Alfred Wegener Institute of Polar and Marine Research, Potsdam

Deutsches Bergbau Museum, Bochum

Direktion Landesarchäologie, Generaldirektion Kulturelles Erbe, Speyer

Federal Institute for Geosciences and Natural Resources, Hannover

German Research Centre for Geosciences (GFZ), Potsdam

Helmholtz-University Group: Compound-specific ^{14}C, Alfred Wegener Institute of Polar and Marine Research, Bremerhaven

Hydroisotop GmbH, Schweitenkirchen

Institute of Botany, University of Hohenheim, Stuttgart

Institute of Environmental Physics, University of Heidelberg, Heidelberg

Institute of Geography, University of Cologne, Cologne

Institute of Geology and Mineralogy, University of Cologne, Cologne

Institute for Geomorphology, University of Bayreuth, Bayreuth

Institute for Geosciences, University of Jena, Jena

Institute for Geosciences, University of Potsdam, Potsdam

Institute for Nuclear Chemistry, University of Cologne, Cologne

Institute of Paleontology, University of Münster, Münster

Institute of Soil Science and Soil Geography, University of Bayreuth, Bayreuth

Landesamt für Denkmalpflege, Regierungspräsidium Stuttgart, Esslingen

Leibniz Institute for Marine Sciences, University of Kiel, Kiel

Photovoltaics Group, Hahn Meitner Institute, Berlin

Research Center Dresden-Rossendorf, Dresden

Hungary

Institute of Nuclear Research (ATOMKI), Hungarian Academy of Science, Debrecen

Israel

Geophysical Institute of Israel, Hebrew University, Jersualem

Italy

Department of Earth Sciences, Universtiy of Turin, Turin

Department of Geology and Geophysics, University of Padua, Padua

Liechtenstein

Denkmalpflege / Archäologie, Hochbauamt Triesen, Triesen

Netherlands

Department of Petrology, VU University Amsterdam, Amsterdam

Norway

Department of Earth Science, University of Bergen, Bergen

Geological Survey of Norway, Trondheim

Nansen Environmental and Remote Sensing Center & Bjerknes Centre for Climate Research, Bergen

Quaternary Geology, The University Centre of Svalbard, Longyearbyen

Russia

Faculty of Physical Science and Technology, St. Petersburg State Polytechnic University, St. Petersburg

Spain

National Center for Accelerators, University of Seville, Seville

Sweden

Department of Geology, Uppsala University, Uppsala

Tandem Laboratory, Uppsala University, Uppsala

Switzerland

Air Pollution / Climate Group, Research Station Agroscope Reckenholz-Tänikon, Zurich

Amt für Städtebau, Stadt Zürich, Zurich

Archäologischer Dienst, Kanton Bern, Berne

Archäologischer Dienst, Kanton Graubünden, Chur

Bookham AG, Zurich

Dendrolabor Wallis, Brig

Department of Anthropology and Ecology, University of Geneva, Geneva

Department of Chemistry and Biochemistry, University of Bern, Berne

Department of Earth Sciences, ETH Zurich, Zurich

Department of Geology, University of Neuchatel, Neuchatel

Department of Geosciences, University of Fribourg, Fribourg

Electrochemistry Laboratory, Paul Scherrer Institut (PSI), Villigen

Functional Polymers Group, Swiss Federal Laboratories for Materials Testing and Research (EMPA), Dübendorf

Institute of Botany, University of Basel, Basel

Institute of Geography, University of Bern, Berne

Institute of Geography, University of Zurich, Zurich

Institute of Geology, University of Bern, Berne

Institute of Geology, ETH Zurich, Zurich

Institute of Geomatics and Risk Analysis, University of Lausanne, Lausanne

Institute of Isotope Geochemistry and Mineral Resources, ETH Zurich, Zurich

Institute of Microengineering, ETH Lausanne, Lausanne

Institute of Particle Physics, ETH Zurich, Zurich

Institute of Solid State Physics, ETH Zurich, Zurich

Kantonsarchäologie, Kanton St. Gallen, St. Gallen

Kantonsarchäologie, Kanton Solothurn, Solothurn

Kantonsarchäologie, Kanton Zürich, Dübendorf

Kantonsarchäologie, Kanton Zug, Zug

Laboratoire Romand de Dendrochronologie, Moudon

Laboratory for Atmospheric Chemistry, Paul Scherrer Institut (PSI), Villigen

Laboratory for Nuclear Materials, Paul Scherrer Institut (PSI), Villigen

Laboratory for Radiochemistry and Environmental Chemistry, Paul Scherrer Institut (PSI), Villigen

Materials Group, Paul Scherrer Institut (PSI), Villigen

Nanomechanics Group, Swiss Federal Laboratories for Materials Testing and Research (EMPA), Dübendorf

Nanometallurgy Group, ETH Zurich, Zurich

Nanoscale Materials Group, Swiss Federal Laboratories for Materials Testing and Research (EMPA), Dübendorf

Oeschger Center for Climate Research, University of Bern, Berne

Reinhardt Microtech AG, Wangs

Section d'archéologie et paléontologie, Office de la culture, Hotel des Halles, Porrentruy

Soil Sciences, Swiss Federal Institute for Forest, Snow and Landscape Reseach (WSL), Birmensdorf

Solid State Chemistry Group, Swiss Federal Laboratories for Materials Testing and Research (EMPA), Dübendorf

Steinel AG, Einsiedeln

Swiss Geotechnical Commision, Swiss Acadamy of Sciences, Zurich

SURF, Swiss Federal Institute of Aquatic Science and Technology (EAWAG), Dübendorf

Thin Films Group, Swiss Federal Laboratories for Materials Testing and Research (EMPA), Dübendorf

Unaxis AG, Balzers

Turkey

Faculty of Mines, Istanbul Technical University, Istanbul

Geological Engineering Department, Middle East Technical University, Ankara

United Kingdom

Department of Earth Sciences, University of Bristol, Bristol

Department of Geography, Aberystwyth University, Aberystwyth

Department of Geography, Durham University, Durham

Department of Geography, Exeter University, Exeter

United States of America

Lamont-Doherty Earth Observatory, Columbia University, Palisades

VISITORS AT THE LABORATORY

Daraoui Abdelouahed
Center for Radiation Protection and Radioecology, University of Hannover, Germany

Naki Akçar
Institute of Geology, University of Bern, Switzerland

Katja Ammon
School of Sciences, University of Edinburgh, United Kingdom

Erica Andreotti
The Institute for Reference Materials and Measurements, University of Insubria, Italy

Katharina Gückel
Center for Radiation Protection and Radioecology, University of Hannover, Germany

Bernhard Kuczewski
Institute for Nuclear Chemistry, University of Cologne, Germany

Walter Kutschera
VERA, Faculty of Physics, University of Vienna, Austria

Jakob Liebl
VERA, Faculty of Physics, University of Vienna, Austria

Barbara May
Institute of Environmental Physics, University of Heidelberg, Germany

Danuta Michczynksa
GADAM Centre, Gliwice, Silesian University of Technology, Poland

Caroline Münsterer
Institute of Environmental Physics, University of Heidelberg, Germany

Aaron Ruiz-Gomez
National Center for Accelerators (CNA), University of Seville, Spain

Hugo Sandman
The Netherlands Organisation for Applied Scientific Research TNO, Zeist, The Netherlands

Zdravko Siketic
Ruder Boskovic Institut, Zagreb, Croatia

Friedhelm von Blanckenburg
GFZ German Research Centre for Geosciences, Potsdam, Germany

Hendrik Wiesel
Institute for Nuclear Chemistry, University of Cologne, Germany

Jane Willenbring
GFZ German Research Centre for Geosciences, Potsdam, Germany

Qiang Zhao
Institute of Nuclear Solid State Physics, University of Leuven, Belgium